Incorporation of Nanoparticles in Polymeric Materials for Medical Applications

by

Christopher John Ward

A dissertation submitted to the Graduate Faculty of
Auburn University
in partial fulfillment of the
requirements for the Degree of
Doctor of Philosophy

Auburn, Alabama
August 3, 2013

Keywords: controlled release, polymer nanocomposites, halloysite nanotubes,
polyurethane, gold nanorods, photothermal shape memory activation

Approved by

Edward W. Davis, Chair, Lecturer of Polymer and Fiber Engineering
Maria L. Auad, Associate Professor of Polymer and Fiber Engineering
Bart Prorok, Professor of Materials Engineering
Xinyu Zhang, Assistant Professor of Polymer and Fiber Engineering

Abstract

Nanomaterials have become a desirable field of research for use in the medical industry. Many modern medical techniques, devices, and medications can utilize nanomaterials for entirely new functions and designs. This dissertation details the results of two studies performed on the use of nanomaterials in polymers for potential medical applications.

One important aspect of the medical field is that of drug delivery. While some delivery methods are commonplace, issues such as extremely high concentrations, repeated doses, and low patient compliance are also commonplace. This results in a need for a more sophisticated, controllable delivery method. This work focuses on the use of two distinct types of nanoparticles for controlled release applications.

Halloysite nanotubes are naturally-formed nanoclay materials. The first study evaluated the use of these nanotubes as drug-loading vehicles incorporated into rate-inhibiting polymeric films, with controlled release being the main goal. The topics addressed under this objective include loading methods of the halloysite nanoclay, effects of loaded compound properties on release, and incorporation of the halloysite into a polymer matrix, poly(methyl methacrylate), to lengthen release. Results suggest that the produced nanocomposite is capable of considerable extended controlled release.

Shape memory polymers are a fascinating branch of smart polymers. Traditionally, the shape memory transition in these polymers is triggered by direct heat. Alternative methods are

required for when direct heat is not applicable, such as in the body. With a more acceptable, non-harmful triggering mechanism, shape memory polymers are capable of controlled release.

The second study investigates a remote triggering mechanism to induce the shape memory effect in a segmented polyurethane. To do this, a method of using non-harmful near-infrared light for triggering is investigated. The photothermal properties of gold nanorods are utilized. The topics addressed under this objective are: synthesis of wavelength-dependent gold nanorods through a seed-mediated process, isolation and stability of the nanorods, incorporation of the nanorods into the polyurethane for the creation of the shape memory nanocomposite, investigation of the effects of the nanorods on the inherent polyurethane properties (thermal, mechanical, shape memory, etc.), and examination of the near-infrared, light-induced shape memory properties of the final nanocomposite.

Acknowledgments

This dissertation represents the summation of intense study and experimentation in the field of nanomaterials and composites. Along the way, there were numerous obstacles, problems, and disasters that would not have been overcome without the help from many groups and individuals.

First off, I would like to thank my parents, Karl and Kathy Ward, for their continuing support and encouragement. Without their help throughout the years of my educational development, I would not be where I am today. Due to their commitment towards providing me with the best education possible and encouragement to take advantage of all that the experiences could give me, I was introduced to endless possibilities that helped steer me toward who I am today. I cannot thank them enough for what they have sacrificed in order to help provide me with the tremendous opportunities and advantages I have had the fortune to achieve.

Next, I would like to thank my advisor, Dr. Edward Davis, without whom, my transition from undergraduate studies into graduate life would have been much bumpier. From working in the lab under his direction as an undergraduate researcher to independent studies under my control as a doctoral student, his continual advice, direction, and support kept me focused. Without his help, I would still be floundering in a myriad of data with no clue how to analyze results and produce conclusions.

Dr. Maria Auad also deserves tremendous thanks and appreciation. During the second part of my doctoral studies, she was constantly striving to help me understand results and plan

experiments. Her knowledge concerning shape memory polymers was an invaluable aid towards the development of a novel shape memory triggering system that has huge potential. In addition, she was never hesitant to provide advice in many facets of life, to which I am very grateful.

I would also like to thank the two final members of my committee, Dr. Xinyu Zhang and Dr. Bart Prorok, as well as my University Reader, Dr. Allan David. I fully appreciate the time and effort that you spent in order to help me accomplish my goal of a doctoral degree. I also cannot fail to extend my gratitude towards the Department of Polymer and Fiber Engineering. I have spent many years within its halls and could not imagine having spent my educational time anywhere else.

Within the department, I would like to thank all of the other individuals that helped my research develop. First, I would like to thank various group members over the years that have helped to critique, support, and explain various results, summaries, and conclusions. These individuals include Gold Darr, Shang Song, Meghan DeWitt, Alicia Eustes, Buket Demir, Bernal Xibaja, Ricardo Ballestero, and a few others. In particular, Shang Song, Meghan DeWitt, and Alicia Eustes were undergraduate students whom I worked with. Their contributions were all significant to me. In addition, much of this research would not be possible without funding, in part, from the Alabama EPSCoR Graduate Research Scholars Program.

Last, but not least by far, I owe a tremendous amount to my fiancée, Samantha Bird. Throughout my entire experience during graduate school, she has been unwaveringly by my side. She has loved and supported me when times have been rough and provided me with the stability that I have needed to survive the process. I will never be able to fully express to her exactly how much she means to me. I cannot wait to be able to call her my wife. I hope that eventually she will understand just how critical she has been in my successes since we first met.

Table of Contents

List of Tables

List of Figures

List of Abbreviations

SEM	Scanning Electron Microscopy
TEM	Transmission Electron Microscopy
DSC	Differential Scanning Calorimetry
TGA	Thermogravimetric Analysis
UV	Ultraviolet
FTIR	Fourier Transform Infrared
DMA	Dynamic Mechanical Analysis
PU	Polyurethane
SMPU	Shape Memory Polyurethane
PMMA	Poly(methyl methacrylate)
CTAB	Hexadecyltrimethylammonium
DMF	N, N″-dimethylformamide
T_g	Glass Transition Temperature
T_{mSS}	Melting Temperature of Soft Segment
T_{mHS}	Melting Temperature of Hard Segment
T_c	Crystallization Temperature
ΔH_{mSS}	Enthalpy of Soft Segment Melting
ΔH_{mHS}	Enthalpy of Hard Segment Melting
ΔH_c	Enthalpy of Crystallization

CHAPTER 1

INTRODUCTION

CONTROLLED RELEASE

Controlled delivery has become a very popular field of study within recent years. This is due mainly to the limitations and problems associated with conventional drug delivery. By definition, controlled release is the release of drugs according to two main characteristics, over extended periods of time and in a targeted manner. The problems that controlled release can solve are many, and can include high initial doses, a need for repeat dosing to maintain drug level, and a lack of sufficient patient compliance. The need for high initial doses arises from the metabolic nature of the human body. The metabolic processes constantly break down the drug and decrease the amount available to the body. If there is not enough drug initially present, then the drug will not reach the desired site. To ensure that a sufficient amount of drug travels to the appropriate site, drugs are introduced to the body at much higher concentrations than are technically required for treatment. This can lead to many unwanted side effects. There are currently solutions to this problem, with the most common solution involving more frequent, but less concentrated doses. This, unfortunately, leads to lower patient compliance; the patient tires of taking so many doses or begins to forget the complicated dosing regimen. Controlled release has the ability to solve these unique problems and allows for a tailorable approach for drug delivery. The modern problems of drug delivery

are solved through either extended periods of release for one dose or the protection of smaller doses from the metabolic processes of the body.

Principles

Controlled delivery has been developed as an alternative to the current techniques of delivering drugs to the body. Of the current techniques, oral administration (ingested tablets or liquids) and injection (intravenous, subcutaneous, or intramuscular) are the most common. Unfortunately, the route that a drug takes through the digestive system can take as long as six hours, thus making the oral route very ineffective [1-2]. This can be especially unacceptable for drugs with short half-lives, meaning that the drug loses its effectiveness in a short period of time. To ensure that a proper amount of a short-half-life drug reaches the intended site, high doses have to be administered. This results in unwanted, sometimes harmful side effects, unforeseen drug dependence [3], and occasionally death [4]. The excess drug that was administered is either degraded early by the body, causing the side effects, or not adsorbed at the desired site. Either way, the excess drug is wasted. This degradation is caused by many mechanisms, including, but not limited to, hydrolysis in the stomach, metabolism in the digestive organs, digestion at the walls of the intestines, and then final degradation at the colon [5-7]. Even with its many problems, this route of drug delivery is still the most common due to its ease and widespread use. The injection route, on the other hand, was developed especially with short-half-life drugs in mind [1-2]. Injection can administer drug directly to the bloodstream, bypassing the digestive tract. Unfortunately, this still does not eliminate the need for high doses. While the drug will reach the intended site faster, the medications are still degraded by metabolic processes. In addition, they can be adsorbed by the liver and removed

by the kidneys. High or frequent doses are thus needed to maintain the critical therapeutic concentration.

The therapeutic concentration level is a very critical parameter. Most medications are only effective within a range of concentrations, which can sometimes be very narrow. If the concentration is too high, irritation or allergic reactions can occur. On the other hand, if the concentration is too low, there is no effective therapeutic value, as shown in Figure I-1.
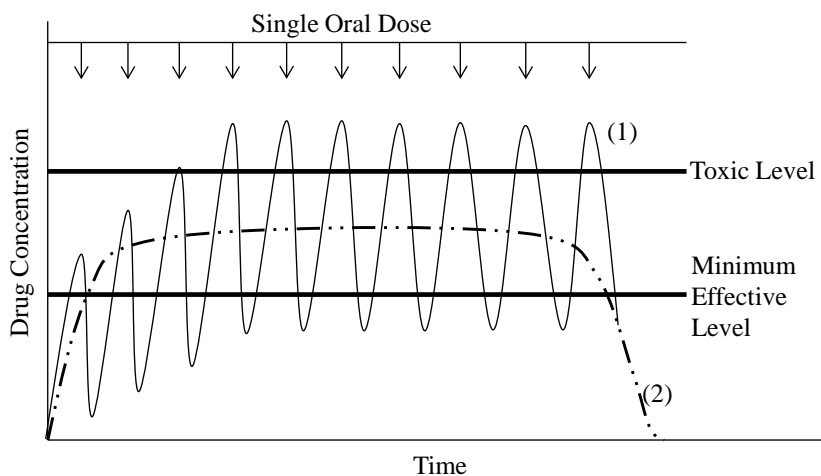
Figure I-1. Typical curves of concentration vs. time for (1) oral doses and (2) controlled release. The curve of injections would appear very similar to the oral dose curve, except that initial concentration would be high, followed by cyclic drops as injections are repeated to keep medication levels high enough. Reprinted with permission from [8], Ward, C.J., M. DeWitt and E.W. Davis, Halloysite Nanoclay for Controlled Release Applications, in *Nanomaterials for Biomedicine*. 2012, American Chemical Society. p. 209-238. Copyright 2012 American Chemical Society.

The repeated doses required with oral and injected medicines result in a cyclical drug concentration [2, 9]. With oral drugs, the drug is introduced into the body and begins to be adsorbed in the small intestine. This causes the drug level in the body to rise. After adsorption slows, however, metabolic processes decrease that level in the body. Another pill is taken and the cycle begins again. The only difference with injection is that it results in an initial high

concentration, followed by a drop. Within these cycles, the level of drug only stays within the optimal concentration level for a short amount of time. Indeed, the upper limit of that window can sometimes be considered toxic, resulting in the need to carefully calculate and monitor doses so that patients do not unintentionally overdose [9-10]. One solution to this problem already in use is to reduce the concentration of the medication and increase the number of doses. Toxicity is no longer a problem, but patient compliance becomes an issue. Many patients, faced with taking pills on a regular basis, will either grow tired with the treatment and disregard instructions or accidentally forget to take the medication, with the result that concentration will once again drop below effective levels.

Faced with the multiple problems outlined concerning traditional drug delivery, controlled delivery has become an increasingly popular field of research. The advantages of controlled delivery of medications are fourfold: i) the level of drug present within the body will remain consistent throughout release, ii) duration of release will be longer, even for those drugs with shorter half-lives, iii) the possibility of side effects and unintentional overdoses will be reduced, and iv) patient compliance should rise with the reduction or elimination of repeated doses or injections [11-12]. Patient compliance studies have shown that issues in this area can lead to problems such as lingering or increasing illness and even possible loss of life, not to mention the increased costs of medical care as a result of lingering treatment [13]. To achieve these goals, controlled release devices must include two key characteristics. First, release, of course, would be required to be of a longer duration than normal. Second, however long the duration is, effectiveness is lowered if the drug has to travel through the body to reach the desired site. Thus, the device needs to be capable of targeted delivery, meaning that the drug is

actively delivered to the site or the drug is passively carried and then becomes active once the site is reached [5, 11, 14].

To categorize controlled release, there are three main descriptive characteristics: release mechanism, targeting method, and delivery route. Release mechanism refers to the mechanical or chemical method of drug release from the device. Mechanisms can include mechanical or osmotic pumps as well as polymeric systems controlled by degradation or diffusion [15]. Targeting methods are the ways that the device is capable of responding to the environment and then allowing release to occur only if that environment or physiological condition is the desired one. These methods include chemical manipulation of the drug, a delivery system that is modified to allow for recognition of environment, and systems that respond to change in temperature, pH, or salinity [14]. Finally, the delivery route refers to the area of the body that the device is located. Injection and oral are still the most prevalent among controlled release, but other types studied are transdermal, buccal, rectal, nasal, pulmonary, ocular, and implantable [14].

Mechanisms

Currently, there are three main mechanisms that are utilized in studies concerning controlled release systems: pumps, degradation of monoliths or films, and diffusion from a monolith or through a film. Of the three categories, pump-based systems are the only systems that absolutely require both surgical implantation and removal. There are two main types within the broader pumps category: mechanical and osmotic. Mechanical pumps are much more common. They are composed of either electrically driven pumps, meaning that the pump is
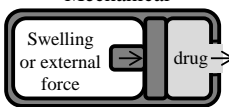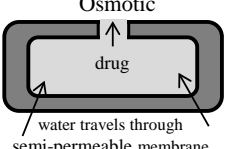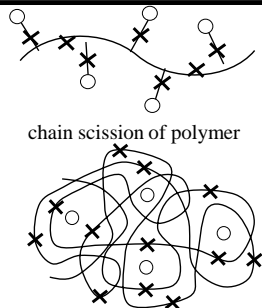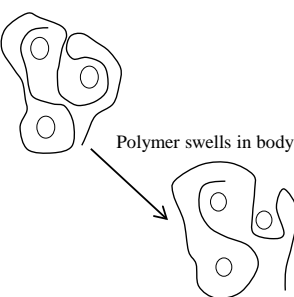
outside the body and drugs are pumped through a catheter into the body, or implanted and based on swelling of a material on one side of a movable membrane. The drug is located on the other side of the membrane and is pushed out when the membrane flexes. Osmotic pumps, on the other hand, are becoming more popular and are much more typically implanted. They are designed with a polymeric membrane surrounding a water-soluble drug. This polymeric membrane is permeable, as water permeates the membrane. Hydrostatic pressure begins to force the drug out and into the body [2, 9, 15]. Osmotic pumps have actually been proven capable of extended release for many days and are popular for the dispense of pain relievers in non-hospitalized patients [16]. Unfortunately, even the smallest osmotic pump is still large when compared to currently researched nanoscale release systems [17]. The main advantage of pump-based systems is that the outlet of the pump can be located right next to the target location in the body, making it a very beneficial type of release when high-side-effect medications are utilized, such as chemotherapy, or when dosing depends on body conditions mandating a dose, such as the release of heparin or insulin to the system [15]. The main disadvantage is the necessity of both surgical implantation and removal.

Another mechanism utilized in controlled release is degradation of polymers. The vision of being able to introduce a delivery vehicle to the body, have it release the drug controllably, and then have the now useless vehicle slowly degrade away harmlessly is very attractive to the medical field. This degradation mechanism can occur multiple ways. Bulk degradation occurs when the entire structure begins to degrade virtually at the same time, both the inside and the surface [18]. This results in relatively quick releases. A notable polymer of this category used for controlled release is poly(lactic-co-glycolic acid), or PLGA. Hydrolysis of the ester links

6

throughout the polymer chain causes the structure to degrade at roughly the same rate throughout the polymer. Typically, these types of structures are designed to self-catalyze their own degradation, meaning that as degradation occurs, the cleaved sections enhance the degradation of the rest of the system [19-20]. The other and more desirable type of degradation is called surface erosion. In this case, the polymer's hydrophobic nature causes water to only attack the surface of the polymer, not allowing water to penetrate inside the device. Zero-order release and more complex release profiles are possible with this type of degradation [19]. Common polymers of this type of degradation include polyanhydrides and poly(ortho esters). Poly(ortho esters) are commonly modified by the addition of basic or acidic components. These act to increase or decrease the rate of degradation, thus increasing or decreasing the release of the drug [19, 21]. A key parameter for all degradation-based release structures is that the polymer and degradation products be non-toxic. Thus, there is no need for surgical removal, although there might still be a need for surgical implantation. To utilize degradation for controlled release, the drug can be incorporated into the polymer by one of two ways. One way involves the physical mixing of the drug with the polymer of choice. The polymer would necessarily need to be in a solvated state. Another involves the chemical bonding of the drug to the polymer chain. This provides a more stable and protective method due to a higher degree of difficulty in breaking the connective bonds through metabolic processes. To induce release of the drug, the polymer backbone or bond holding the drug to the polymer will be cleaved by hydrolysis or enzymatic reactions [9, 15]. This leaves the drug to disperse into the body. A key issue with this method of drug release, however, is that all systems degrade differently, depending on the polymer used and the area of the body that the

system is located in. In addition, some systems will degrade more by bulk degradation than by the more desired surface degradation.

Table I-1. Primary mechanisms of controlled release. Reprinted with permission from [8], Ward, C.J., M. DeWitt and E.W. Davis, Halloysite Nanoclay for Controlled Release Applications, in *Nanomaterials for Biomedicine*. 2012, American Chemical Society. p. 209-238. Copyright 2012 American Chemical Society.

	Introduction	Release	Removal
Pumps	surgical implantation	Mechanical Swelling or external force → drug → Osmotic drug water travels through semi-permeable membrane	surgical removal necessary
Degradation	all sites of administration except ocular and transdermal	chain scission of polymer	no further removal; scission products must be non-toxic
Diffusion	All sites of administration	Polymer swells in body	surgical removal may be required

Diffusion-based systems are significantly different from degradation-based systems in mechanism as well as application. In mechanism, aqueous fluid diffuses into the polymer matrix, but does not cause cleavage of chemical bonds. Two main types exist: i) transport of

the drug takes place through molecular diffusion through the chains of the polymer without fluid penetration, and ii) fluids penetrate the matrix, swelling the material, and diffusion of the drug occurs as a result of micropore formation [2, 9, 15, 22-23]. The important difference is that release is controlled through solubility of the drug in the fluid for the second case, instead of diffusion through the polymer.

Targeting Methods

In controlled release studies, there are two broad targeting methods. Each encompasses many subcategories of targeting. The first method involves the modification of a drug, making it inactive before introduction to the body. Once reaching the desired site, the drug is then reactivated by a controllable transformation [14, 24]. For example, Prodrugs are introduced into the body and then activated by a secondary compound that is introduced when the prodrug has reached the area [25]. Unfortunately, this can be a very difficult process to design. To counteract this disadvantage, this method was modified. This modification involves the use of a chemical transformation during the entire route through the body. Along the route through the body, predictable, chemical transformations take place due to physiological conditions. Once the desired site is reached, the predicted number of transformations has taken place and the drug is once again active to treat the site [14].

The second broad method of targeting uses a carrier to protect the drug during transport through the body. Once the carrier reaches the delivery site, the drug is released through a variety of mechanisms. Carriers can include macromolecules, microspheres, and nanoparticles [14]. Directed release, called location targeting, from these carriers can be activated in several

ways. Temperature gradients can be used with intentional inflammation at the active site. Additionally, magnetic particles can be utilized either in the carrier or as the carrier, after which a magnetic field can hold the carrier at the afflicted site for the duration of the release. Passive targeting can be used as well, in which microsphere size is used to target specific areas. The microspheres will lodge in different sized capillaries to release drug. The designed size of the microsphere will ultimately fit in the desired size capillary [14, 26]. This can be taken one step further with nanospheres. These can actually lodge in the pores of specific cells. Drug carriers are being researched that will penetrate cancer tumors and then lodge specifically in the cells to release the medication [26].
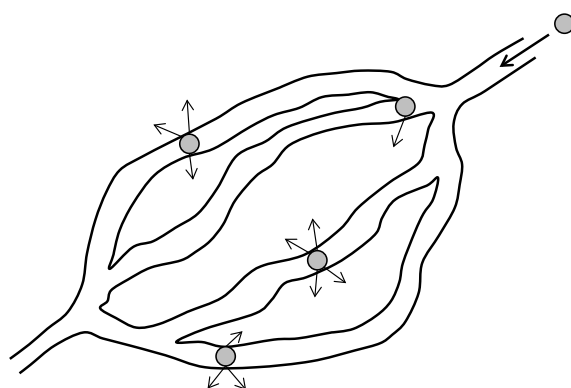
Figure I-2. Drug targeting achieved through size of micro (or nano) particles. Particles are lodged into the capillaries and begin to release. Reprinted with permission from [8], Ward, C.J., M. DeWitt and E.W. Davis, Halloysite Nanoclay for Controlled Release Applications, in *Nanomaterials for Biomedicine*. 2012, American Chemical Society. p. 209-238. Copyright 2012 American Chemical Society.

Delivery Routes

Delivery route is the third descriptive characteristic of controlled release. There are many different routes, including buccal, sublingual, transdermal, injection, and oral. Under study, however, are devices that utilize controlled delivery to improve release in other routes, such as ocular, implantable, nasal, and pulmonary. All release routes are summarized in Table I-2.

Buccal and sublingual routes are commonly described together. Buccal refers to the route where drugs are administered between the cheek and gums, while sublingual refers to the route where drugs are administered under the tongue. Compared to the oral route, these two routes are much more effective because medication enters directly into general circulation through the jugular vein, bypassing the digestive system [5, 11, 14]. Due to the sensitivity of this route, however, drug release is short acting, excluding many types of controlled release. Some saliva-activated adhesive structures have proven to be effective, however [14, 22], and nitroglycerine tablets for angina have been a commercial system of drug release for years.

Transdermal delivery also bypasses the digestive system. Delivery through the skin allows for access to the blood vessels under the dermis and hypodermis layers [5, 11, 14, 27]. Transdermal delivery also allows for the use of short-half-life drugs due to quick application as well as quick removal of the release agent if necessary. Perhaps the most important advantage is that patient compliance can be much higher with this method because it is the least invasive. Two types of systems are used for transdermal release: membrane-controlled or monolithic. The first involves the use of a reservoir that contains the drug. Once attached to the skin, slow diffusion occurs through a membrane into the epidermis. The second system is much simpler and only involves application directly to the skin, with no rate-determining properties [2, 5]. Controlled release systems already exist for this route: treatment of motion sickness with scopolamine [28], treatment of angina with nitroglycerine release [29], and smoking cessation patches that release decreasing amounts of nicotine [5]. There is also research underway in patches that will release small amounts of anesthesia for post-surgery pain or chronic conditions [5].

Table I-2. Drug administration routes, their key aspects, and experimental and commercial controlled release systems utilizing the route. Reprinted with permission from [8], Ward, C.J., M. DeWitt and E.W. Davis, Halloysite Nanoclay for Controlled Release Applications, in *Nanomaterials for Biomedicine*. 2012, American Chemical Society. p. 209-238. Copyright 2012 American Chemical Society.

Route	*Key Points*	*Experimental Systems*	*Commercial Systems*	*Reference*
Buccal and Sublingual	bypasses digestive process, enter the body through the jugular vein	saliva-activated adhesive systems	nitroglycerine tablets for angina	[5, 11, 14, 22]
Transdermal	large surface area for absorption, high barrier properties of epidermis	patch that releases anesthesia for pain relief	patches that release scopolamine, nitroglycerine, and nicotine	[5, 11, 27-30]
Ocular	protective actions of the eye make sustained release difficult	controlled release contact lenses		[5, 14, 31]
Implantable	requirement of surgery for implantation and sometimes removal	biodegradable polymer implants that release treatment for bone infections and bone growth	drug-eluting, biodegradable implants	[2, 32-33]
Injection	subcutaneous, intramuscular, and intravenous	hydrogels, microparticles, and polymers to release proteins and polypeptides	polymer nanoparticles to release prostate cancer drugs	[34-35]
Oral	small intestine most effective release site, difficult to travel through digestive process	flotation tablets, bioadhesive polymers	erodible tablets and capsules, natural polymer matrices that swell	[5, 9, 11]
Nasal	ease of deployment, sinus cavities have high absorption capability	mucoadhesive release of anti-Parkinson drugs		[5, 14]
Pulmonary	large absorption area in lungs	microspheres for the release of steroids	inhaled insulin-releasing treatment	[14, 36-37]

Injection is another very popular route for drug delivery. This includes subcutaneous, intramuscular, and most commonly, intravenous. Continuous injection into the body requires training and constant monitoring, thus making it a difficult prospect for patients to medicate themselves. As noted, however, progress has been made in developing controlled release systems that will lodge in certain areas of the body due to size restrictions. Large microspheres, typically larger than 25 microns, will be trapped very quickly and release at the area of injection, while some smaller particles may be able to reach all the way to the lungs through the circulatory system [5, 14]. Once again, time to the desired site is faster than the oral route due to direct introduction into the circulatory system [38].

The most common drug delivery route is oral. The main disadvantage of the oral route is that the drug has to make it through the gastrointestinal system. The main absorption into the body is in the small intestines, past the stomach. Travel to and through the small intestines takes upwards of three hours, a length of time too short for most controlled release systems. To overcome this liability, studies have examined how to extend this release utilizing flotation tablets that resist gastric emptying, bioadhesive polymers that attach to the intestinal walls, and drugs that will slow intestinal motility. Most medical personnel are generally hesitant to use these drugs, however [5, 11].

Of the non-traditional drug delivery routes, ocular is the most interesting and promising. Medication has been administered in eye drops for years. They are applied topically to the eye in high concentration due to cleansing mechanisms of the eye. These high concentrations can cause problems, so controlled release methods are needed. Contact lenses have shown great

promise in being that controlled release method [39]. The cleansing methods of the eye are still an issue in keeping the medication in the eye, but since the drug releasing structure is now solid and cannot be washed away, controlled release can be used [31].

The implantable delivery route is the route most often studied for controlled release. Studies have demonstrated that release, when the device is surgically implanted into the body, can occur for more than 30 days [16]. Normally, polymeric release devices are used, with release occurring through the previously described degradation or diffusion mechanisms. Many research groups are experimenting with biodegradable implants, to limit trauma to the body. A few examples of this type of implant include an implant composed of polyhydroxyalkanoate to release antibiotics [32] and a scaffold composed of poly-(di-lactide/glycolide) to release bone growth osteotropic factors [33].

Nasal delivery routes are already being utilized for some drug sprays, but controlled release devices are only under study. It is a very desirable route, due to its ease of deployment and noninvasive nature, as well as the sinus cavities' high absorption capability. The drawback, however, is that the particles that release drugs need to be large enough to ensure that the particles do not pass through the sinuses and then into the lungs [5, 40]. The problems that still exist with this method are reproducibility and uncertainties dealing with mucus interaction.

The problem with the pulmonary route is that there is major loss of drug via the mouth and then to the stomach. While the absorption area in the lungs is huge, because of the loss in the mouth, large quantities of medication have to be delivered. To solve this problem, more study

is required to determine how to make certain that the drug reaches the lungs and then attaches to the walls of the lungs, most likely with aerosol or nebulizer delivery [14].

Current studies in literature concentrate on the controlled release of compounds mainly via the implantable route. The controlled release studies in the following chapters were designed with this type of release in mind. Controlled release systems composed of nanoparticles and polymeric matrices are focused upon. The first study deals with naturally-formed nanoclays and poly(methyl methacrylate). Nanoclays are described in the following sections as a controlled release possibility of increasing popularity. The second study involves the creation of a possible controlled release system composed of gold nanoparticles and shape memory polyurethane. This system is specifically examined for its potential to act as a remotely-activated controlled release system.

NANOPARTICLES FOR CONTROLLED RELEASE

There has always been a pressure to make drug delivery systems smaller, stronger, and less frequent. The addition of nanoparticles to make nanoscale systems has been shown to be very effective in achieving these goals. In addition, these systems are capable of encapsulating the drug to increase solubility, allowing for quicker release due to increased specific surface area, and yet can be designed for sustained releases longer than traditional methods [41]. One of the more important advantages of using nanotechnology in controlled release is for the possibility of targeting the release. Depending on the type of release and application of release, there are multiple types of nanoparticles that can be utilized. Some of the more popular categories

include lipid-based nanoparticles, polymer-based nanoparticles, dendritic materials, metallic nanoparticles, and nanoclays.

Lipids can form very similar structures to polymeric micelles that are called liposomes. Bilayers are created whereas the heads surround and protect the drug and interact with the aqueous solution to create a stable structure [42]. In addition, depending on the nature of the drug, a single layer can be formed with the hydrophobic end protecting the drug [19, 41, 43-44]. Even though the size of these particles can be relatively small, roughly from 20 to 500 nm [45], the inherent problems that can make the addition of liposomes to release systems difficult are that the lipoproteins inside the body react with liposomes. Thus, a high enough concentration of liposomes needs to be introduced, leading to difficulties in application as well as cost [41-42, 44, 46].

Polymeric nanoparticles are becoming very popular in the controlled release field. Block copolymers form very similar structures to liposomes. One block of the copolymer is hydrophobic while the other is hydrophilic. In addition, the benefit of using block copolymers over liposomes is the possibility of crosslinking the polymer to provide extra stability, thus increasing time before degradation and increasing release time. Unfortunately, a drawback of this method is that only hydrophobic drugs can be used, as bilayers cannot be formed [44]. Common polymers for the hydrophobic block include poly(ortho esters), while polyethylene oxide is the common polymer for the hydrophilic block. This type of system has been shown to be very effective for tumor treatment, as polymer micelles have been shown to accumulate in tumor tissues due to their colloidal nature [43]. A new micelle system using amphiphilic

poly(N-isopropylacrylamide) (PNIPAM) has used this property to incorporate anti-tumor drugs for treatment [41, 47].

Another class of polymer-based nanoparticles is dendrimers. These polymers are created by repetitive synthesis reactions to create three-dimensional structures. The structures can be synthesized very small, as low as three nanometers [48]. The key for this structure is that it can entrap the drug compounds. In addition, the branches of the structure can be "grown" outward (divergent) to trap the drug in the branches, or inward (convergent) to entrap the drug in the center. Lending feasibility for drug release in different circumstances, this complex structure can be created from many different polymers, allowing for design complexity [42-44]. A great example of this type of carrier is the delivery of 5-flourouracil, an anti-tumor treatment. It is very toxic, thus damaging en-route to the body. Poly(amido amine) dendrimers are capable of conjugating with the treatment, protecting the body from its toxic effects until the tumor is reached [43, 49].

a)

20 − 500 nm

b)

50 - 150 nm

c)

≥ 3 nm
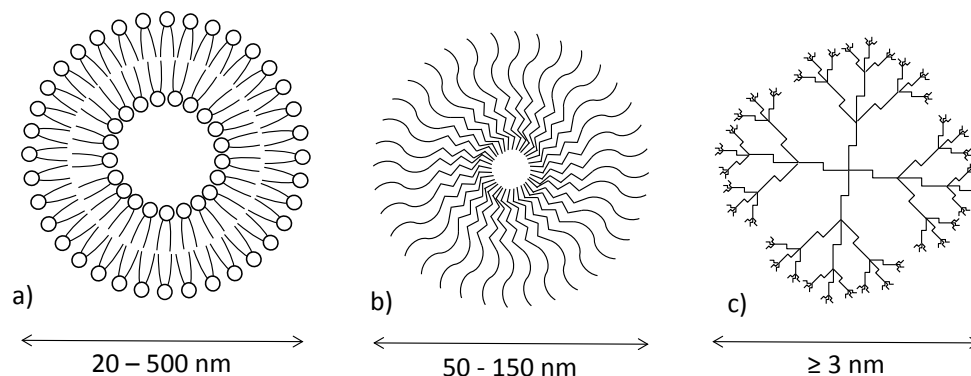
Figure I-3. a) Liposome composed of a bilayer of hydrophilic (circles) and hydrophilic tails (lines), b) Polymeric micelle composed of a diblock polymer with hydrophobic sections towards the inside (zigzag lines) and hydrophobic sections towards the outside (curved lines), c) Dendrimer with branches capable of trapping desired compounds . Reprinted with permission from [8], Ward, C.J., M. DeWitt and E.W. Davis, Halloysite Nanoclay for Controlled Release Applications, in *Nanomaterials for Biomedicine*. 2012, American Chemical Society. p. 209-238. Copyright 2012 American Chemical Society.

Another two categories of nanoparticles include nanoclays and metallic nanoparticles. Nanoclays are mined nanoparticles with natural origins, with a wide array of compositions, properties, and availability. They are currently used and studied for many different applications. Metallic nanoparticles are not quite as common and are used more for their usefulness in targeting and tracking [42-43]. Both types of nanoparticles are utilized in this research and are explained fully in subsequent sections.

Nanoclays

Nanoclays are a relatively new branch of nanomaterials that have found a wide array of popularity due to their abundance and low costs. In addition, they have been found to have many different applications for use as nanomaterials. There are four basic groups available: kaolinites, smectites, illites, and chlorites [50]. For controlled release applications, however, smectites are mainly used, due to their layered composition of tetrahedral sheets of silica fused to an octahedral sheet of alumina [51]. The nanoclays belonging to this group include montmorillonite, laponite, halloysite, hectorite, beidillite, nanotronite, and saponite. Previous studies with these materials have shown that incorporation into polymer structures can affect changes in polymer properties of tensile strength, bending strength, modulus [52], rheological properties [51, 53], diffusion rates [54], and reduced thermal transfer [55]. In addition, reduced thermal expansion coefficients and absorption properties have been documented [56-57].

Montmorillonite was the first nanoclay studied for its use in controlled release. Formed through the reaction of certain volcanic ash with water and magnesium, montmorillonite consists of a stacked array of sheets, two of silica and one of alumina [50-52]. The interstitial

space between the layers is capable of being loaded with drug. The ionic nature of the silica layers provides a high enough cation exchange capacity to bind the layers of the montmorillonite to the drug ionically. During loading, the separation between layers increases, an action called intercalation, allowing for more drug to be loaded. Research groups have experimented with using montmorillonite to release drugs such as ibuprofen, 5-flourouracil, promethazine chloride, buformin hydrochloride, sertraline, timilol meleate, and tetracycline hydrochloride [58].

Recently, however, nanocylinders have been gaining attention due to their ability to capture and hold materials within the lumen of their tubes. Halloysite is one such material that is extensively studied for controlled release.

Halloysite

Halloysite is a type of nanoclay that is naturally found in nanocylinder formation. While the composition is similar to montmorillonite, halloysite is actually only composed of two layers, one of silica and one of alumina, with the chemical formula ($Al_2Si_2O_5(OH)_4$ x nH_2O). Most often, these two layers are found rolled, creating a tube-like structure of concentric layers [46, 59-65]. The tubes can vary in length from 500 to 1000 nanometers, with the diameter ranging from 15 to 300 nanometers [62-63, 65]. Figure I-4 shows an SEM picture as well as a diagram of the layers of halloysite.
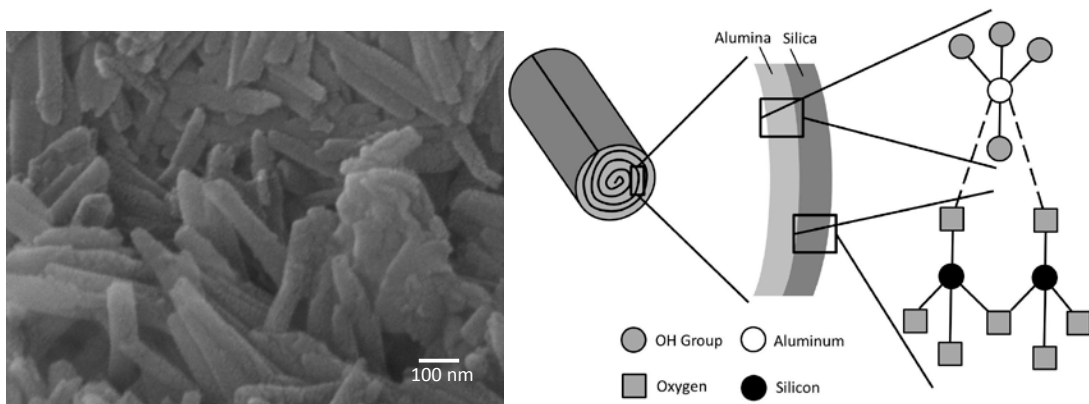
Figure I-4. SEM of halloysite nanotubes at 100K magnification and schematic of halloysite structural hierarchy. The alumina layer is on the concave side of the rolled sheet. The silica layer is located on the convex surface. These layers are bound together through a layer of oxygen. The outer surface of the twinned layers is covered with charged oxygen and hydroxyl groups that allow for binding of adsorbed species. Reprinted with permission from [8], Ward, C.J., M. DeWitt and E.W. Davis, Halloysite Nanoclay for Controlled Release Applications, in *Nanomaterials for Biomedicine*. 2012, American Chemical Society. p. 209-238. Copyright 2012 American Chemical Society.

Several theories exist as to why the layers roll. One contends that as the alumina and silicate layers are weathered, the layers of hydration cause a packing disorder which is relieved when the layers roll [60, 62-64]. Another theory states that unbound hydroxide groups on the alumina side will cause instability versus the oxygen backbone on the silica side. The layers will roll to create a more stable form. Halloysite has been studied for various applications over the years. These applications include catalysis for petroleum cracking, nanoreactors to fabricate nanowires and nanoparticles, and absorption of materials such as dyes, stains, chemicals, and pollutants [59]. In addition to these applications, like montmorillonite, halloysite can be loaded with drugs. It also has a high cation exchange capacity so that the drug can bind to the surface of the tubes. Unlike montmorillonite, however, drug can also be bound to the inside of the lumen via the hydroxyl functional groups.

Controlled release of a variety of compounds has been studied. Paint additives, pesticides, herbicides, lubricants, and cosmetics are capable of being loaded into halloysite and then released [59]. A great example of this type of release is anti-corrosion additives found in some paints. Halloysite carriers are loaded with benzotriazole, included in paint, and then applied [59, 64, 66-68]. This will extend the life of the coating, reducing the amount of reapplications needed. Similarly, bioprotection agents, such as iodobutlypropyl carbonate, have been loaded and released to combat marine fouling [59, 62].

CONTROLLED RELEASE FROM HALLOYSITE

The release of pharmaceutical compounds from halloysite has become the main focus of research. The first study concerning this issue was performed with tetracycline hydrochloride, a hydrophilic drug, and khellin, a hydrophobic vasodilator [69]. Release of tetracycline occurred over the course of ten hours, while the release for khellin had a duration of a week. Other drugs have since been evaluated, including diltiazem hydrochloride, propranolol hydrochloride, nifedipine, furosemide, and dexamethasone [63, 70-72]. Studies have also been performed on extending the release from halloysite utilizing polymer, chitosan, and gelatin. Using a layer-by-layer approach, release rates were shown to be reduced by 75% [70]. In addition, coating of diltiazem chloride and propranolol hydrochloride by chitosan significantly delayed release as well as a reduced the burst, the rapid initial release common with several nanoparticle-based systems [72]. One study that utilizes a polymer and halloysite for a specific application is a study involving the use of polyethylene glycol-coated halloysite to treat canine periodontitis. Once injected into the mouth, the liquid gel solidifies. The release was shown to last on the order of several days to several weeks [71].

Drug release from halloysite occurs multiple ways. Due to halloysite's tubular nature, the drug can be loaded one of three places: on the surface of the tubes, inside the lumen of the tubes, and crystallized between the tubes. Release occurs through a combination of diffusion along the tube and ionic desorption from the inner wall of the tube. The initial burst, mentioned before, corresponds to rapid release of the crystallized drug between the tubes. Throughout literature, there exists major variations in release duration and amount, depending on what study is being examined and what drug is released. For example, tetracycline has been shown to have a release time up to 37 hours, with a very high release percentage [71]. Nifedipine, furosemide, and dexamethasone demonstrate release percentages of greater than 70%, with very low burst percentages [62-63, 73]. Another drug, khellin, has been shown to release for very long periods of time, up to 195 hours [69]. The differences between releases can be explained by differences in solubility, surface interaction with the halloysite, diffusion rates, and charge of the molecules.

Table I-3. Initial burst amounts, time of full release, and extent of release for pharmaceutical compounds utilized in controlled release studies. Reprinted with permission from [8], Ward, C.J., M. DeWitt and E.W. Davis, Halloysite Nanoclay for Controlled Release Applications, in *Nanomaterials for Biomedicine*. 2012, American Chemical Society. p. 209-238. Copyright 2012 American Chemical Society.

Drug	Initial Burst (%)	Time of Release (hrs.)	Extent of Release (%)	Reference
tetracycline hydrochloride – two loadings	27 - 41	2.3 - 37	75 - 95	(87, 88)
tetracycline hydrochloride – three loadings	12 - 57	2 – 10	75 - 80	(85, 88)
tetracycline hydrochloride – four loadings	69	1.3	75	(88)
propranolol hydrochloride	27	>8	>90	(86)
diltiazem hydrochloride	98	0.6	100	(86)
nifedipine	6	>5	>70	(73, 74, 89)
furosemide	10	>5	>70	(73, 74, 89)
dexamethasone	8	>5	>70	(73, 74, 89)
khellin	1	195	10	(85)
nicotinamide adenine dinucleotide	20	6	87	(85)

Finally, brief studies have been performed on release from halloysite through a rate-slowing polymer film. Ward et al. experimented with degradable poly(vinyl alcohol) films. Results indicate that release is slowed dramatically with the initial burst eliminated [74]. In addition, montmorillonite is utilized with the same system. Release results are compared between the two systems, with and without montmorillonite. It is shown that the addition of montmorillonite to the polymer creates a longer release when compared to a system with halloysite. The possible explanation is an extra tortuous pathway for release diffusion of the drug. When release is studied for just pure halloysite and montmorillonite, however, release

for both is very similar, meaning that the tortuous pathway only has an effect when the montmorillonite is incorporated into the polymer.

Currently, controlled release studies from halloysite mainly focus on release straight from the nanotubes. While this does result in short controlled release profiles, longer duration times are usually required. Thus, fewer studies extended their scope and began examining the encapsulation of these nanotubes in polymeric materials to extend release. In most studies, this encapsulation dealt with shell-type encapsulation, such as the chitosan shells described earlier. The studies performed in the following chapters include a study incorporating the halloysite in polymeric films for increased release duration. These films mimic a type of drug release device that would utilize monolithic structures and the previously described degradation and diffusion mechanisms. In addition, the properties of the release compound are rarely studied. Depending on the various properties, effects on the controlled release behavior can be apparent. Thus, studies are performed that examine how compound properties, such as molecular size, charge, and solubility, affect release from pure halloysite.

METALLIC NANOPARTICLES

Nanoparticles are defined as particles that have of at least one dimension less than 100 nm. The importance of this for metallic nanoparticles lies with the fact that the mean free path of electrons on the surface of metals in standard conditions is generally about 10 to 100 nm [75-78]. Once the size of the metallic nanoparticle reaches these low values, surface effects predominate. Because of larger relative surface areas, the interaction potential of the nanoparticles over that of the bulk material is increased and there is much higher interfacial

interaction. Due to the high relative surface area, transition metal nanoparticles are used in nanocatalysis [77]. In noble metals, the decrease in size of the nanoparticles results in resonant photons and surface plasmon resonance. This surface plasmon resonance occurs when an increase in the wavelength of light is shone on the nanoparticle, dramatically amplifying its effect. This type of result can be very useful in certain areas such as fluorescence, Rayleigh scattering, and RAMAN scattering, making noble nanoparticles attractive in fields such as optical detection and imaging [75, 79-85]. Indeed, one of the main reasons that metallic nanoparticles are so interesting is that these optical properties are so strongly dependent upon shape and size. The interaction between the conduction electrons and the incident radiation leads to significant, characteristic absorption in the ultraviolet, visible, and near-infrared spectrum [76-78, 82, 86]. When in the visible spectrum, unusually bright colors that are extremely dependent on particle dimensions are observed. This phenomenon is not observed in the bulk material. Control over the shape and size of metallic nanoparticles is a key factor for their potential use in these applications. The surface plasmon resonance, a key parameter in this research, is very dependent on the shape and size.

The characteristic of surface plasmon resonance, the most important aspect of metallic nanoparticles for this research, is a result of electron interaction with light. With the oscillation of the electromagnetic field at a resonant frequency of light, electrons in the conduction bands in metallic nanoparticles begin to oscillate as well [79, 83, 87]. The oscillation forces the electron away from the metallic core. In turn, forces restrict this movement and draw the electrons back. This creates an even higher oscillation than what was originally imparted. The resulting absorption of light is very distinct and can be observed by such simple

characterizations such as UV-vis-NIR. Naturally, this absorption is dependent on many characteristics of the nanoparticle, such as size, shape, structure, and even surrounding medium [79-80, 83, 87]. Metallic nanospheres consistently absorb in the visible region, while other shapes and configurations show results in the UV or even near IR regions. While nanospheres will only exhibit one peak, meaning one plasmon band, nanorods will exhibit two [75, 83, 86]. This arises from the two main dimensions of the nanorod. The first plasmon band is called the transverse plasmon band, corresponding to the absorption and light scattering along the diameter of the rod. This band will compare to the same plasmon band of metallic nanospheres of a similar diameter. The second plasmon band of metallic nanorods corresponds to the absorption and light scattering along the length of the nanorod and is called the longitudinal plasmon band. This peak under UV-vis-NIR examination will be able to shift to lower or higher wavelengths, unlike the peak of the transverse plasmon band. This shift to lower or higher wavelengths depends mainly on the aspect ratio of the nanorod, or the length-to-diameter ratio. The higher this ratio, the higher wavelength of the longitudinal plasmon band absorption.

Of large importance to this research is the ability of metallic nanorods to absorb the incident light and transfer that energy to heat. This is called the photothermal effect. Essentially, the conduction band electrons, excited from the surface plasmon resonance, decay to the ground state. The excess energy is released in the form of heat [88-89]. Interestingly, depending on multiple factors such as laser power, irradiation time, and nanorod concentration under the laser, temperature increases in aqueous solutions have been documented from about 10°C to as much as 1000°C [90-91].
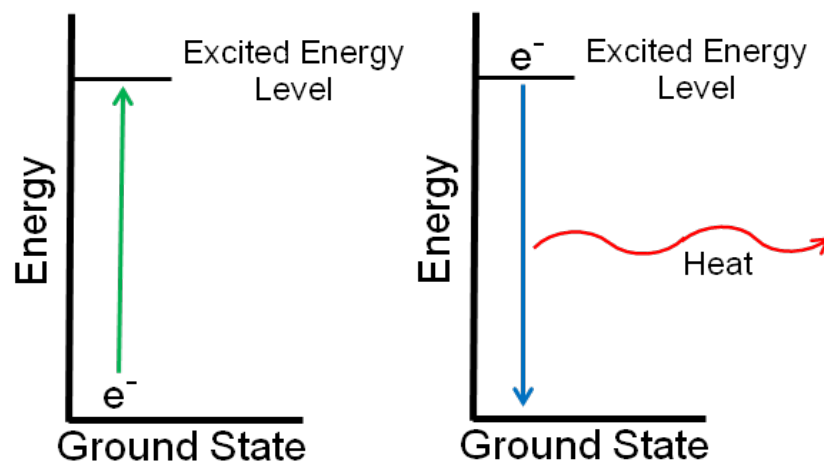
Figure I-5. Representation of the photothermal effect.

There are a few applications that already use this effect in the medical field. Many researchers are examining the possibility of utilizing the photothermal heating of nanoparticles for drug release capabilities as well as the more prominent therapeutic uses. It has been shown that even small changes in temperature can cause lasting damage to pathogens, cancer cells, and even tumor tissues [92]. With the photothermal effect, these temperature changes can be created in localized areas, allowing for very specific treatment.

The metallic nanoparticles used in the following chapters are gold nanorods. They will be used for their photothermal properties and their viability to be used as a trigger in shape memory behavior.

GOLD NANORODS

While all noble metallic nanoparticles exhibit the surface plasmon resonance to some degree or another, gold nanoparticles are the best characterized. In general, nanorods are defined as

having an aspect ratio between one and about twenty-five, while any larger, the particles are defined as nanowires [83]. In addition to having several beneficial properties and possible applications, there are a variety of methods for synthesizing the gold nanorods. Possible applications include uses in fields such as medical, electronic, aerospace, and even fashion. What makes gold nanorods more suited to these applications than other materials are their tailorable properties. Gold nanorods have been demonstrated to be producible with a broader range of properties of interest, meaning an easier ability to tune these properties to the right values.

Synthesis

Of the myriad of synthesis techniques for gold nanorods, the template method, electrochemical method, and seed-mediated method are by far the most common [76, 82, 93]. Even within these three, however, seed-mediated growth of gold nanorods is considered the foremost method, due to its extreme ease of tailoring the nanorods for specific applications and properties. The template method is top-down synthesis, as the gold is grown on a nanoporous template.   Both electrochemical and seed-mediated are considered bottom-up, with electrochemical occurring through the dissolution of gold plates and deposition on or near a platinum plate. Seed-mediated growth involves the combination of reagents to effect the growth of nanorods inside soft rod-like micelles to prevent agglomeration of rods. The template and electrochemical methods are introduced in the next sections. The seed-mediated approach, however, is introduced in a later major section, due to the extreme breadth of introduction and eventual choice as experimental technique.

Template Method

One of the initial techniques for creating gold nanorods is named the template method. It is so named because a nanoporous template is used, within which the gold nanorods are grown. The template can then be removed and the nanorods utilized [77, 94-96]. This theoretically simple method became the initial technique of examining gold nanorods of various aspect ratios and their properties and characteristics. Initially, this method was developed to create microscopic electrodes of conducting metals on the surface of polymeric substrates. It was noticed, however, that upon the usage of various sizes of nanopores within the template, the color of the resulting composite was changed [96-97]. Later, it was discovered that the nanorods could be removed from the template and dispersed within water or solvents, creating more useful nanorod solutions.

To create the nanorods, a conductive layer is sputtered onto a typically alumina template membrane. This conductivity gives the foundation for electrodeposition. Gold is then deposited within the pores of the alumina, onto the conductive base. Once the nanorods are fully grown, the conductive material and alumina template are selectively dissolved, with some type of stabilizer to keep the nanorods separate. Finally, the nanorods are dispersed in either water or a solvent by sonication or agitation [98-99].

The alumina template is the source of both the control of growth and this method's main limitation. Because the nanorods are grown within the nanopores of the template, the diameter and length of the nanorods can be controlled by increasing the diameter and depth of the nanopores [77, 100-101]. Additionally, length of the nanorods can be controlled by the amount

29

of gold deposited during the process [102]. Because this technique involves the use of a template, the growth is necessarily only on a monolayer. Thus, the yield is extremely low and time-consuming [103].

Electrochemical Method

The electrochemical method is more complicated and also less understood. It does provide for a higher yield of nanorods, however. Typically, this method consists of the two electrodes that are present in electrochemical setups [77, 103-105]. A gold metal plate exists as the sacrificial anode, while a platinum plate is the cathode. The solution that both plates are submerged in is a binary surfactant system. The first cationic surfactant is hexadecyltrimethylammonium (CTAB), which functions as both the electrolyte in the solution as well as the stabilizer to prevent the agglomeration of the nanorods. The secondary cationic surfactant is usually much more hydrophobic and present in a small amount. A typical surfactant is tetradecylammonium (TCAB). This surfactant serves as the rod-shaping agent, giving the CTAB micelles more structure. In addition, acetone and cyclohexane are incorporated into the system. The acetone serves to loosen the micellar framework of CTAB to allow incorporation of the smaller amounts of TCAB, while the cyclohexane plays a not completely understood role in enhancing rod-like shapes [106].

During the actual process, the gold anode is consumed, forming $AuBr_4^-$. The CTAB complexes with these anions and travels to the cathode. Here, reduction occurs and nanorods begin to form. One major drawback to this method is that the process of how rods begin to form is still not clear. It is not understood whether the rods nucleate on the cathode surface or

just above the surface inside the micelles [76-77]. Regardless, sonication is commonly needed to either shear the nanorods off of the cathode or shear them away from the cathode. A measure of control that can be added to the system can take the form of a silver plate behind the platinum plate. As will be discussed in more detail in the seed-mediated section, silver ions that are a result of the plate being present during electrolysis will result in a more controlled aspect ratio.

Characterization

One of the most common characterization methods for gold nanorods is transmission electron microscopy. This provides visible evidence that nanorods are produced, along with evidence that other shapes are present as well. In addition, qualitative analysis can be made toward the homogeneity of the size and characteristics of the rods produced.

As previously mentioned, the surface plasmon resonance results in visible absorption of light at specific wavelengths.   Gold nanospheres exhibit one peak in the visible region, most commonly near 500 nm.   The height of this peak is directly related to the amount of nanospheres present in the system. With nanorods, however, a second peak occurs, related to the longitudinal plasmon absorption. Because the diameter of the nanotube is comparable to that of nanospheres, the primary peak remains at around 500 nm. The location of the second absorption peak depends on the nanorod aspect ratio, which is controlled by many factors associated with rod production [80, 103, 107-108]. The larger the aspect ratio, the higher the absorption wavelength. In addition, as well, the larger the aspect ratio, the smaller the intensity [87].

Properties and Applications

Gold nanoparticles, and in particular rods, are so vastly studied and used because of their relative ease to create and functionalize. In addition, gold has been shown to be superior at carrying bio-active molecules as well as for its use in sensing applications, even more so than silver nanoparticles [80-81]. Also compared to silver nanorods, gold nanorods have been shown to have better tunable properties during synthesis, much stronger absorption characteristics, and easier surface functionalization [103]. Not to mention, gold has been show to be much more stable in oxidative environments.

Many of the applications of gold nanorods are within the optical field. This is not surprising due to the fact that optical properties of gold nanorods are the most prevalently studied and are what makes metallic nanoparticles, in particular, very interesting. Many are examining gold nanorods for their usefulness in sensing applications, where the nanorods will specially attach to certain areas or items within the body. It is then possible to detect the nanorods via processes such as dark field microscopy and even optical microscopy [109-111]. Nanorods are modified to be attracted to certain cancer cells. Upon attachment, color change is visible in contrast to the cancer cells and only the cancer cells. These cells are effectively surrounded by the tale-tell color of the nanorods.

Additionally, there are multiple medical uses that make use of gold nanorods' ability to absorb light and then release heat. Nanorods can be modified to preferentially bind to certain kinds of harmful cells. Upon binding and near infrared light being shined upon the body, these particles will produce heat, killing the harmful cell while still inside the body [109, 112-114]. Many

studies have already been performed in this area, resulting in the pulsed laser technique of inducing damage to harmful cells. Technically, all metallic nanoparticles will exhibit this effect, but gold nanorods have been proven to be better due to nanorods' more efficient ability to absorb radiation [115]. This photothermal heating is also useful in nanocomposites, where the heating of the nanoparticles by light will result in a heating of the matrix material. The result could include shape memory effects in shape memory polymers or even just general heating of the entire material, depending on the applications. In addition, this photothermal effect has been modified for use as drug-releasing technology as well. One route involves using the heat produced to cleave the bonds holding drugs to the nanorods [92, 116-117]. Another route is the use of a polymer that will contract or expand upon application of heat [116, 118-119]. Upon expansion, pores open, releasing the drug.

SEED-MEDIATED GROWTH OF GOLD NANORODS

Seed-mediated growth of gold nanorods involves the use of previously made spherical seeds to create monodisperse colloid particles. Initially, this technique was used to create spherical gold by which a weak reducing agent, typically hydroxylamine, reduces Au^{3+}. It was found, however, that while this process did result in nanospheres, it was difficult to selectively pick certain sizes, as the reducing agent reduced the gold too much and growth had already started by the time the seeds were added [120-122]. As a result, a wide range of sizes were produced. The next improvement involved citrate stabilization of the nanorods as well as testing different reducing agents to slow the growth. While this showed some success in limiting growth until the seed could be added, it was still found that the reducing agent needed to be added at a controlled rate to prevent full reduction of the gold [75, 77, 79, 123].

A much more controlled modification of the previous method was introduced by Murphy. This method utilizes seeds prepared with sodium borohydride and the growth of nanorods prepared by the use of ascorbic acid, a weaker reducing agent. In addition, the growth was now stabilized by surfactants. In the presence of these surfactants, the ascorbic acid was not capable of fully reducing the gold salt until the seed was added to the solution [75, 77, 79, 124-125]. This resulted in much more uniform sizes at higher yields. Additionally, Murphy et al. discovered that the addition of silver ions, in the form of silver nitrate, affects both yield and aspect ratio. These silver ions also affect mechanism of growth, making it necessary to discuss seed-mediated growth process as two categories: with and without silver nitrate [75, 108, 124, 126-127].

Seed-mediated growth was first performed without silver nitrate. Murphy created the multi-step process whereas spherical seed nanoparticles are first grown, stabilized by sodium nitrate and reduced by sodium borohydride [75, 127]. This seed solution is then added to a CTAB stabilized solution of aurochloric acid ($HAuCl_4$). The gold is then reduced to Au^I by the addition of ascorbic acid. Results were very promising, with yield as high as 90% and aspect ratio as high as around 20 [128]. The presence of silver nitrate in the growth solution, as was discovered later, provides for a better measure of control on the growth of the nanorods. Unfortunately, this additional measure of control results in a marked decrease in aspect ratio [75, 127].

Nikoobakht and El-Sayed implemented the use of CTAB in the seed solution in addition to its presence in the growth solution [86]. It was proven that with sodium citrate-capped seeds, a

large portion of the nanoparticles that were grown were not cylindrical. With CTAB present in the seed solution as well, these results could be significantly modified, with a new result of smaller side-product spherical particles [77, 108, 124].

Process Variation

Within the seed-mediated growth method of gold nanorods, the reagent concentrations and environmental conditions play an important role in the growth and final properties of the nanorods. With simple changes in these factors, significant changes develop. Many research groups have studied these effects, from the effects of micelle formation to the necessity of silver nitrate. Throughout the growth process, all factors seem to have been studied, with the exception of sodium borohydride.

The concentration of CTAB has been proven to be very important to the growth of nanorods. Although the critical micelle concentration for CTAB is much lower than 0.1 M, this concentration is very important to reach for the growth of nanorods [103]. It is believed that CTAB plays more than just a simple roll of being the rod-like template for growth. Interestingly, results have shown that there is a critical range for the CTAB concentration. At lower concentrations, nanorods begin to precipitate and are unable to be redispersed. On the other hand, concentrations of CTAB that are too high destabilize the nanotubes as well, even producing other shapes at the expense of rods [80, 82, 129-130].

The trend for differences in gold ion concentration is very interesting. As the concentration increases, then nanorods with higher aspect ratios can be produced. At a certain level, though,

aspect ratio begins to decrease, proving that there is a critical level that results in higher aspect ratio rods [86, 131].

Interestingly, it has been shown that with an increase in silver ion concentration, there is an increase in aspect ratio of the nanorods, to a certain point. Similar to gold ion levels, at a critical level, aspect ratio then begins to decrease again [79, 86]. In addition, silver ions raise the yield percent as well, mainly due to the fact that they inhibit growth of any other than rod-shaped particles [75, 82-83, 103, 132].

On the other hand, increasing amounts of ascorbic acid has been shown to reduce both rod length and yield. The reason for this has been has been attributed to quick reducing of the gold and very quick application of the reduced gold to the seed [131]. With this fast application, rod growth is not primary and multiple shapes occur. Additionally, it can be proven that addition of more ascorbic acid after rod growth is complete can lead toward increasing rod length [126]. The reason behind this is that there is still unreduced gold present in the system. Once reduced, more gold ions can deposit onto the nanorods. Care needs to be taken, however, that only the minimum amount of ascorbic acid is used initially. Too much ascorbic acid added in the beginning of growth has been shown to lead to many different shapes of nanoparticles due to the fast reduction of gold [129].

As the amount of seed added to the growth solution decreases, the aspect ratio will increase [131, 133]. This is logical due to the availability of growth sites. As the amount of gold stays the same and the number of growth sites decrease, there is more gold available per growth site,

resulting in longer nanorods. The diameter may increase as well, but as discussed in the growth mechanism section, growth preferentially occurs at the ends of the nanorods. Additionally, however, there are some results to suggest that, at first, when seed amount is increased, a slight increase in aspect ratio can be measured [79, 131, 133]. This can occur when the length decreases normally, but the diameter will decrease even quicker, forcing a slight increase in aspect ratio temporarily. Alternatively, some research suggests that with small amounts of seed, there is not enough seed to grow nanorods and instead, nucleation will occur on all facets of the seed, with larger seeds grown instead of nanorods [134].

With respect to seed age, it is sensibly wiser to use fresh seed in contrast to older seed. While the older seed has a more uniform size distribution, it also is much more capable of having developed shapes other than spheres. The fresh seeds, however, will nearly completely be spheres, which are proven to be more beneficial to rod growth [135].

Temperature has been shown to play an important factor in growth of the nanorods. It has been shown that with a lowering of the growth temperature, higher aspect nanorods can be formed [80, 107, 136-137]. Similarly, it was found that as the temperature is increased, then the aspect ratio of the nanorods decreases. In addition, it was discovered that at lower temperatures, a higher yield of nanorods was also obtained. A tentative explanation for this effect contends that at higher temperatures, CTAB has an increased tendency to associate with each other to form the micelles, but at lower levels of micelles available for nanorod growth. Another explanation explains that the additional heat helps to reduce extra gold after original growth has finished. The extra reduced gold then might preferentially attach to the outside of

the nanotubes, creating higher diameter rods of the same original length [126, 137]. The aspect ratio would then be lower.

Another possible control over nanorod growth is through the use of pH. Research has shown that pH does effect nanorod growth to some degree. Although it is still not quite understood why or even exactly how much pH effects growth, it was documented that different pH values will result in different yields of nanorods as well as multiple different variations in shape after growth [124]. Indeed, higher pH values have been shown to reduce the distribution of shapes, by eliminating triangular shapes [85]. It can be reasoned that pH can affect the stability of the CTAB micelles, thus reducing its capability of supporting nanorod growth.

While stirring of the seed and growth solutions upon combination of all reagents has always been a part of the procedure, it has recently been studied that this is absolutely necessary for the growth of higher aspect ratio rods. While stirring studies have not been performed on each step of the procedure, it was found necessary to stir both the seed solution and the growth solution in order to promote rods of higher wavelength absorption, meaning higher aspect ratios [81]. Thus, amount of stirring is one more way to be able to tune the properties of the nanorods.

Growth Mechanism

It is very important that the actual growth mechanism of gold nanorods be understood in order to understand how to control that growth. Unfortunately, much of the growth mechanism remains unclear, although there are certain theories that have garnered support. Due to the

overwhelming support for the seed-mediated growth method as well for the fact that this growth method is the one being proposed for this research, only the growth mechanism for seed-mediated growth will be explained in detail. Once again, however, there are two different explanations for the mechanism: one for without silver nitrate and one for with silver nitrate.

It has been proposed that the CTAB absorbs onto the gold nanorods in bilayers, meaning that cationic headgroups bind to the surface of the gold in the first monolayer and the tailgroups associating between the first and second monolayers [75, 77, 83, 138]. Because of this, it is supported that the headgroup of CTAB preferentially binds to the sides of the nanorods instead of the faces at the tip [125, 139]. Each wall of the nanotube is one of five of the pentahedral shape of the nanotube. Tests have been performed showing that length of the surfactant tail will substantially affect the length and yield of nanorod formation [75, 140]. As the tail grows longer, the van der Waals interactions between the tails grow larger. This allows for longer rod formation and higher yield due to the extra stability provided by these higher interactions. In rise of these theories, it was proposed that CTAB forms the micellar protection for the gold nanorods in a "zipper-like" fashion, shown in Figure I-6.
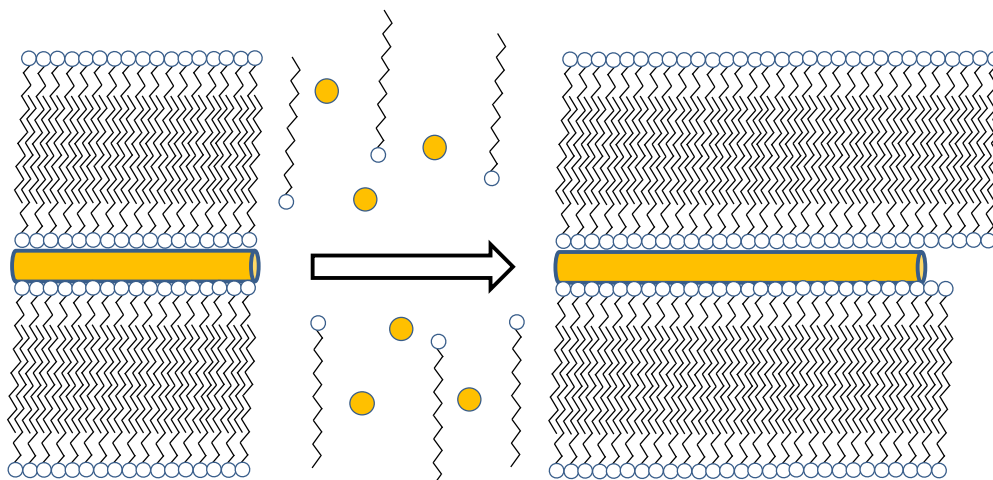
Figure I-6. The bilayer formation of CTAB (zigzag lines) on the nanorod (orange rectangle) as gold ions (orange circles) are introduced. This is the "zipper-like" formation.

This means that, as gold ions are attracted toward the growing nanorods, the CTAB attaches to these ions as they themselves attach to the nanorod. This grows the CTAB micelle as well as the gold nanorod [86, 108, 125, 138, 140-141].

The presence of silver nitrate in the growth solution results in a better measure of control on the growth of the nanorods. As mentioned before, this additional measure of control results in a decrease in aspect ratio. It is suspected, but not fully proven, that the silver ions from the silver nitrate combine with the loose bromine from the CTAB [83, 86, 103, 130]. The AgBr would then adsorb to the particle surface, inhibiting further growth. Originally, this process was thought to be more complicated due to the possibility of the silver reducing at the same time as the gold, but ascorbic acid is too weak to also reduce the silver [75, 84].

There has been a large amount of research on the seed-mediated growth of gold nanorods. Since it is described as a very straightforward method with high yield, many research groups utilize the method to create the nanorods needed for further experimentation. In addition, there

are studies that have examined how to control the properties of the nanorods by modifying the growth process. Studies have not been performed, however, with the intent on tailoring the dimensions of the nanorods by the modified growth process. This is necessary when utilizing the dimension-dependant plasmon properties for their eventual incorporation into shape memory polymers. Thus, the studies in the following chapter will examine how to modify reactant amounts and ratios in order to tailor nanorod aspect ratios to achieve specific sizes and plasmon absorbance properties.

SHAPE MEMORY POLYMERS

Shape memory polymers are one type of material in a broad category of smart materials. Essentially, they are a type of polymer that can be deformed from a permanent shape into a temporary shape. Due to some outside stimuli, usually heat, the shape can reform to the original. This happens as the polymer is heated past a critical temperature, often called the switching temperature [142-144]. Depending on the type of shape memory polymer, this temperature can be the melting or glass transition temperature. The common polymers that are capable of exhibiting shape memory response are polyurethanes [145-146], epoxies [147-148], polyethylenes [149], polyolefins [150], styrene-based polymers [151], and acrylate-based polymers [152]. They each have various advantages and disadvantages, although it has been shown that segmented polymers, especially polyurethanes, exhibit the most perceptible, and easiest to control, effects.

In contrast to shape memory alloys, which have been studied for much longer periods of time, shape memory polymers have become attractive recently due to the fact that they are easier to

process, have a much lower density, are cheaper to create, and have much larger possible strains [153-155]. Some shape memory polymers have been documented to have strains as high as 700% as compared to 10% for shape memory alloys [153, 156-157]. Unfortunately, however, there are also disadvantages toward using such a material. Because of the polymer's relatively low modulus, as compared to shape memory alloys, shape memory polymers exhibit low recovery forces, meaning that recovery is more difficult, depending on the application [153]. In addition, they have been shown to have longer recovery times, as well as a low number of repeatable strain and recovery cycles [158].

The actual mechanism of the shape memory effect may vary, but there is essentially one broad mechanism that all shape memory polymers follow [142-144]. These elastomeric polymers consist of two phases. One of the phases is responsible for the memory of the shape. This memory is held though either physical or chemical cross-links and keeps this phase rigid. The other phase is responsible for shape movement, or the reversible shape recovery. This is the phase where a thermal transition is reached, causing melting or movement. Passing this critical thermal transition, the lower transition phase, the one responsible for movement, will either move or melt, allowing for the rigid phase to resume its original configuration. This type of effect is utilized in shape memory polymers by deforming the entire polymer to a new shape. When the critical thermal transition is passed for the lower transition phase, the rigid phase is then allowed to move back to its original shape. Essentially, the original deformation is storing energy in the rigid phase that is then released when the thermal transition is reached. With shape memory alloys, this cycle of deformation and recovery can occur many times. With polymers, however, the number of achievable cycles is reduced and, while the deformed state

42

should be able to be held indefinitely, it has been found that most polymers will eventually deform to the original shape without heat application. This is mainly due to polymeric viscoelasticity [144].

There are many applications for shape memory polymers. These applications can include items such as the obvious heat-shrinkable films, tapes, and tubes [149], as well as temperature sensors [143], data recording devices for reversible data storage [143], and actuators [154-155], in which the polymeric devices can perform repeatable tasks with reversing temperature conditions. The medical field has also demonstrated beneficial applications as well, from self-tightening sutures and bandages [159], medical actuators [160-161], and even to smart stents that expand to fit any size blood vessel once placed inside the body [162-163]. In addition, shape memory polymers are quite capable of being utilized for controlled release of pharmaceutical compounds, with the initiation of heat, or the irradiation of near-infrared light.

Types

Researchers have used many ways to categorize shape memory polymers. Of the most general categorization, there are those that switch at the glass transition temperature or the melting temperature [164]. Some classify them according to how they are activated: thermal, light, electricity, solvent, pH, magnetic, etc [142]. Others group the polymers according to if they are physically cross-linked or chemically cross-linked [143, 164]. The most popular method of categorizing them is through their chemical structure. The four resulting categories are (i) chemically cross-linked glassy thermosets, (ii) chemically cross-linked semi-crystalline

rubbers, (iii) physically cross-linked amorphous thermoplastics, and (iv) physically cross-linked semi-crystalline block copolymers [143-144].

The first group, chemically cross-linked glassy thermosets, is the simplest type of shape memory polymers. Typically, the transition temperature is the glass transition of the lower transition phase. Because of the chemical cross-linking, this class of shape memory polymer shows excellent recovery [144]. In addition, tuning of the properties can occur with the varying of cross-link density. Unfortunately, however, because the cross-linking is permanent, hence being called a thermoset, once the polymer is synthesized and cured, there is no possibility for reshaping afterward. Also, because the glass transition temperature is generally utilized, the transition can be broader than if the melting temperature is used. This results in some slightly slower recovery responses [143].

The second group, chemically cross-linked semi-crystalline rubbers, utilizes the melting transition for recovery. This results in a sharper transition, thus resulting in quicker recovery times [143]. In addition, because this material utilizes the melting temperature, the polymer is more compliant and rubbery below the critical temperature, since it will most likely be above its glass transition. To tailor the recovery of this type of polymer, the degree of crystallinity is a changeable factor, of course still related to the degree of cross-linking. In fact, because the melting temperature is utilized, full crystallization will occur at lower temperature, allowing for a stronger deformation shape, or higher shape fixity while deformed [143-144].

The third category, physically cross-linked amorphous thermoplastics, is similar to the first in that glass the transition temperature is used as the critical temperature, but different in that there are no chemical cross-links. Because of this, there is some limited possibility to re-process these materials. Polymers in this class are typically phase-separated block copolymers, with soft phases that will respond by melting or reaching the rubbery plateau at the glass transition when the critical temperature is reached [144]. The hard, rigid crystalline or rigid amorphous phases will store the kinetic energy needed for shape recovery. Because even the hard phases still exhibit a lower transition due to physical cross-linking instead of chemical cross-linking, it is possible to process both phases above this second transition. Amorphous shape memory polyurethanes are a common polymer in this category.

The final group, physically cross-linked semi-crystalline block copolymers, is very similar to the previous group, with the difference that, due to the semi-crystalline regions, the melting temperature is exclusively used as the critical transition temperature. The soft segments of the polymer will crystallize at lower temperatures, once again allowing for high shape fixity [143]. As well, this type of polymer may be re-processable at higher temperatures. The segmented shape memory polyurethane used in this research falls into this category [143-144].

Among the most common category of thermally-induced shape-memory polymers, there are a few important classes. This is another way that shape memory polymers can be classified. The first group is a subset of the physically cross-linked shape memory polymers: linear block copolymers. Among the linear block copolymers are those where the critical transition temperature for shape memory transition is the melting temperature of one segment. These

include mainly polyurethanes, a topic discussed more thoroughly in the next section. Another inclusion into this category are polyesterethers, where poly(ε-caprolactone) acts as the soft segment and the melting temperature of it is the transition temperature [165-166]. Similar polymers to these include polyesterurethanes and polymers with urethane hard segments and polyisoprene soft segments [167-168]. Also among linear block copolymers are those polymers where the glass transition of a segment is the switching temperature. Many polyurethanes will utilize this type of switching, mainly those that are thermosets [169].

Another class of thermally-induced shape memory polymers includes polyesters. Interestingly, the shape memory properties of this class of polymer are added to the polymer by a reaction [170]. Normally, the ketones in a copolyester will be reduced to alcohols by simple organic reactions. An example of this type is poly(ethylene-co-propene-co-carbonoxide), where the degree of reduction controls the glass transition temperature. Thus the switching temperature can be controlled over a large range. At the lower temperatures, shape memory effects are limited, but at conditions above room temperatures, the shape memory response is more noticeable.

A third class includes covalently-crosslinked polymers. This is a very complicated class of polymers in that ionizing radiation is used to crosslink the polymer. After crosslinking, the glass transition of the polymer can be utilized as the transition temperature, while the crosslinks provide the rigid phase necessary for recovery. This type of crosslinking can work with polyethylene and many of its copolymers [171]. For some polymers, however, the ionizing radiation degrades the polymer chains, resulting in no useful properties. Thus, two

different types of polymers, poly(ε-capralactone) and polymethylvinylsiloxane for example, can be blended together [172]. The radiation will then create cross-links between the two. Covalent crosslinks can also be added to the polymer through synthesis. Condensation reactions of monomers of tri-functional natures or copolymerizations of monofunctional monomers with oligomeric cross-linkers have proven capable of this type of shape memory addition [152].

Segmented Polyurethanes

Segmented polyurethanes are an ideal polymer for shape memory use due to their definitive segments and their naturally phase separating natures. They are synthesized through the condensation polymerization of a diisocyanate and a high molecular weight diol. A low molecular weight diol is then used as a chain extender to create the long polymer chains. The subsequent polymer is then formed of two segments: the long-chain high molecular weight diol, which is the soft phase, and the diisocyanate and chain extending low molecular weight diol, which acts as the hard or rigid phase [173]. As explained in the previous section, the soft phase is responsible for the transition and allows for shape recovery, while the hard phase stores the energy after deformation and causes the return to original shape due to its rigidity [174-175]. The polymer will be solid below the critical transition, which will be melting in the case of this type of polymer. This occurs due to the hard segments' ability to hydrogen bond with themselves and form semi-crystalline regions [175]. Normally, thermal energy is used to trigger the shape memory response of this type of polymer. Even this proposed research, however, will technically utilize thermal energy, just not directly applied.

Shape Memory Triggering Mechanisms

As mentioned previously, the main method of triggering the shape memory behavior of shape memory polymers is through thermal application. This can either occur through the transition temperatures of glass transition or melting. For glass transition temperatures, the amorphous phase of the block copolymer that has the lower transition temperature will begin to move once that temperature has been reached. The higher glass transition temperature amorphous phase stays in the glassy region and is responsible for recovery. For melting temperatures, a very similar mechanism occurs except that the segment responsible for the melting is composed of crystalline regions. Once the crystalline regions are melted, then that segment is capable of movement.

There are other methods of shape memory triggering, however. Some involve just an indirect method of thermal application. These are labeled as indirect heating methods. One of the more common examples of this is light-induced shape memory polymers. While the light, or laser, is an indirect method of triggering, heat is still produced for the shape memory effect. Normally, this heat is produced when the light is absorbed by conductive fillers in the polymer. The fillers absorb the energy of the light, and through the photothermal effect, release the absorbed energy as heat. Carbon nanotubes, carbon black, and conductive ceramics have been studied as these fillers [176-177].

Another example of indirect heating involves the inclusion of magnetic nanoparticles into the polymer. These nanoparticles are usually iron oxide cores coated in silica [178]. Upon the application of an alternating magnetic field, heat is produced. Multiple shape memory

48

polymers have been shown to be viable for this method. The most promising was a biodegradable multiblock copolymer of poly(p-dioxanone) and poly(ε-capralactone). For medical applications, however, an alternating magnetic field applied to the body is not desirable, if not just for the reason that the machinery needed would be large, and expensive to use.

There are other methods of shape memory activation that do not use heat, however. The first is an indirect actuation by the temporary lowering of the glass transition. This occurs mainly through the introduction of water or a similar system. As the water is absorbed into the polymer, it acts as a temporary plasticizer, lowering the glass transition and allowing for shape memory recovery [179-180]. For example, the glass transition of a polymer is above room temperature. Upon water absorption, the glass transition is reduced to below room temperature. The temperature of the water environment is now above the glass transition temperature and shape memory actuation is achieved. It has been proven that this effect can be controlled, depending on the degree of moisture uptake as well as time of immersion in the water. Interestingly, in a completely different, but related method, one study has shown that one segment of the polymer can be water soluble [181]. As the segment dissolves, permanent shape recovery occurs. The only downside is that there can be no return to the temporary fixed shape due to the disappearance of the soft phase. For either method, application for the medical field is small. Controlled release would prove difficult if shape memory activation occurred the moment the body's environment cause shape memory behavior.

A final technique for shape memory actuation is through light inducement. While light has been described for shape memory activation previously, the light was used for indirect heating. In this case, certain polymers are composed of photocrosslinked bonds that, upon application of the laser, are cleaved, allowing for shape memory actuation [182-183]. While this could be used in the medical industry, a specialized polymer and/or polymer modification would have to be utilized. Other methods need to be developed that make use of existing polymers and their properties.

Shape Memory Parameters

While shape memory polymers have many distinct characteristics and properties, there are two main parameters that are important to general characterization. They are exhibited during two distinct points of the shape memory behavior. During traditional shape memory behavior, there are three main stages: deformation, fixing, and then recovery. Deformation occurs when the polymer is heated, or placed under a similar shape memory triggering method, and is elongated to a set length. Because the polymer is above the shape memory transition temperature, it is capable of being elongated to much higher values. The segment responsible for switching is capable of motion. Once the polymer is elongated, then the second stage, fixing, begins. This involves the cooling of the polymer back below the transition temperature and allowing the polymer to permanently take the shape of the elongated length. Loading is then released, but the polymer stays in the elongated shape. Fixity, one of the two main parameters, is taken from the fixing stage. Regardless of the fact that the temperature is reduced below the transition temperature, full elongation is not kept. There is usually a slight loss in strain once the load is removed. The amount of strain that is kept is labeled as the fixity

and has units of percent, as in the percent of the strain that the polymer is capable of holding when load is released [184-186]. Following the fixing, the third segment involves recovery of the film to the original shape. Heat is normally reapplied to the polymer and the temperature once again rises above the transition temperature. The switching segment moves and the other segment, the rigid phase, is capable of returning to its original shape. The second main parameter, recovery, is taken from this part of the shape memory behavior. Due to fatigue within the polymer, the recovery of the film usually does not quite reach completely back to the original shape. Thus, the recovery, the second parameter, is the ability of the polymer to reach the original shape [144]. Its units are percent as well, and is calculated based on the amount of strain returned out of the entire strain applied during the previous cycle. Traditionally, the previous cycle is always used as the reference when calculating recovery. Figure I-7 displays the traditional shape memory behavior curves of polyurethane and how fixity and recovery are calculated.
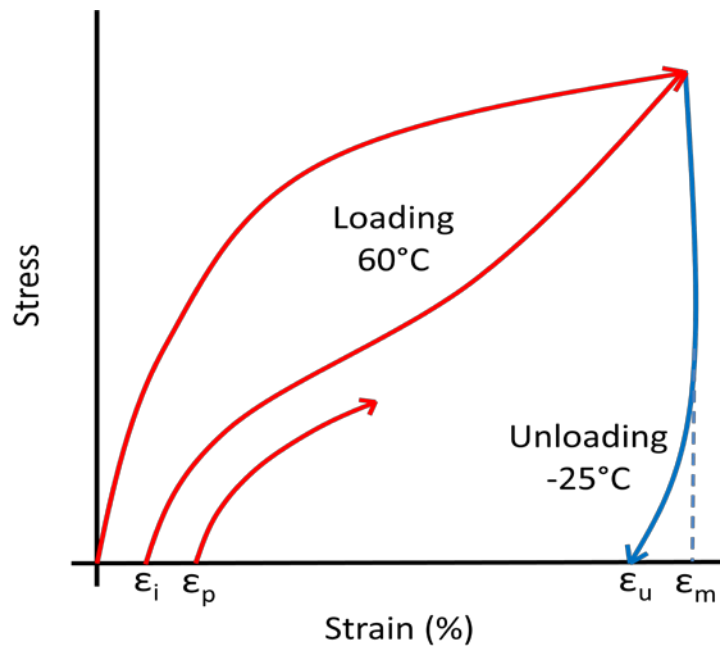
Figure I-7. Representation of stress vs. strain graph for shape memory behavior.

Fixity is calculated according to Equation 1.

$$Fixity\ (\%) = \frac{\varepsilon_u}{\varepsilon_m}\ \text{x}\ 100 \tag{1}$$

Recovery is calculated according to Equation 2,

$$Recovery\ (\%) = \frac{\varepsilon_m - \varepsilon_p}{\varepsilon_m - \varepsilon_i}\ \text{x}\ 100 \tag{2}$$

where ε_m is the maximum strain in the cycle (300%), ε_u is the residual strain after unloading, ε_p is the residual strain after recovery, and ε_i is the residual strain after recovery of the previous cycle. The first cycle of Fig I-7 is the characteristically different cycle of this type of polyurethane and is usually disregarded for data.

As mentioned before, shape memory polymers come in a variety of types with a handful of different triggering mechanisms. Due to differing reasons, these mechanisms can be proven unacceptable for medical applications. For this reason, the research in the following chapters investigates a new triggering mechanism more suitable for medical applications. Gold nanorods and their photothermal properties are incorporated into shape memory polyurethane. The viability of near-infrared light to then trigger the photothermal effect of the nanorods is studied. The resultant heat produced is examined for its potential to trigger the shape memory behavior of the polyurethane. A comprehensive review of the behavior and its dependence on the properties of the nanorods is undertaken and reported.

RESEARCH OBJECTIVES

There are two main objectives associated with this research. While there are many applications in the medical field that can benefit from the use of nanomaterials, two distinct applications are

investigated. Within each main objective are two minor objectives that are necessary towards the complete study of the objective. The main objectives and their minor objectives are as follows:

i) The first main objective involves the incorporation of halloysite nanoclays into a polymeric matrix in order to control the release of a model antibiotic, tetracycline hydrochloride. The goal of this objective is to demonstrate the ability of halloysite and the polymeric matrix to synergistically slow the release rate for extended release possibilities (Chapter II).

   a. The first minor objective is to study the loading and release from pure halloysite in order to understand how to best utilize the nanotubes in order to result in a controlled release profile.

   b. The second minor objective involves the study of the incorporation of the drug-loaded halloysite into a polymeric matrix in order to greatly extend the release of the drug.

ii) The second main objective is to investigate a new triggering method for the shape memory behavior of segmented shape memory polyurethanes. This new triggering method involves the use of near-infrared light and the photothermal properties of gold nanorods instead of the traditional direct-heat triggering or the less common light-cleavage of chemical bonds.

   a. The first minor objective is to study the seed-mediated growth of gold nanorods and to understand how to control the growth in order to result in desired photothermal properties needed for shape memory behavior (Chapter III).

   b. The second minor objective entails the incorporation of the gold nanorods into the shape memory polyurethane and the study of the shape memory behavior triggered by a near-infrared light source (Chapter IV).

CHAPTER II

CONTROLLED RELEASE FROM HALLOYSITE NANOTUBES

INTRODUCTION

As mentioned in Chapter I, montmorillonite was the first nanoclay studied for its use in controlled release. The interstitial space between the layers is capable of being loaded with drug, with studies concerning controlled release of ibuprofen, 5-flourouracil, promethazine chloride, buformin hydrochloride, sertraline, timilol meleate, and tetracycline hydrochloride [58].

Recently, however, nanocylinders have been gaining more attention due to their ability to capture and hold materials within the lumen of their tubes. Halloysite has become the more common. In fact, the release of pharmaceutical compounds has become the main focus for halloysite. Many drugs have been evaluated, including, but not limited to, tetracycline hydrochloride, khellin, diltiazem hydrochloride, propranolol hydrochloride, nifedipine, furosemide, and dexamethasone [63, 69-72]. Studies have also been performed on extending the release from halloysite, utilizing polymers, chitosan, and gelatin. Release rates have been shown to be reduced when utilizing these materials as coatings and matrices, sometimes by many orders of magnitude [70-72].

In this chapter, similar effects were studied, but with an added level of scrutiny that deals with how certain properties will affect the release if modified. First, different methods of halloysite loading were analyzed. These methods are mentioned in literature, but no direct comparisons of the methods have been undertaken. Thus, many previous results in the literature can show vast differences in release profiles, with no explanation as to why. In addition, multiple types of halloysite were examined for their viability for controlled release. These types include a standard halloysite with narrow sizes from Sigma-Aldrich and two other halloysites which are reported to differ greatly in length. This is also a current problem in halloysite research. There is no attention paid to the different types of halloysite, leading to a possible explanation of vastly different release profiles documented. The effects of the loaded release compound were studied as well. Various dyes, of very similar natures, but with key differences, such as size and charge, were used to determine how the properties of the loaded compound affect the controlled release profiles. Finally, the effects of incorporation of drug-loaded halloysite into a polymeric matrix, poly(methyl methacrylate) were studied. For this to succeed, the degradation of tetracycline was measured, and the long-term release from the nanocomposite system was monitored. Thus, the main goal of this chapter is to provide a more detailed study on controlled release from halloysite, how to reconcile the large differences in release profiles seen in current controlled-release studies utilizing halloysite, and to provide initial results on how halloysite and poly(methyl methacrylate) can synergistically work as a controlled-release nanocomposite.

MATERIALS AND METHODS

Halloysite

Three types of halloysite nanoclays were compared for this research. The first was purchased from Sigma-Aldrich. The other two are purported to be of varying sizes, with one considered a "short" length and the other a "long" length.

Loading of the Halloysite

Loading of the halloysite was performed through one of two methods. In both cases, the halloysite was first ground, sieved with a 240 mesh screen, and then dried at 80°C for 24 hours. Simultaneously, a 20 mg/ml drug solution was prepared by adding 2 grams of tetracycline hydrochloride, 95% purity and purchased from Sigma-Aldrich, to 100 mL of an ethanol:water (90:10 by weight) mixture.

In method one, an excess amount of drug solution, roughly 6 grams of drug solution per one gram of halloysite, was mixed with the prepared halloysite. A vacuum was then pulled on the mixture to withdraw the air from the lumen of the tube. Bubbles were seen on the surface of the suspension as the air was removed. The vacuum was then quickly released, allowing a pressure gradient to form, drawing the drug solution into the lumen. This vacuum process was then repeated two or three more times to ensure full loading, until no more bubbles could be seen on the surface of the suspension. Following the final vacuum and release, the solution was centrifuged, the supernatant removed, and the nanotubes dried under vacuum.

The second method used the same saturated solution, but in a lesser amount. The solution was mixed with halloysite in a one to one weight ratio. The result was a thick paste. The paste was applied to the same vacuum cycles, but centrifugation was not needed. The nanotubes were dried under vacuum, after which a second measure of one to one drug solution was added. The vacuum cycles were repeated and the nanotubes were dried once again. With this method, there is no waste of drug and the amount of drug loaded can easily be calculated.
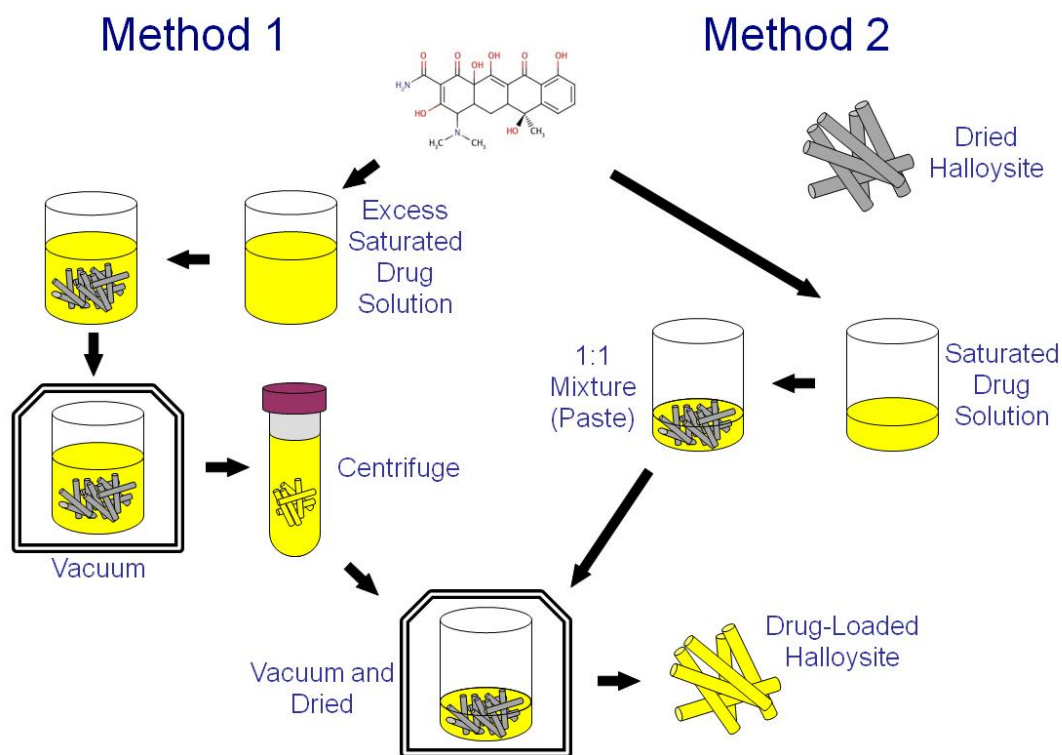
Figure II-1. Halloysite loading methods.

Following the loading of either method, the resulting drug-loaded halloysite was ground and then stored in a cool, dry, and low-light environment.

For some experiments, dyes were loaded instead of tetracycline. Dye-loading occurred in a very similar fashion to the second loading method of the drug-loading section. The dye solutions were created so that the final concentration in water resulted in an absorbance value of two in an ultraviolet (UV) spectrophotometer. Loading then occurred exactly as the second method of drug-loading. Finally, after the dye-loaded halloysite was created, the halloysite did not need special storage condition, as the dyes are much more stable. They only needed to be kept dry to stop large amounts of agglomeration.

The dyes used include acid blue 25 (MP Biomedicals), acid blue 9 (Spectrum), reactive blue 19 (Acros Organics), rhodamine B (Alfa Aesar), and rhodamine 6G (EMD Millipore).

Washing Methods

To determine if the initial burst could be removed, two washing procedures were used. The first involved placing twice-loaded halloysite onto the surface of a vacuum filter funnel and 100 mL of deionized water was added to the halloysite for five minutes. The water was then pulled through the filter paper, through the halloysite. The second process involved mixing the twice-loaded halloysite with 40 mL of water in a centrifuge tube and centrifuging for five minutes. The supernatant was decanted and 40 mL of water was again added, followed by centrifugation and supernatant removal. A final wash cycle occurred with 20 mL of water to keep both procedures equivalent. The resulting halloysite from both methods were dried and then tested for release.

Preparation of Drug-Releasing Films

Solution casting techniques were used to create drug-loaded films. Poly(methyl methacrylate) (PMMA), purchased from Sigma-Aldrich, was used as the polymer, with acetone as the solvent. The polymer and solvent were mixed with a bottle roller at a 1:3 ratio by weight until the polymer was completely solvated. The solution was then cast into an aluminum dish and the solvent allowed to evaporate under vacuum at room temperature. Drug-loaded halloysite was added to the solvated mixture by mechanical mixing at 25% of the dried film.
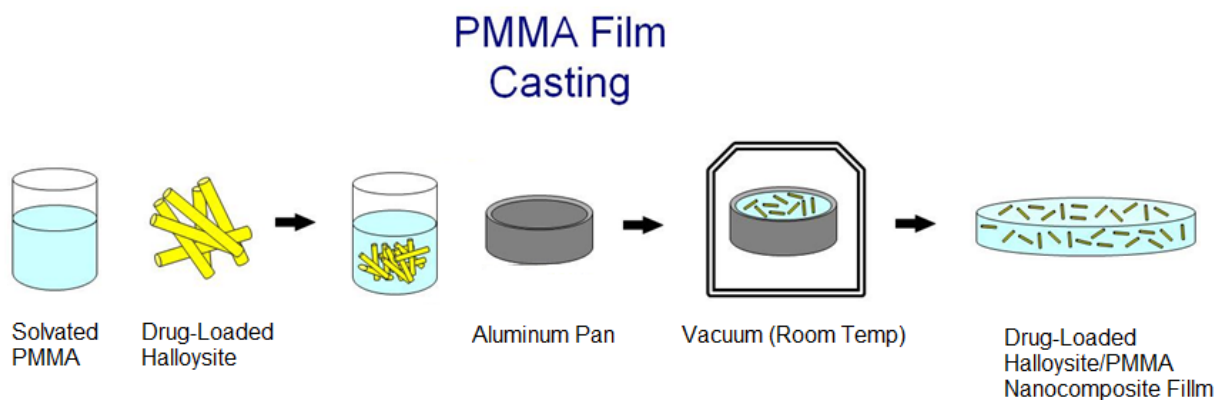
Figure II-2. Casting of Nanocomposites.

Release Method

Release from pure halloysite was evaluated by adding roughly 0.02 grams of drug-loaded halloysite (DLH) to 40 mL of a 10 mmolar phosphate buffer, pH 6.8, in a 50 mL centrifuge tube kept at 37°C. During desired measurement intervals, the tube was centrifuged at 5000 rpm for 5 min.

Release from pure films and drug-loaded films was evaluated in a similar procedure as for pure halloysite. 13 mm film samples, weighing about 0.12 grams, were suspended in 40 mL of the

same buffer solution and kept at 37°C. Control tubes of phosphate buffer and equivalent amounts of tetracycline were also prepared due to the degradation of the drug over time.

TECHNIQUES

Ultraviolet (UV) Spectrophotometry

Concentration and controlled release from halloysite was evaluated using a ThermoSpectronic Genesis 6 UV spectrophotometer. An aliquot of the supernatant (about 3 mL) was removed after centrifugation, inserted into a disposable poly(methyl methacrylate) cuvette, and then placed into the spectrophotometer slot. The absorbance value at 362 nm was measured and compared to the experimental calibration curve in order to determine the concentration of the sample at that specific time. The aliquot was then returned to the tube and the tube shaken to re-suspend the halloysite. The wavelength has been shown to be a peak wavelength of tetracycline for absorption.

Concentration and controlled release from nanocomposites was also evaluated using the ThermoSpectronic Genesis 6 UV spectrophotometer. An aliquot of the release buffer (about 3 mL) was removed in a very similar process to pure halloysite, measured in the UV-vis at 362 nm, and compared to the experimental calibration curve. The aliquot was then returned to the tube. At the same time, an aliquot was removed from the degradation constant tube and used as the control in the UV-vis. This eliminates degradation effects of long-term exposure of the drug to light and heat.

Thermogravimetric Analysis

Degradation analysis was performed using a thermal gravimetric analyzer (TGA; Thermal Instruments Q500 TGA). The samples were placed in the platinum weighing pan. The procedure simply ramps the temperature from room temperature to 1000°C at a rate of 10°C/min and measures weight loss over time.

Scanning Electron Microscopy

Small amounts of halloysite were examined under a scanning electron microscope (SEM; Zeiss EVO 50 Variable Pressure SEM). A few milligrams were spread over the surface of conductive microscopy carbon tape, which was attached to the top of an SEM grid. A thin layer of gold was sputtered onto the halloysite to enable conductivity, at which point the stub was examined in the SEM.

RESULTS AND DISCUSSION

Halloysite

As mentioned, three types of halloysite were purchased in order to choose an acceptable type for study. SEM images of the three are shown in Figure II-3.
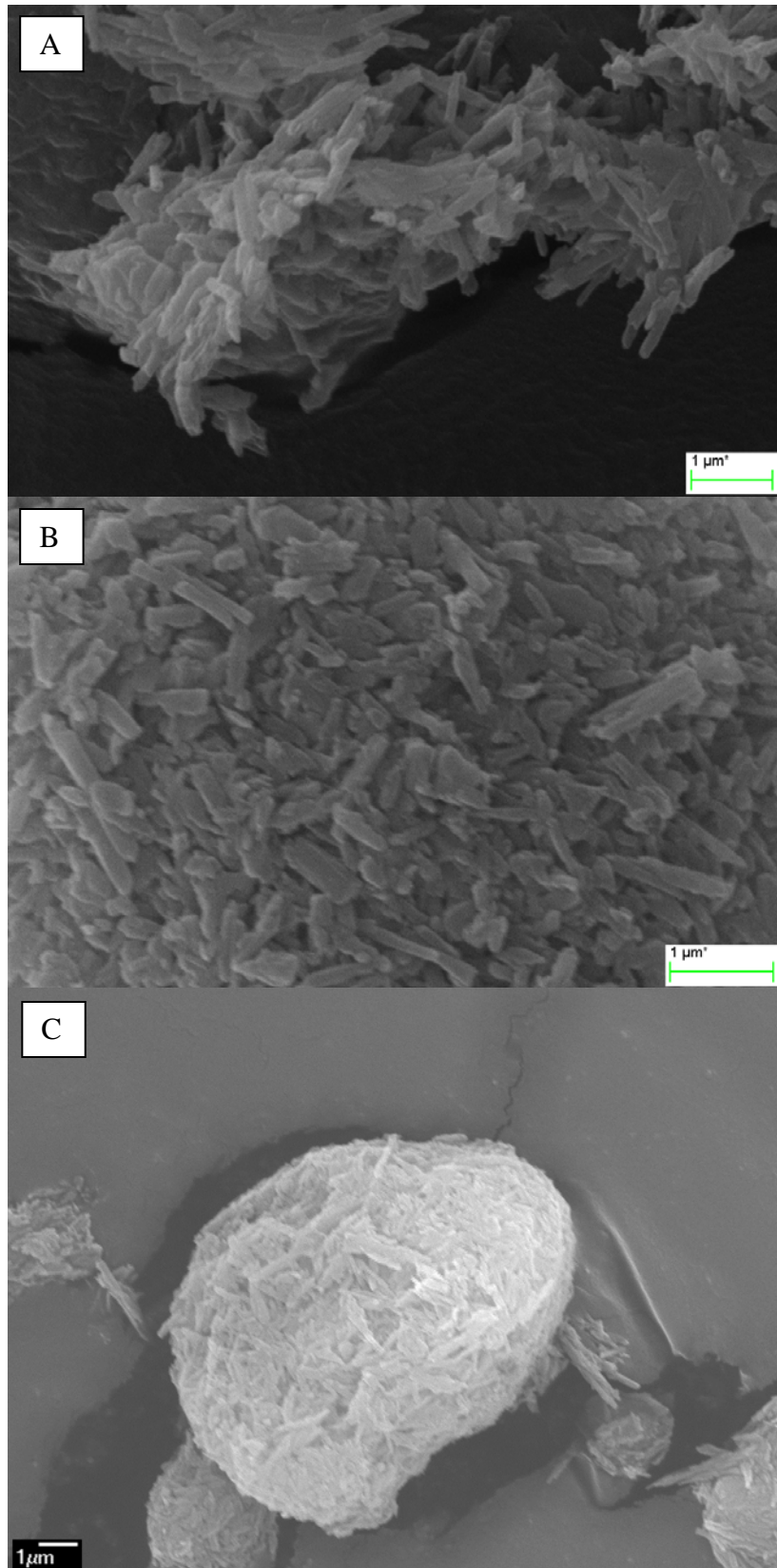
Figure II-3. Sigma halloysite (A), short halloysite (B), and long halloysite (C).

It is difficult to capture crisp images of halloysite, even with a conductive, gold coating. The "short" and "long" halloysite were the most difficult to image. Regardless, there is a clear increase in length for the "long" halloysite vs. the "short." "Long" halloysite is typically longer than 1 micron. Also evident when capturing images was that there is a large range of sizes for both "short" and "long" halloysite types, while the range of sizes for the Sigma halloysite was much smaller.

From this, the Sigma halloysite was chosen for further experimentation due to its ease of image capturing and smaller size differentials. The SEM image in Figure II-4 is a more magnified view of the Sigma halloysite.
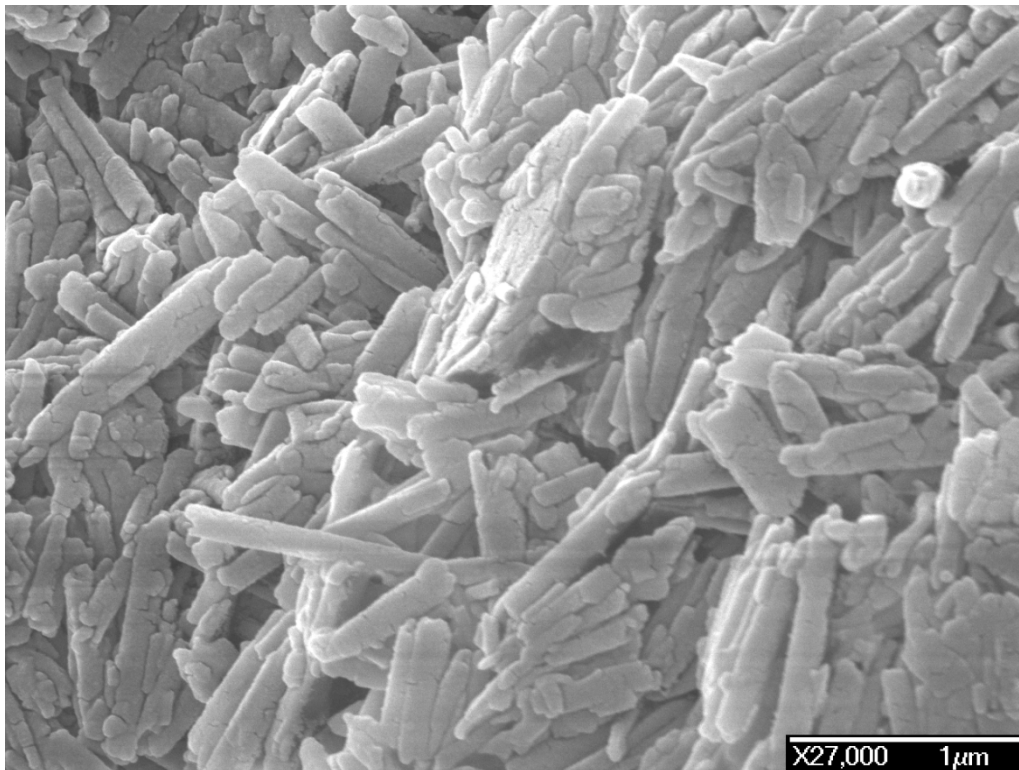
Figure II-4. Sigma halloysite.

Common lengths for this halloysite can range from 800 nm to 1200 nm. The diameter is commonly 100 nm to 200 nm. In addition, the inner lumen of the nanorods can be seen in Figure II-4.

Calibration Curve

A calibration curve is necessary in order to determine the concentration of released compounds. To create the curve, known concentrations of the loaded compound, tetracycline, were created in the phosphate buffer. These solutions were then measured in the UV spectrophotometer in order to determine the requisite absorbance values. The resulting calibration curve is displayed in Figure II-5.
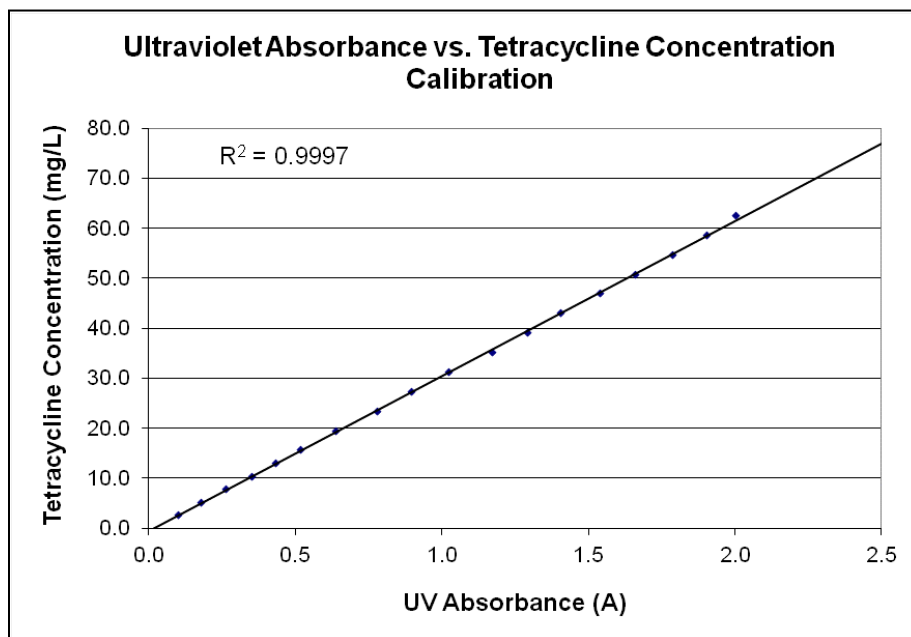
Figure II-5. Tetracycline calibration curve. The independent variable is on the y-axis in this case so as to be able to create an equation to solve for an unknown concentration when an absorbance value is measured.

As can be seen, there is a strong linear trend relating drug concentration to absorbance, with an R-squared value of 0.9997. Backwards extrapolation even leads to a absorbance value of very close to zero when the concentration is zero mg/mL. This is accurate, considering that the pure phosphate buffer was used as the reference for this measurement. From this calibration curve, an equation can be derived in order to solve for concentration of unknown samples (Figure II-5).

$$y = 31x - 0.4301 \qquad (3)$$

This equation links the absorbance (x) to the concentration (y), in mg/mL.

Effect of Loading Method

Loading method is an essential step of the process of release of drugs from halloysite. As can be seen in Figure II-6, there is a significant difference in the two loading cycles. The first method, involving excess amounts of the drug solution loaded into the tubes, with the excess eventually removed, resulted in the highest amount released for a similar amount of halloysite. Full release occurred on the order of about one hour, with an initial burst of roughly 85% of the final release amount.
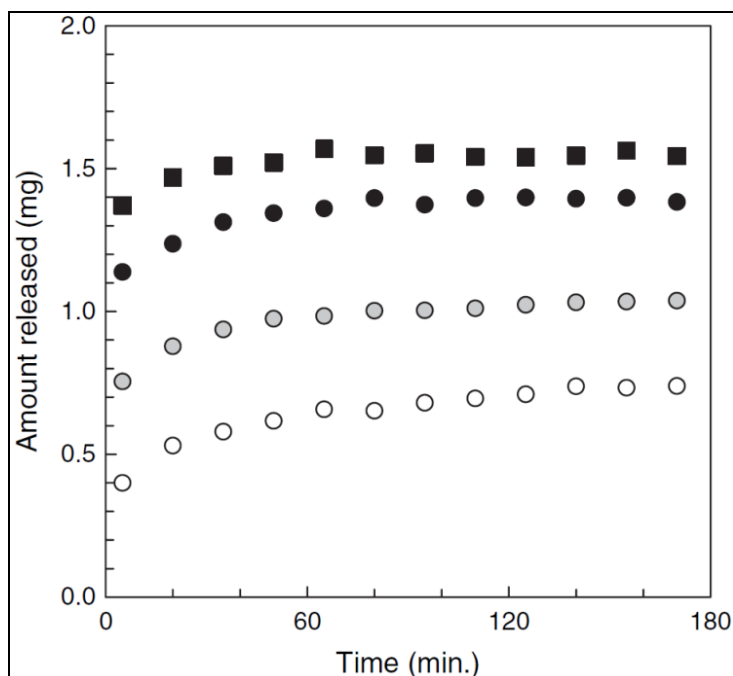
Figure II-6. Mass released of tetracycline hydrochloride from halloysite based on number of loading cycles and method of loading. Black squares are prepared from Method 1, while circles represent Method 2. Black represents four loading cycles, shaded represents three, and open represents two. Reprinted with permission from [74], Christopher J. Ward, Shang Song, and Edward W. Davis J. Nanosci. Nanotechnol. vol.10, pp.6641-6649 (2010). Copyright American Scientific Publishers.

The second method, on the other hand, consisting of 1:1 ratios of drug solution to halloysite by weight, resulted in smaller release amounts and initial bursts. Examining Figure II-6, it can be seen that as the amount of loading cycles increase, the final amount released also increases, as can be expected. In fact, release amounts approximately double when doubling the number of loading cycles from two to four. This infers that with the second method of loading, the number of loading cycles will linearly increase the amount of drug that will eventually release. Also, the times for full release and initial burst percentages change depending on the number of loading cycles. From two, to three, to four loadings, the time of release decreases from 2.3, to 2, to 1.3, and the initial burst increases from 41%, to 57%, to 69%, respectively. This is reasonable, considering that the area inside the lumen is static. There is only a certain amount

of drug that can be loaded there. On the other hand, the outside of the nanotube can hold progressively more drug. Finally, it too, reaches a point of saturation, though, leaving the drug to crystallize between tubes. This crystallization is what releases with the initial burst. As more loadings occur, more drug crystallizes between the tubes, resulting in higher burst percentages. At the same time, because more drug releases very quickly, release levels off at a quicker rate, resulting in faster overall release. These results are contrary to what is reported in the literature. Lvov et al. utilized the first loading method, whereas an excess amount of drug solution was mixed with the halloysite [63]. His results indicate virtually no burst effect, although unspecified washing procedures were stated to be utilized before release. On the other hand, Kelly et al. used a vacuum filtration washing procedure [71]. They discussed the fact that they could calculate loaded amount. In their case, however, release from just halloysite was demonstrated for many days. This has not been reproduced in any other study.

To determine if the initial burst can be removed, the two washing procedures were used. The resulting curves, shown in Figure II-7, demonstrate a shift downward in the curves from previous release curves. Both washing procedures resulted in removing about 30% of the loaded tetracycline, but the shape of the curves remain very similar to that of the twice-loaded, unwashed halloysite release curves. Thus, the burst effect was reduced, but not the steady release. It can be construed that the washing removes the loosely bound tetracycline of the interstitial spaces, which thus contributes to the initial burst amounts. The previously mentioned study by Lvov et al. must have used a similar washing procedure, as the results are comparable.
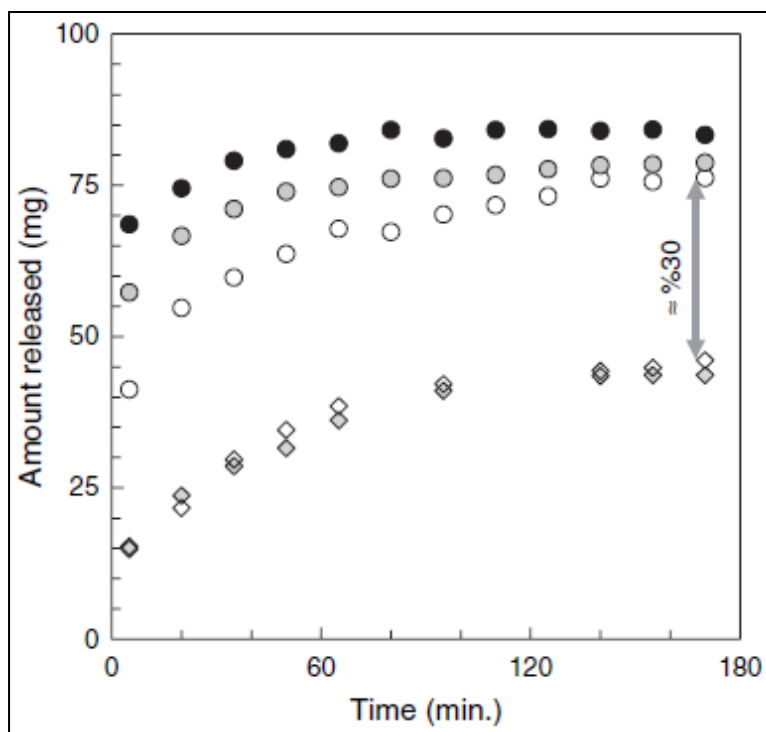
Figure II-7. Fraction released for multiple loadings using Method 2; open circles are twice loaded, grey circles are thrice loaded and black circles are quadruple loaded; open diamonds are samples washed using centrifugation process, grey diamonds are samples washed using filtration. Reprinted with permission from [74], Christopher J. Ward, Shang Song, and Edward W. Davis J. Nanosci. Nanotechnol. vol.10, pp.6641-6649 (2010). Copyright American Scientific Publishers.

Effects of Loaded Compound Properties

Release characteristics are not determined solely by type of release delivery or loading method, but also on the properties of the loaded material. Properties such as size, charge, and polarity can add variability into the release. To demonstrate this, dyes were loaded instead of tetracycline hydrochloride. These dyes are more stable and much easier to find with small differences between them. For example, there are many dyes that have very similar structures, but can be smaller or larger than each other, or contain extra charges.

Rhodamine B and 6G were used due to their very similar structures. The main difference between the two is that Rhodamine 6G possesses an ethyl side group that hinders hydrogen bonding to the carboxylic group. This, in turn, lowers the solubility of the dye into the aqueous release medium. The effect of this difference was demonstrated when the two are loaded into halloysite and released (Figure II-8).
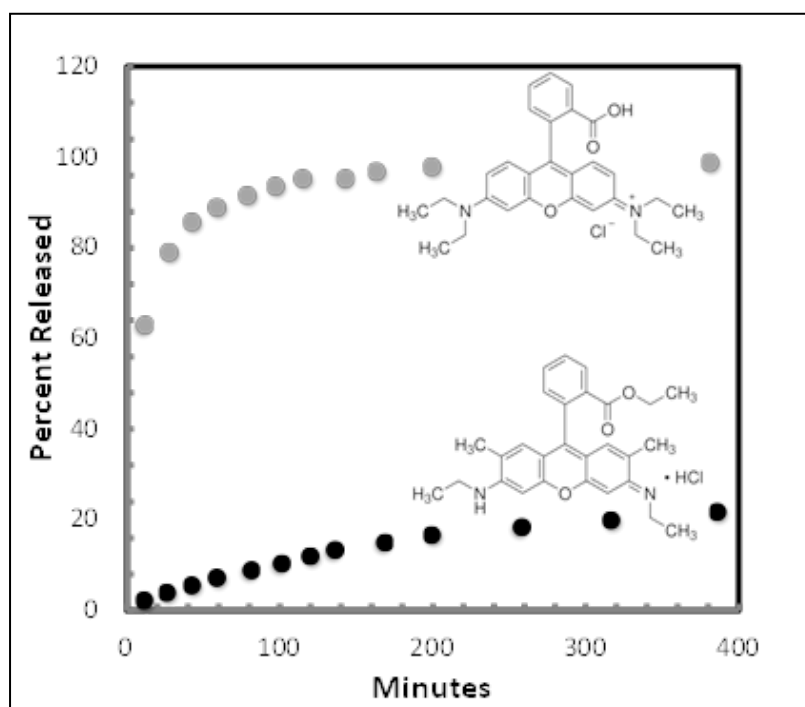
Figure II-8. Percent released of rhodamine B and rhodamine 6G from halloysite. Black circles represent rhodamine 6G and shaded circles represent rhodamine B. Reprinted with permission from [8], Ward, C.J., M. DeWitt and E.W. Davis, Halloysite Nanoclay for Controlled Release Applications, in *Nanomaterials for Biomedicine*. 2012, American Chemical Society. p. 209-238. Copyright 2012 American Chemical Society.

It is shown that the lower solubility of rhodamine 6G hinders overall release, even eliminating the initial burst seen for rhodamine B.

Size and charge of the loaded compounds are important as well. As mentioned before, loaded compounds can bind to the nanotubes via ionic interaction. It follows that compounds with differing charge will bind to halloysite with varying strength. Three dyes were utilized to examine this effect. Reactive blue 19 possesses two negative charges, acid blue 25 possesses one negative charge, and acid blue 9 possesses three negative charges and one positive charge for a net charge of negative two. Comparing reactive blue 19 to acid blue 25, there is a difference in magnitude of charge, as well in size. While reactive blue 19's larger size would be expected to hinder release through the nanotube, its larger negative charge serves to repel the dye away from the surface of the negatively charged nanotube faster, as can be seen in Figure II-9.
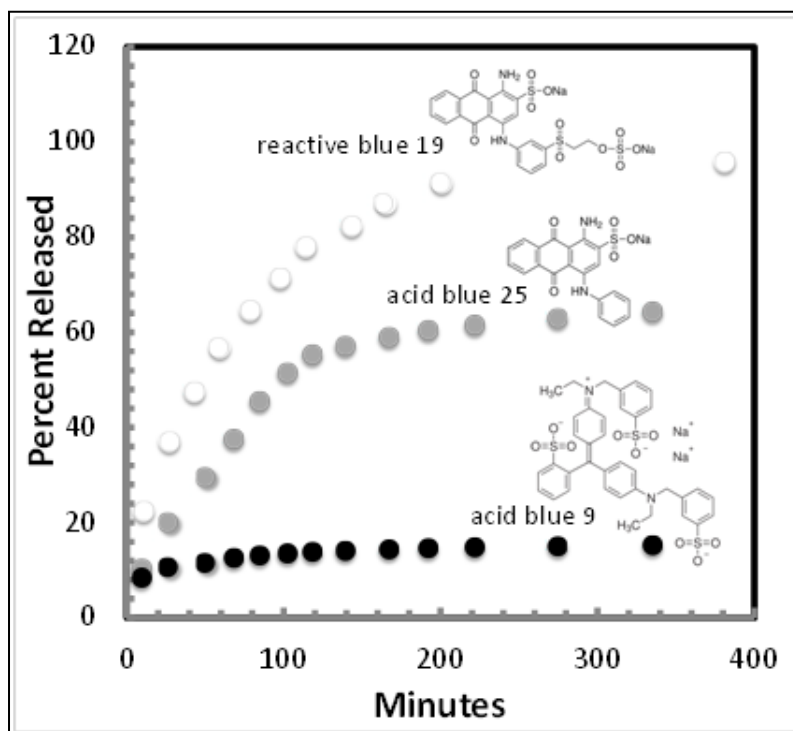
Figure II-9. Release as a function of size and charge. Black circles represent acid blue 9; shaded circles, acid blue 25; and open circles, reactive blue 19. Reprinted with permission from [8], Ward, C.J., M. DeWitt and E.W. Davis, Halloysite Nanoclay for Controlled Release Applications, in *Nanomaterials for Biomedicine*. 2012, American Chemical Society. p. 209-238. Copyright 2012 American Chemical Society.

Examining acid blue 9, its size is larger still than either of the other two. Examining its charge, however, there are three negative charges. This would be expected to cause a quicker release than is shown, even with size effects playing a role. There is also one positive charge, however, allowing for closer association with the halloysite on that side of the dye molecule. Size would logically play some role, however, as Gan et al. determined that increasing molecular size off the loaded compound resulted in dramatic slowing of release from silica nanoparticles [187].

Thermogravimetric Analysis of Halloysite

Both halloysite and drug-loaded halloysite were subjected to thermogravimetric analysis to analyze the percentage of drug loaded into the halloysite. Figure II-10 displays the analysis performed.
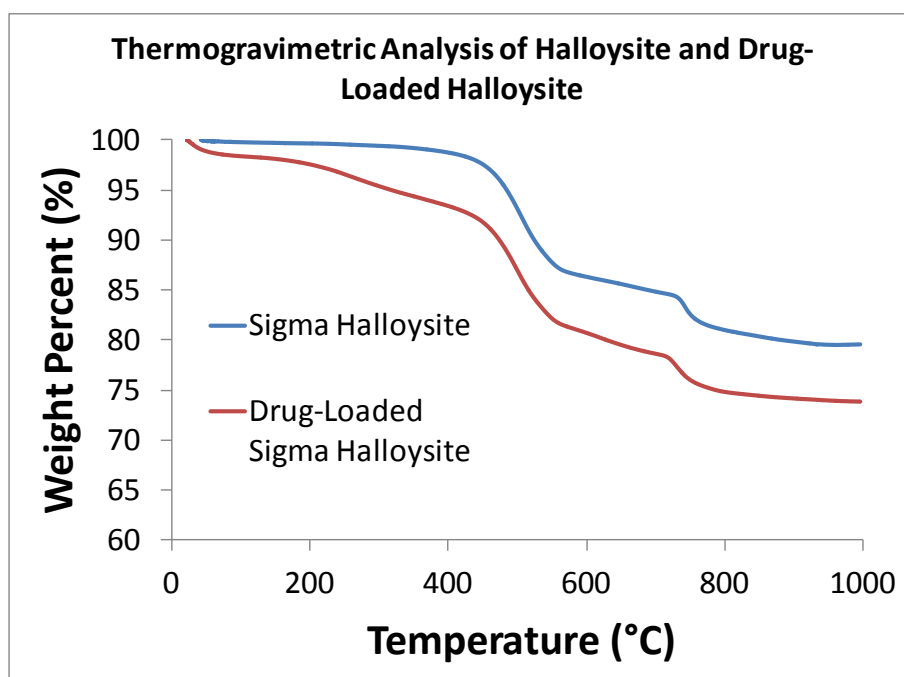
Figure II-10. Thermogravimetric analysis of halloysite and drug-loaded halloysite.

The Sigma halloysite, before drug-loading, demonstrated two distinct temperatures of weight loss, at around 500°C and then again at around 700°C. These weight losses most likely are the decomposition of trace elements bonded or associated with the halloysite nanotubes. The nanotubes themselves are impervious to these temperatures and will not completely decompose. In all, around 79.5% of the weight of pure halloysite remains upon reaching 1000°C. When drug-loading the halloysite, a difference in weight loss can be seen. Very early in the heating process, a weight loss is seen when the weight of tetracycline is lost. It is already known that tetracycline is easily susceptible to both and light and heat and degrades very easily. The end result for the drug-loaded halloysite was that a little less than 73.9% of the weight remained. To roughly calculate what percentage of drug-loaded halloysite is tetracycline, one only has to subtract the final values of the curves. Thus, tetracycline composed roughly about 5.64% of the mass of drug-loaded halloysite.

Tetracycline Degradation

Like many drugs, tetracycline hydrochloride has a certain shelf life. With exposure to both light and heat, the drug undergoes chemical degradation. This was observed when measuring a concentration of the drug in the release buffer over time. Figure II-11 details this degradation.
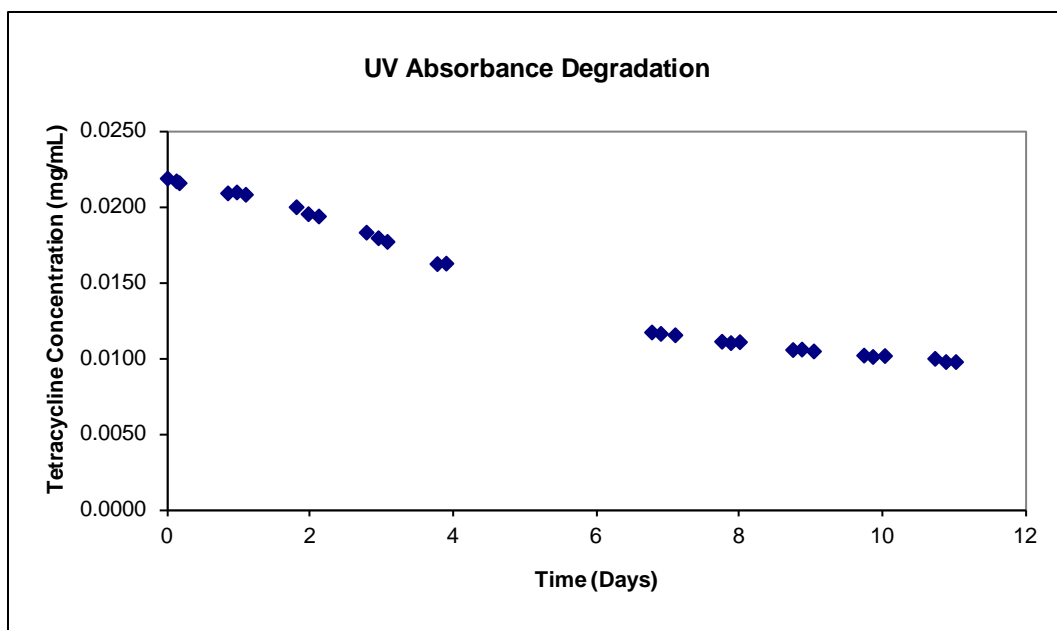
Figure II-11. Degradation of tetracycline.

Degradation of the drug is minimal for the first few hours, which is why the degradation did not need to be taken into account for release from just halloysite, which only released for a few hours. With the release from films, however, the potential for release times is much higher, thus degradation should be taken into effect. This effect is documented by multiple studies. For example, Loftin, et al. demonstrated that temperature changes are a large cause of degradation in all of the tetracycline family [188]. To counteract this degradation, a control was set that consisted of a concentration of pure drug in the release medium. As the drug decayed, this concentration was used as the control when measuring with the UV-vis.

Controlled Release from Nanocomposite Films

Incorporation of the drug-loaded halloysite into polymeric films was expected to enhance the duration of the release, based on either the diffusion or degradation mechanisms discussed before. When the drug-loaded halloysite was incorporated into poly(methyl methacrylate)

films, release rate was shown to slow dramatically (Figure 9). Because aqueous solutions do not serve as solvents for PMMA, the release medium does not swell the films. Release occurs, therefore, by molecular diffusion. In Figure II-12, release through halloysite from the film is compared to tetracycline released purely from the film.
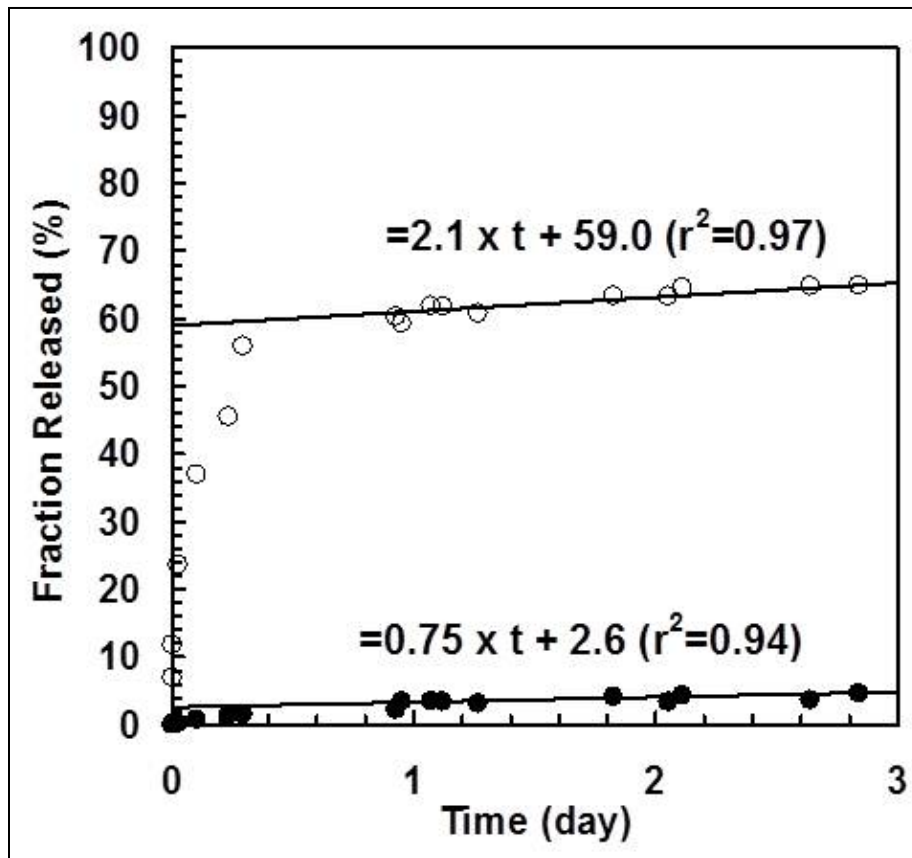
Figure II-12. Release of tetracycline from PMMA Films. Films with pure tetracycline are open circles, and films with dug loaded halloysite are shaded circles. Linear fits are applied only to the data collected after 10 hours. Reprinted with permission from [74], Christopher J. Ward, Shang Song, and Edward W. Davis J. Nanosci. Nanotechnol. vol.10, pp.6641-6649 (2010). Copyright American Scientific Publishers.

Both show a very gradual release curve after a certain amount of time. Pure tetracycline release exhibits a strong initial release of about 60%. On the other hand, there is virtually no initial burst when halloysite is involved. This is very important, demonstrating how halloysite

is a necessary component in this two-component drug delivery system. In addition, after a larger release rate occurs for the first 10 hours or so, release is linear afterwards for both releases. Halloysite continues to exhibit a definite effect, however, as the rate of release for pure tetracycline release is roughly three times that of when release is through halloysite and then from the film. While there are not many studies yet that incorporate halloysite into a polymer for nanocomposite release, Wei et al. have demonstrated similar release for their system of halloysite and poly(methyl methacrylate) bone cement [189]. They did not study the differences in release from pure halloysite and their nanocomposite, but their nanocomposite release showed a similar constant release for at least 10 days.

CONCLUSIONS

Halloysite has been shown to be a very viable material for the release or enhancement of release for controlled release applications. Its rolled nature is very useful for its ability to be loaded with a compound. Of the three types examined, the Sigma halloysite proved the most viable mainly due to a smaller fluctuation in sizes, evidenced by the SEM images capable of being taken. Following the choice of halloysite, a simple calibration for the chosen drug, tetracycline hydrochloride, was performed in the release medium, achieving the method for concentration measurement once release began.

From that point, it was possible to begin release studies, initiated by a study on which of two possible loading mechanisms was more effective. It was discovered that, although the excess loading method did result in successful controlled release, the 1:1 loading methods resulted in controlled release and a calculable loaded amount. In addition, this second method resulted in

smaller initial bursts, allowing a conclusion that the excess drug from the first method was not really loaded but merely crystallized to the surface of the nanotubes and not effectively controlled when released. A study concerning washing methods discovered that certain methods would allow for the removal of the burst effect without hindrance or degradation of the controlled release portion of the release curve.

In order to understand the release of the drug and how the release could possibly be slowed or more controlled, a dye study was performed in which it was discovered that the properties of the loaded compounds do, indeed, affect the final release. Solubility is an important property, with the more soluble drug in the release medium resulting in a quicker release. In addition, charge is shown to play a dominant role, as more negatively charged compounds release faster as they are repelled away from the negatively charged surface of halloysite. Finally, it was observed that the larger-sized compounds may result in a slower release, but charge effects overcome the possible size effects.

The final section of this chapter dealt with the incorporation of the drug-loaded halloysite into a polymer matrix of poly(methyl methacrylate) in order to further hinder release and create a true controlled release device. After discovering the eventual degradation of halloysite and realizing the necessity of compensating for this, release from the new nanocomposite was demonstrated to have a release over multiple days, with a potential release of much longer. In addition, the burst effect near the beginning of release was virtually eliminated.

While the controlled release of pharmaceutical agents from halloysite and similar materials has been studied before, this chapter delved into elements of the release that has not been examined. The studies on loading method and compound properties are particularly new and valuable to the enhancement of this field of controlled release from nanomaterials.

CHAPTER III

SYNTHESIS OF GOLD NANORODS

INTRODUCTION

Gold nanoparticles have been shown to be simple to functionalize and stable under oxidative environments [103]. They are also relatively easy to synthesize in the spherical form and have been used for their inherent properties for many years [82, 103]. There are many applications being actively researched for the possibility of using gold nanorods. These applications can include biomedical sensing, cancer treatment, and as carriers for bioactive compounds [109, 112, 116]. Several synthesis routes have been developed for the production of gold nanorods, including multiple template methods, variations of electrochemical methods, and photochemical methods [76-77, 82]. However, these routes suffer from low yield of the nanorods, damage to the nanorods due to necessary purification steps, and many times, low quality products due to lack of substantial control over the growth. The most commonly used method is the seed-mediated approach, where nanorods are grown from small spherical gold nanoparticles [76, 79, 83, 123]. This approach utilizes a surfactant to stabilize growth and guide nanorod formation over the formation of other shapes. In addition, some variations of this technique utilize silver ions that promote the formation of nanorods, but also reduce the aspect ratio [86, 132].

For many gold nanorod synthesis methods, tailoring the aspect ratio can be difficult. The possible tailoring procedures are limited to duration of growth, such as with the electrochemical and photochemical methods, difficult modifications of the nanotemplates in the template method, or purification steps with the electrochemical methods [76-77, 82]. With the seed-mediated approach, however, there are many more techniques for the tailoring of aspect ratios. The easiest method is to vary reagent concentrations and growth environment. Sao et al. demonstrated that increasing chloroauric acid amounts will result in higher aspect ratio nanorods until a critical level is reached where aspect ratio decreases again [131]. Increasing ascorbic acid amounts, however, have been shown to decrease the aspect ratio of the nanorods, even leading to the production of alternate shapes at higher levels [129, 131]. After becoming a pioneer of the seed-mediated growth of gold nanorods, Murphy et al. discovered that the introduction of silver nitrate results in a beneficial effect of improving yield, but with decreasing aspect ratio [83, 86, 132]. The actual mechanism of the silver nitrate interaction is not yet completely understood, however. Because of the introduction of more nucleation sites, Pérez-Juste et al. has demonstrated that higher amounts of seed particles introduced into the growth solution will result in lower aspect ratio nanorods [133]. Finally, higher temperature of the growth solution has been documented to result in lower aspect ratio nanorods, due to decreased CTAB association tendency and resultant lower stabilization [136].

This chapter examines the role of these studied parameters, as well as examining the role of the ratio between the chloroauric acid and ascorbic acid. The ideal ratios between the two compounds have not been previously reported. Additionally, control over seed nanoparticles is

attempted through manipulation of seed reagents, and the subsequent effects on nanorod growth are presented. Both of these effects have not been examined before in literature.

The surface plasmon resonance is used as the primary indication of shape and shape selectivity. Surface plasmon resonance occurs when the electromagnetic field forces conduction band electrons to begin to oscillate [79, 83]. This results in two distinct absorption peaks in UV-vis-NIR spectra for colloidal gold nanorods. One peak corresponds with the transversal plasmon (along the shorter axis of the nanorods), while the other corresponds with the longitudinal plasmon (along the longer axis). The transversal plasmon peak is usually located around 520 nm, but the longitudinal plasmon peak is red-shifted depending mainly on the aspect ratio of the nanorods; larger aspect ratios result in higher wavelength absorption peaks [108]. These longitudinal plasmon peaks are used to demonstrate control over the aspect ratio.

MATERIALS AND METHODS

Synthesis of gold nanorods in this research occurred in a two-step process. First, a seed solution was prepared in which chloroauric acid ($HAuCl_4$), bought from Sigma-Aldrich, was reduced by sodium borohydride ($NaBH_4$), from Fluka. The prepared seed solution could then be added to a growth solution containing more reduced chloroauric acid to promote rod growth. The silver ion-assisted approach was utilized with the addition of silver nitrate ($AgNO_3$), from Sigma-Aldrich. After a desired period of time, nanorods grew and could be measured and characterized.

Reagent Solutions

Five solutions were used in the creation of gold nanorods. Of the five, three were prepared as stock solutions and used for a couple of weeks, while the other two were prepared fresh. The three stock solutions were the CTAB (purchased from Sigma-Aldrich), $HAuCl_4$, and $AgNO_3$. The L-ascorbic acid, from Sigma-Aldrich, and $NaBH_4$ solutions needed to be made fresh with each growth. The CTAB solution was made at 0.1 M in deionized water. Once made, the solution required heating at 60°C to fully go into solution and needed to be continuously warmed above room temperature to keep in solution for the age of the stock. The $HAuCl_4$ solution was made at 0.0086 M in DI water and was stored in light-free conditions. Similarly, the $AgNO_3$ solution, at 0.01 M in DI water, was stored in lightless conditions. Of the fresh solutions, L-ascorbic acid was prepared at 0.1 M in DI water and $NaBH_4$ was made at 0.01 M in DI water. The $NaBH_4$ solution needed to be created and then cooled until ice-cold.

Seed Preparation

The seeds that were formed from the $HAuCl_4$ reduction were stabilized in the CTAB solution. 10 mL of the CTAB solution (clear) was pipetted into a vial. 290 μL of the $HAuCl_4$ solution was then introduced into the CTAB solution. The mixture was slowly inverted three times to ensure complete mixture. At this point, the solution was a deep yellow color. 601 μL of fresh, ice-cold $NaBH_4$ solution was then added to the mixture and the final mixture was carefully swirled for two minutes. The solution immediately began to turn to a light to murky brown color. The seed solution was kept at 37°C in a water bath to grow for two hours to ensure that there were only gold nanospheres when used for the growth solution. After the two hours, the solution had started to become a pink to red color. Three seed growth temperatures were tested

in order to evaluate the effect on eventual rod growth: 28°C, 37°C, and 40°C. Chloroauric acid amount was varied to study its effect: 0.11, 0.2, 0.29, and 0.38 mL.

Growth Preparation

Growth solution was prepared in a similar fashion. First, 10 mL of the CTAB solution was added to a vial. 130 μL of the $AgNO_3$ solution was introduced and the mixture slowly inverted three times. The mixture was still clear at this point. Next, 580 μL of the $HAuCl_4$ solution was added, followed by another three inversions. At this point, the solution had turned a deep yellow color. 55.2 μL of the L-ascorbic acid solution was added to the mixture. After swirling, the solution turned colorless. The previously made seed solution, after sitting for two hours, was added to the mixture in the amount of 24 μL. The solution was stored in a water bath at 28°C. Typically, the nanorods were left to grow for at least two hours. After growth had begun, color change could be documented, starting with a very light pink.
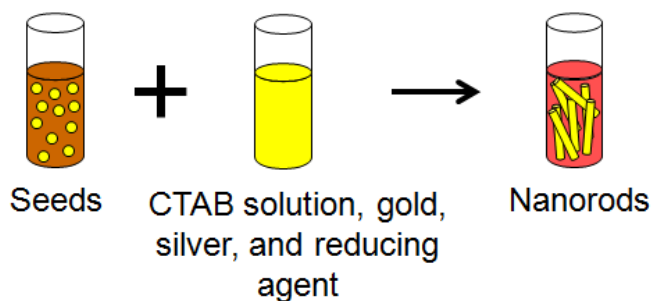
Figure III-1. Nanorod Synthesis.

To test the effect of variations in reactant concentrations, the amounts of silver nitrate, $HAuCl_4$, and ascorbic acid were changed. Silver nitrate amounts studied were 50, 70, 90, 110, 130, 150, 170, 190, and 210 μL, with three replicates per value. While the normal amount of $HAuCl_4$ utilized was 580 μL, new amounts tested were 300, 440, 720, and 840 μL, with five replicates

for each value. Ascorbic acid amounts were examined at 25, 40.1, 55.2, 70.3, and 80.4 µL, also with five replicates per value. Nine different growth variations were tested, with three different $HAuCl_4$ amount values (560, 580, and 600 µL) and three different ascorbic acid amount values (53.3, 55.2, and 57.1 µL). This resulted in seven different ratios of $HAuCl_4$ to Ascorbic Acid. One ratio of 10.51 was repeated three times to give a measure of how an increase in volume of both reactants, but at the same ratio, will affect growth. Finally the amounts of seed that were examined were 6, 24, 48, 72, 96, 120, 144, 170, and 194 µL.

TECHNIQUES

UV-vis Spectrophotometry

Nanorod growth characterization was normally performed on a Shimadzu UV-2450 UV-vis spectrophotometer. Absorption spectrum was taken from 1000 nm to 200 nm in a polystyrene microcuvette. A microcuvette containing deionized water was used as a reference. Growth solutions were kept at growth temperature until measurement is taken. Normally, measurement was taken two hours and four hours after growth was initialized. For analysis of growth control, data is presented predominately using the wavelength and absorbance intensity of the peak for the longitudinal plasmon effect. This is due to the fact that the longitudinal plasmon effect is the one dependent on nanorod aspect ratio. Samples were returned to seed and growth solutions immediately after measurement.

Transmission Electron Microscopy

A Transmission Electron Microscope (TEM; Zeiss EM 10C 10CR) was used to visualize selected samples. Small drops of the growth solution were dropped onto formvar-coated,

83

copper TEM grids and allowed to air dry. Because the CTAB can block transmission of the electrons, excess CTAB was commonly removed in two centrifugation cycles of 10 minutes, each at 14,462 xg.

RESULTS AND DISCUSSION

Growth of Seeds

With seed-mediated growth, seeds are small nanospheres that are inhibited from growing further by the type of reducing agent used in the process. Growth can be followed by the UV-vis, as the spheres begin to be visible near the 520 nm wavelength after about 15 minutes of growth. This growth can be seen in Figure III-2.
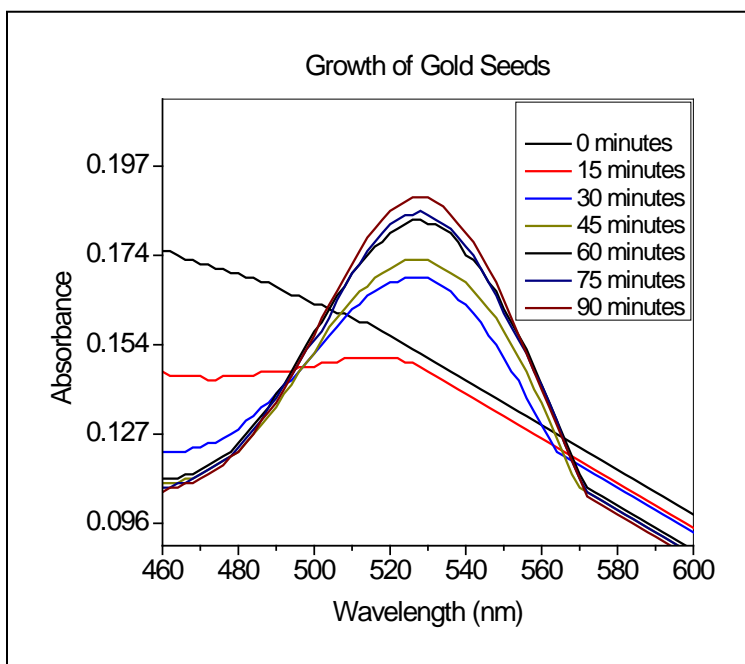
Figure III-2. Growth of gold seeds over 1.5 hours.

The growth of the gold seeds has not previously been reported in the literature. Even more surprising is that when UV spectra of growing gold nanorods are displayed, the transverse

plasmon peak that should be present for the gold seeds at initial times of nanorod growth is also not present. An example occurs during the study performed by Alekseeva et al [79]. It is clearly demonstrated that gold seeds do absorb at the wavelength of 520 nm, but is not truly examined by others researching this field.

Growth of Nanorods

A growth solution was purposely designed to attempt and grow only spheres and interrupt rod formation. As shown in Figure III-3, results, when compared to correct rod growth, indicate that when only spheres are present, the 520 nm absorption peak is the only visible peak.
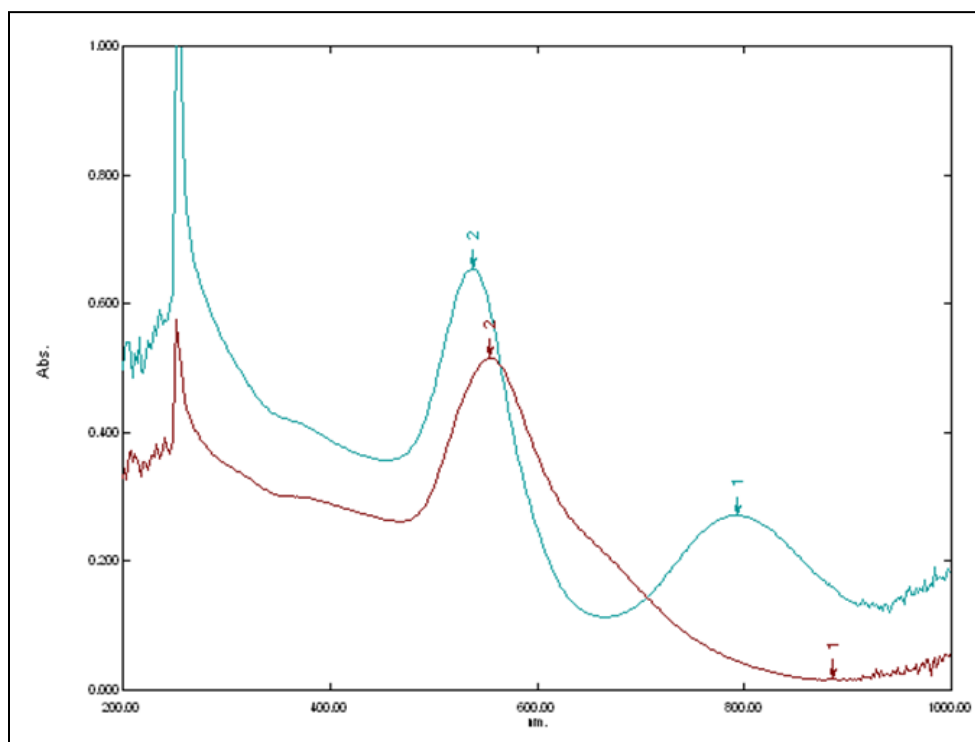
Figure III-3. UV-vis spectrum with the red plot containing no nanorods and the blue plot containing nanorods.

When rods are present, however, another peak occurs. According to literature, this peak can occur in a large range, but in Figure III-2, the peak occurs very close to 800 nm. Additionally,

while most literature suggests that the 520 peak should not noticeably shift, there is a slight red shift when nanorods are not present compared to when they are. It is possible that with the solution containing no rods, there are also other shapes present which slightly shift the peak away.

When examined under TEM, rods are shown to be present, as can be seen in Figure III-4. In addition to rods, however, rather large spheres are present as well.
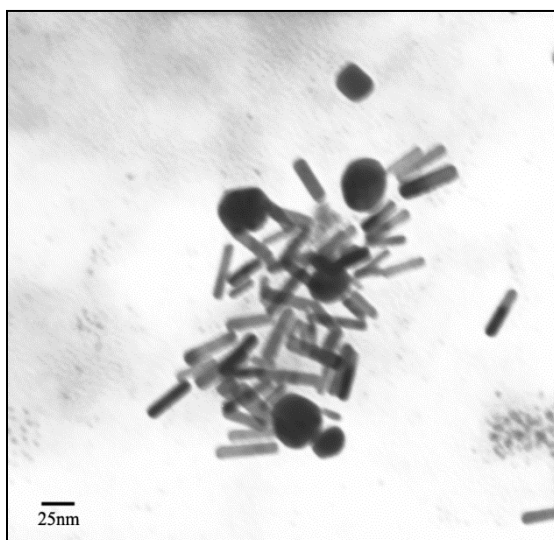
Figure III-4. TEM image of gold nanorods with gold nanospheres present as well (200 KX magnification).

The resulting nanorods have a length of about 36 nm and a width of about 6 nm, an aspect ratio of 6. This lower aspect ratio is expected, since silver nitrate was purposely added to the synthesis procedure for that reason. It is expected that if the silver nitrate were not added, then the rods would be longer, but less numerous. In addition, the amount of spheres and other shapes would increase. As can be seen as well, in Figure III-4, there is a slightly larger range of widths than is desired. This larger range of widths, with the lengths roughly the same,

means a broader range of aspect ratios as well. This is undesirable when designing for specific properties, due to changes in absorbance properties.

As mentioned, the absorbance properties of the longitudinal plasmon peak are dependent on aspect ratio of the nanorods. This is demonstrated in Figure III-5. Three aspect ratios of nanorods are shown in TEM pictures. As the aspect ratio increases, the peak absorbance value that they absorb at for the longitudinal plasmon effects increases as well.
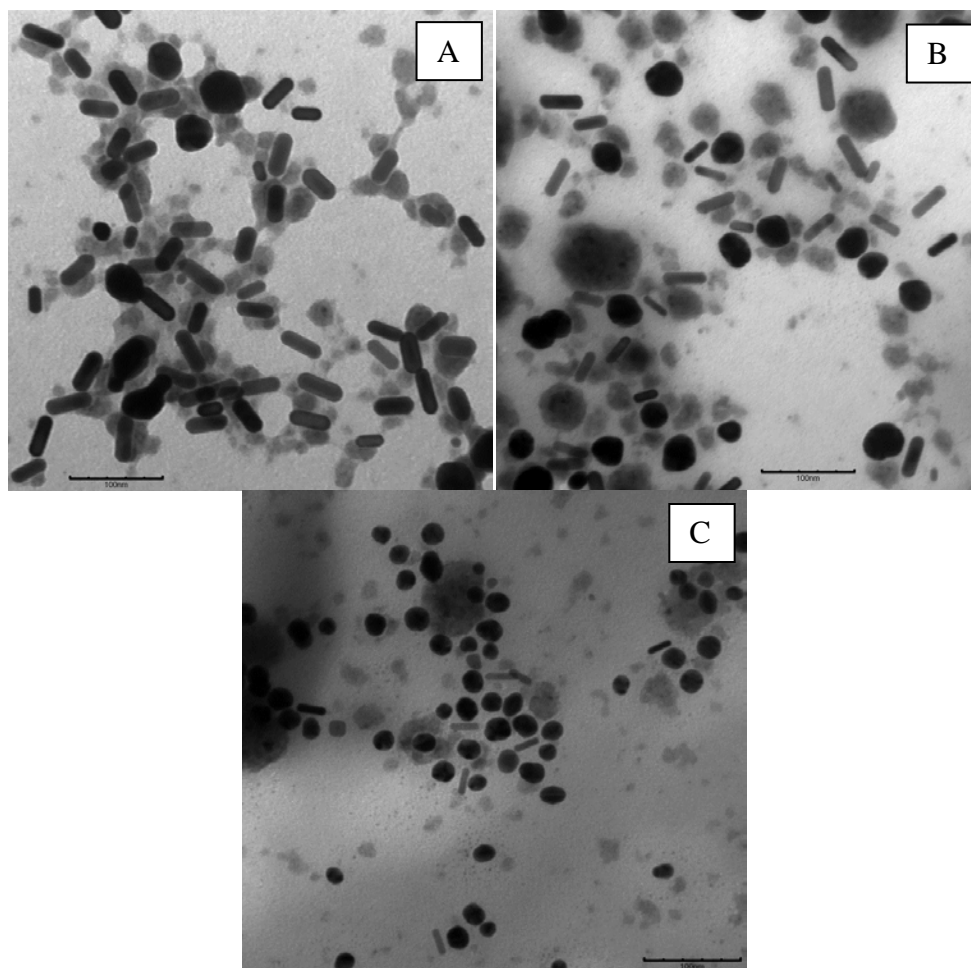
Figure III-5. TEM images of gold nanorods of increasing aspect ratios: Nanorods in A have an aspect ratio of 2.3 and have a peak absorbance of 710 nm; Nanorods in B have an aspect ratio of 3.4 and have a peak absorbance of 804 nm; Nanorods in C have an aspect ratio of 3.8 and have a peak absorbance of 831 nm. The scale bars for all three are 100 nm.

It is interesting to see that, although the lengths in Figure III-5-C are smaller than the lengths in the other two, the aspect ratio is larger, demonstrating the fact that peak wavelength is dependent on nanorod aspect ratio and not length. Because the laser used in subsequent sections is an 808 nm laser, aspect ratios of about 3.4 are desired because they exhibit peak wavelength values very close to 808 nm.

Variation of Synthesis Factors

To try to narrow the range of aspect ratios as well as to vary the absorption values of the nanorods, synthesis factors were studied and varied. The goal is to be able to use these factors in different amounts and values to be able to tune the absorption values to desired levels, thus resulting in desired properties. Throughout this study of synthesis factors, there are two common measurement parameters. The first is the wavelength of absorption. The wavelength reported is the wavelength of the peak of the plasmon absorbance. Normally, the wavelength is reported only for the longitudinal plasmon absorbance. This is due to the fact that this peak shifts due to changes in the nanorod aspect ratios. In some cases, however, peak wavelength is reported for the transverse plasmon absorbance. It can be inferred that, as the wavelength of the peak increases for the longitudinal plasmon, the average aspect ratio of the nanorods also increases. The other measurement parameter measured is the absorbance intensity at that peak wavelength.

Chloroauric Acid in Seed Solution

Chloroauric acid present in the growth of seeds is very important towards the final properties of nanorods. As shown in Figure III-6, with increasing levels of gold ions present, both peak

wavelength values and absorption values generally decrease. It can be inferred that with increased levels of gold ions present, larger seed spheres are grown. These larger seeds, when utilized for nanorod growth, yield larger diameter nanorods. This, in turn, leads to smaller aspect ratios. In addition, as the seeds are larger, there are fewer gold ions present in the growth solution per seed, with the result of one of two situations: shorter nanorods or fewer grown nanorods cause the decrease in absorbance intensity. It can already be seen that shorter nanorods are present, but the decrease in intensity could be a combination of both possibilities.
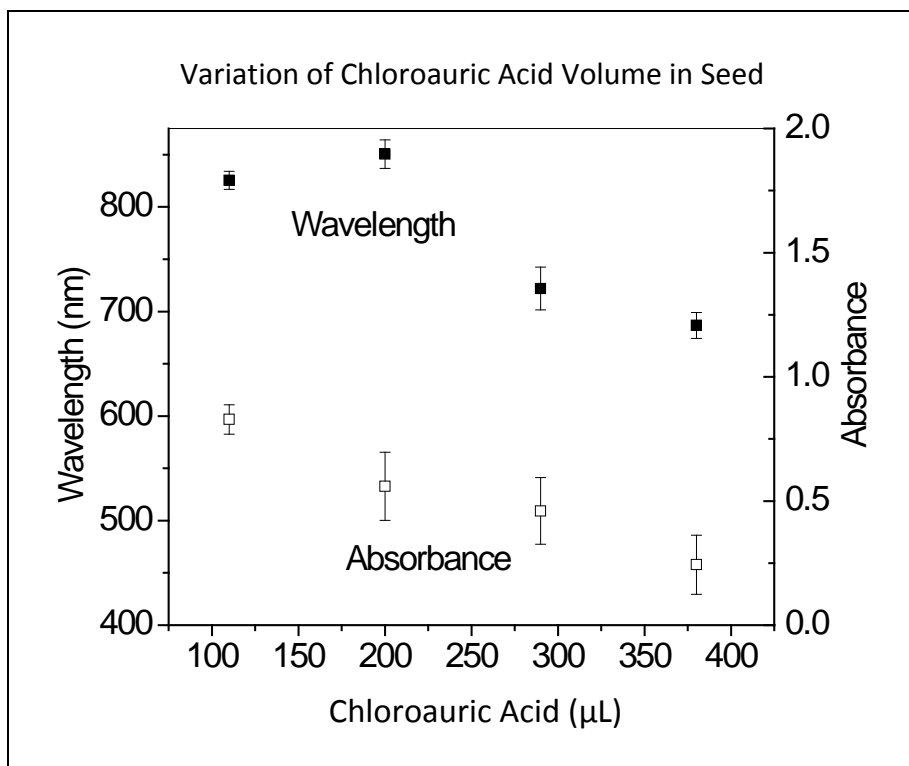
Figure III-6. Wavelength and absorption values for the longitudinal plasmon peak of nanorods grown with variations in chloroauric acid amounts in seed growth.

Temperature of Seed Growth

Three temperatures were examined for growth of seeds: 28°C, 37°C, and 46°C. 37°C was the original temperature, while 28°C was chosen because it is the growth temperature and it was

desired to see how the seed would grow at the lower temperature. 46°C was chosen because it is the same change in temperature as the lower temperature from the normal temperature, but in the higher direction. While studies have examined the effects of growth temperature on nanorod growth, this study is the first to analyze the effect on nanorod growth due to seed growth temperature. UV-vis-NIR results for absorption intensity and peak wavelength of the longitudinal plasmon absorption are presented in Figure III-7.
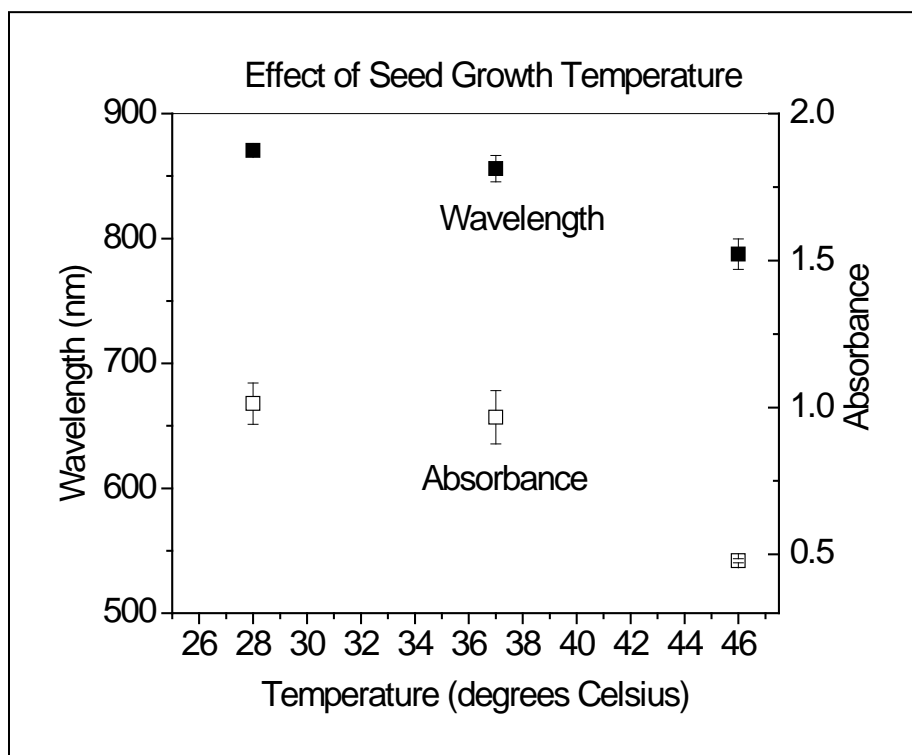
Figure III-7. Wavelength and absorption values for the longitudinal plasmon peak of nanorods grown with variations in temperature of seed growth.

Results indicate that as seed growth temperature increases, both wavelength values and absorption intensity decrease. It can be theorized that with increasing temperature, more gold is reduced, forming larger seeds. This is very similar to theories regarding temperature effects on the growth of nanorods. Literature suggests that at higher growth temperatures, larger

diameter rods are produced with lower aspect ratios due to the higher reduction of gold [137]. Similarly, the seeds can obtain larger diameters, resulting in the growth of lower-aspect-ratio rods. Larger seeds will grow into nanorods with larger diameters, but shorter lengths. In addition, it has been suggested that at higher temperatures, CTAB possesses an increased association tendency, forming more stable micelles, but fewer of them [126]. It can be reasoned that with the formation of fewer seed spheres, fewer nanorods are able to grow, reducing the yield. Similar reasoning can be provided for this development as in the previous section. Shorter nanorods or fewer grown nanorods cause the decrease in absorbance intensity. Smaller aspect ratio nanorods are known to be present due to the decrease in wavelength values, but with previous documented proof of CTAB tendency in the literature, the decrease in intensity could also be a result of fewer nanorods present.

Seed Solution in Growth Solution

As the amount of seed solution added to the growth solution is increased, there are more seeds present in the system for growth. This results in more nanorods grown, but with a drawback of shorter nanorods since the total amount of gold is constant. This occurs because there are more nucleation sites available for growth. This results in fewer and shorter rods. Thus, with shorter nanorods, diameter will remain the same and the resultant aspect ratio will be reduced. This result is presented in Figure III-8, where there is an initial jump in wavelength value with increasing seed amount, but only in the very beginning. After that, there is only a declining trend.
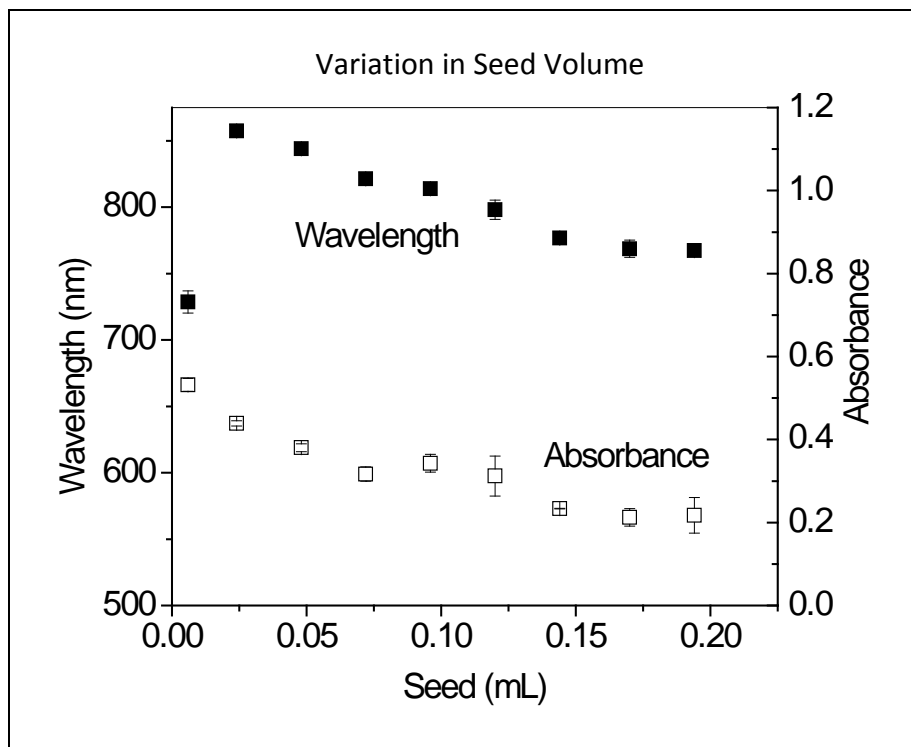
Figure III-8. Wavelength and absorption value trends with variations in seed concentration.

The brief rise in wavelength value at low concentrations has been documented, with the explanation that with small amounts of seed, nucleation will occur on all facets of the seed, with larger seeds grown instead of nanorods [134]. In addition, the absorption value decreases as well. While there may be more nanorods present in the system, at lower wavelength values, intensity decreases due to lower energy plasmon effects from shorter nanorods.

Chloroauric Acid in Growth Solution

Different amounts of $HAuCl_4$ were added to the growth solution just before growth was initiated. These values included 300, 440, 580, 720, and 840 μL. It can be reasoned that if the gold ion concentration is too high, there will not be enough ascorbic acid for full reduction. Indeed, when the solution becomes colorless after ascorbic acid addition, complete reduction

of the gold is occurring. With higher amounts of chloroauric acid, 720 and 840 μL, the

solution still possessed a yellow tint or full yellow color, meaning that full reduction had not

occurred. Interestingly, the solutions made with 720 μL of chloroauric acid were a very pale

gold, but one repetition turned a slight pink color, suggesting that growth began for that one

repetition. This means that the critical value of chloroauric acid is around 720 μL. Literature

does suggest that a critical value can be reached, but no such direct values are reported [131].

Examining the UV-vis data, shown in Figure III-9, it is confirmed that no growth occurs for the

higher values. Full reduction of all gold ions is necessary for nanorod growth.
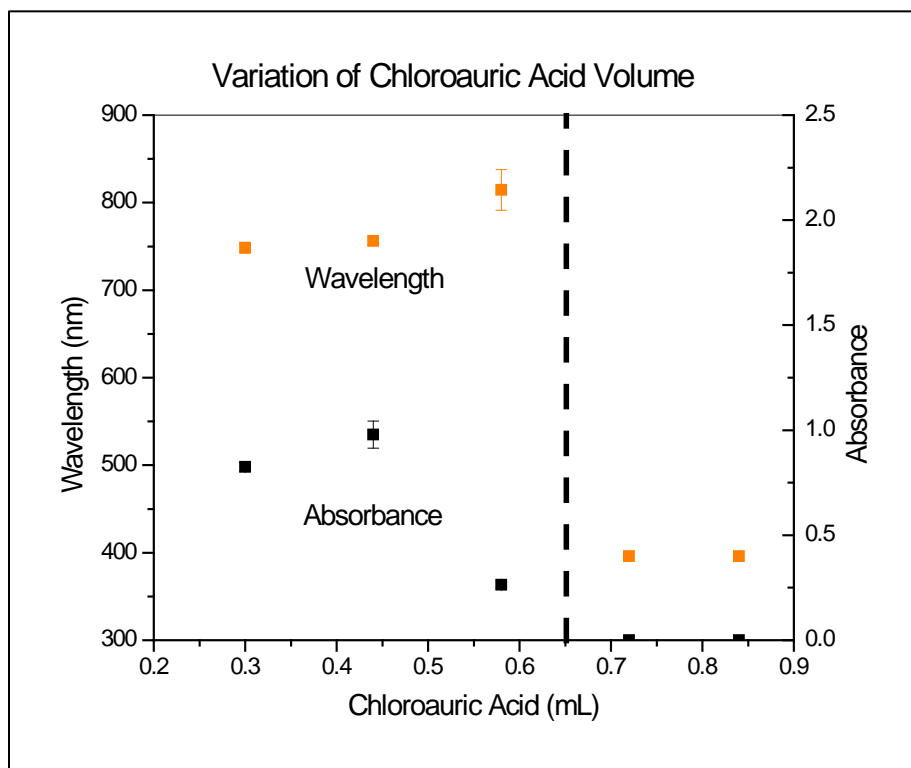
Figure III-9. Wavelength and absorption value trends with variations in HAuCl$_4$ amounts.

When full reduction did not occur, only a peak around 400 nm could be observed in the UV-vis

spectrum. This corresponds to unreduced gold in the HAuCl$_4$. Interestingly, and not reported

in the literature, not only did no growth of nanorods occur when full reduction did not occur, but the seeds were completely consumed as well. This effect can only be explained by the growth of other types of shapes, but is still not truly understood at this time. Examining Figure III-8, it can be seen that before reaching the critical value of too much $HAuCl_4$, an increase in $HAuCl_4$ corresponds to an increase in aspect ratio. The absorption values behave differently, however. There is a slight increase initially, with increasing $HAuCl_4$, before a decrease until reaching the critical value of reduction. This suggests that, even though more gold ions are being introduced into the system, the total number of nanorods produced decrease due to the longer lengths being produced. This correlates to the fact that at higher wavelengths and, thus, higher aspect ratios, a higher absorbance intensity should result. Instead a decrease is seen, due to fewer nanorods present.

Ascorbic Acid

Ascorbic acid variation resulted in very similar results to that of chloroauric acid variation. Amounts of ascorbic acid used included 25, 40.1, 55.2, 70.3, and 80.4 µL. Once again, full reduction did not occur for all concentrations. The gold was not fully reduced and the solution retained a yellow tint. At higher amounts (55.2, 70.3, and 80.4 µL), nanoparticle growth could be confirmed by gradual change in color from colorless to pink.

Unfortunately, UV-vis results for absorption wavelength display no obvious trends, shown in Figure III-10.
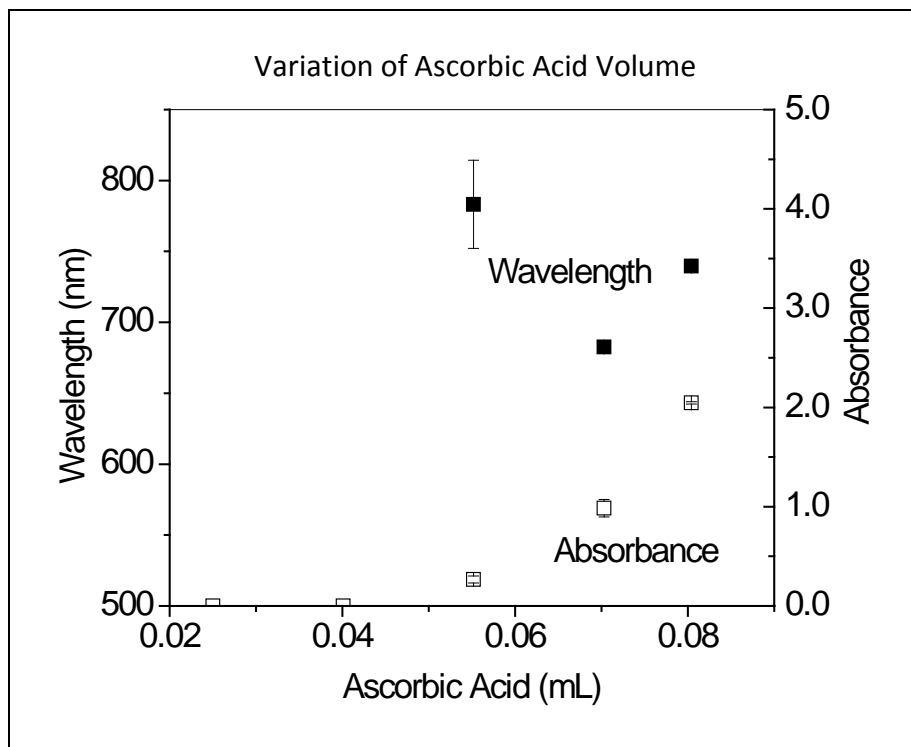
Figure III-10. Wavelength and absorption value trends with variations in ascorbic acid amounts.

However, for the two highest amounts of ascorbic acid, the transversal and longitudinal peaks had begun to combine. While the general trend during this phenomenon of combining peaks is for increasing ascorbic acid amounts to result in an increase in wavelength, the actual mechanism behind these unusual results is still unknown at this time. With respect to absorption intensity, however, there is an obvious trend towards a higher intensity. This occurs due to the larger amounts of reduced gold in the system. Among literature viewpoints, one concerns the fact that after nanorod growth, additional ascorbic acid can be added to further lengthen nanorods by reducing more gold [126]. It is possible that with more ascorbic acid added initially, more nanorods will be grown. This can be rationalized by the fact that the intensity dramatically increases, but wavelength only fluctuates. Either larger aspect-ratio nanorods are grown to increase the intensity, which can be shown not to be the case, due to

fluctuation but still definite reduction in peak wavelength, or a higher number of smaller aspect-ratio nanorods are present. In addition, similar to the $HAuCl_4$ variation, at low amounts of ascorbic acid, similar to at high amounts of $HAuCl_4$, no nanorods were created. This resulted in the same 400 nm peak as before when $HAuCl_4$ is still present in the system.

Chloroauric Acid/Ascorbic Acid Ratio

Nine different ratios were tested, with the following amounts: 560, 580, and 600 μL of chloroauric acid paired with 53.3, 55.2, and 57.1 μL of ascorbic acid. These values were selected so that when 560 μL of chloroauric acid and 53.3 μL of ascorbic acid were pared, the ratio equaled that when 580 μL of chloroauric acid and 55.2 μL of ascorbic acid were pared. The same occurred for when 600 μL of chloroauric acid and 57.1 μL of ascorbic acid were pared. The ratio for all three equal 10.51:1 (chloroauric acid:ascorbic acid). This was done in order to determine if there are any differences in increasing reagent volumes with the same ratio.

Results, shown in Figure III-11, indicate that there is an increasing peak wavelength with increasing ratio of chloroauric acid to ascorbic acid, meaning that larger aspect ratio nanorods are grown.
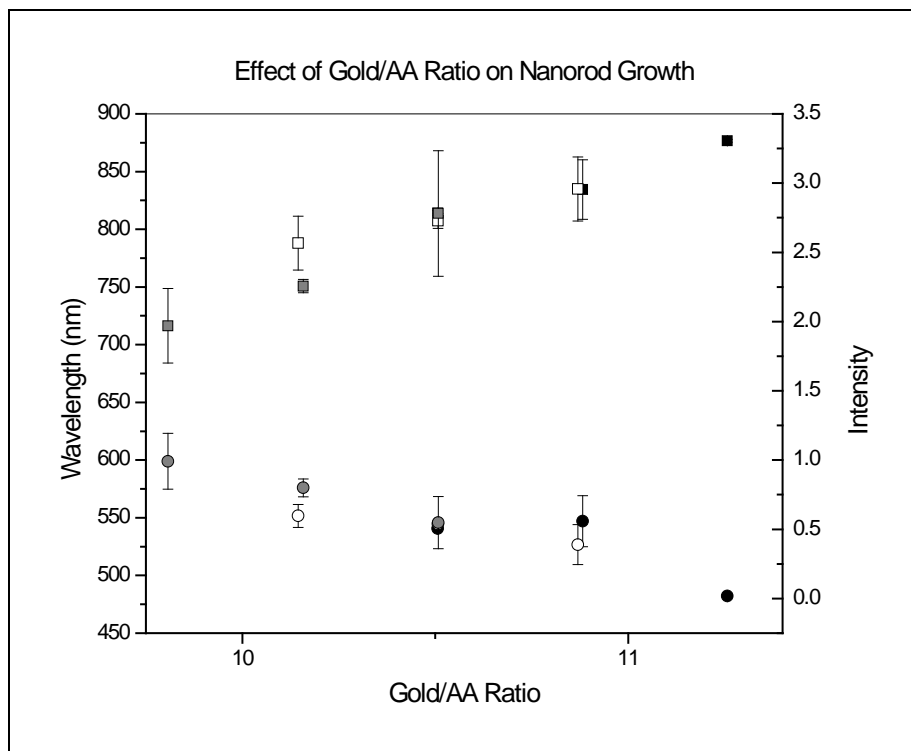
Figure III-11. Wavelength and absorption values for the longitudinal plasmon peak of nanorods grown with variations in chloroauric acid to ascorbic acid ratio in nanorod growth. Square symbols indicate wavelength while circles indicate intensity. Dark symbols indicate 53.3 μL ascorbic acid, open symbols indicate 55.2 μL, and grey symbols indicate 57.1 μL..

Intensity decreases with increasing ratio. This could indicate that fewer nanorods are grown, especially as wavelength increases. In addition, when analyzing the data points for when the ratio is the same, but reagent volumes increase, there is no visible difference in wavelength or absorbance intensity values. This means that increasing amounts of gold do not wholly account for larger aspect ratio nanorods, as some literature results contend.

Silver Nitrate

Literature contends that the addition of silver nitrate improves yield and tuning capability of gold nanorods, while at the same time, reducing the aspect ratio by two or three times. The role of silver nitrate in the seed-mediated growth of gold nanorods has always been a subject of

theory and conjecture, with no proof of how silver ions stabilize nanorod growth or why this stabilization results in smaller aspect ratio nanorods. One possible explanation occurs with the theory of silver combination with loose bromine from the CTAB [75]. This combination adsorbs to the surface of the nanorods during growth, both to the outer surface, stabilizing nanorods and prohibiting other shapes, and to the ends, capping growth at shorter lengths.

The silver nitrate amount was varied from 50 to 210 μL, at intervals of 20 μL. In literature, research groups suggest that as silver nitrate concentration is increased, wavelength values hit a peak value before decreasing again. In addition, it is believed that intensity of absorption will increase for the longitudinal plasmon peak.

As can be seen in Figure III-12, absorption intensity can be observed to actually reach a peak at 130 μL, meaning that this is the point at which stabilization due to the silver nitrate reaches peak efficiency. While a direct link cannot be made between concentrations of different wavelengths, the fact there is a peak suggests that there is higher stabilization. Before this point, the nanorods can generally be said to absorb at similar wavelengths. Thus, if the absorbance increases to a maximum value, then more nanorods can be assumed to be present. After this point, due to a decrease in wavelength, either fewer nanorods are produced or there are similar amounts of nanorods with smaller aspect ratios. Because the wavelength value increases, again, however, the aspect ratio is known to have increased, resulting in the conclusion that fewer nanorods actually are produced after the peak value. In addition, two peaks are observed in the absorption wavelength for the longitudinal absorption. While this effect is not yet fully understood, it is possible that this occurs when the intensity begins to

decrease. As the stability of the nanorods due to the silver ions begins to decrease, the growth of the nanorods reverts back to how growth occurs with no or less silver ions present. In that case, higher-aspect-ratio nanorods are grown, with less stable properties and a broader spectrum of sizes [127].
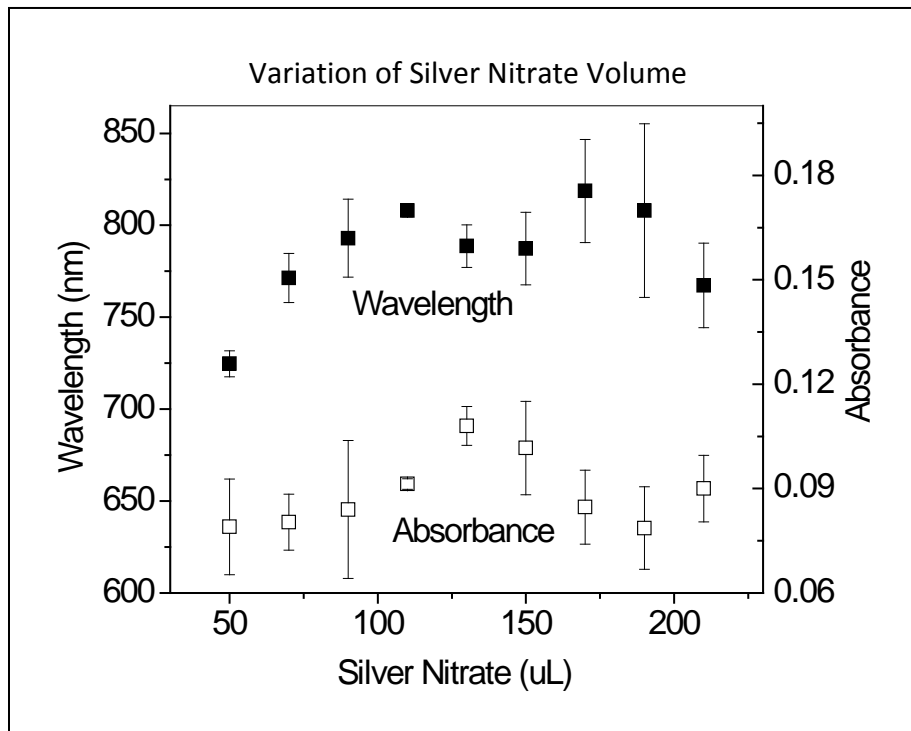
Figure III-12. Wavelength and absorption value trends with variations in silver nitrate concentration.

Literature only suggests an increase in yield potential with increasing silver nitrate amounts. Results here suggest that absorption intensity actually reaches a peak, with a complicated relationship between silver nitrate interaction and stability of nanorod growth.

CONCLUSIONS

Studies regarding the roles of reagent amounts on the growth of gold nanorods utilizing the seed-mediated synthesis technique have been undertaken. In particular, these studies have focused on the reagents in the seed preparation and nanorod growth. Within seed preparation, chloroauric acid, the gold ion source, has been shown to play a crucial role in seed size, with larger seeds occurring with increased amounts of chloroauric acid. This results in shorter-aspect-ratio nanorods due to larger diameter of starting seed templates. In addition, temperature of seed growth on final nanorod properties was examined. It has been found that with increased temperature, resultant nanorods have smaller aspect ratios.

Concerning nanorod growth, the added amounts of seed solution, chloroauric acid, ascorbic acid, the ratio between the two previous, and silver nitrate were examined. Differing amounts of seed solution added to the nanorod growth clearly demonstrated that larger amount of seeds present will result in smaller aspect-ratio nanorods. This occurs due to the availability of gold ions with increasing amounts of seed spheres. Chloroauric acid and ascorbic acid have been confirmed to be very interrelated, with mirror image results of both wavelength and absorption intensity. Too many gold ions or too little ascorbic acid will result in no nanorods grown at all. In addition, the ratio between the two has been shown to have a critical role on growth, with a steady increase in wavelength and decrease in intensity for absorption with increase in ratio. The role of silver nitrate is shown to be complicated, not surprising considering that the role of silver ions in the mechanism of growth is not yet agreed upon. Two wavelength peaks were characterized, with increasing and decreasing stability of CTAB micelles a likely explanation.

CHAPTER IV

SHAPE MEMORY BEHAVIOR OF POLYURETHANE/GOLD NANOCOMPOSITES

INTRODUCTION

Shape memory polymers, as mentioned, are one type of smart material. They utilize a switching temperature, which is just a critical temperature in the thermal properties of the polymer, to allow the material to deform from a temporary, strained shape back into a permanent, fixed shape [142-144]. For the purposes of this chapter, this critical temperature is the melting temperature of one phase of commercial polyurethane. This phase is the soft phase with the lower melting transition of the two phases, the soft and hard. Polyurethane shape memory polymers are considered to be the most responsive type of shape memory polymer and, being a common type of segmented shape memory polymer, are, by far, the easiest to control [145-146].

Polyurethane is synthesized through the condensation polymerization of a diisocyanate and a high molecular weight diol. A chain extender is then used to create the long chains needed, usually a low-molecular weight diol. Thus, the polymer is divided into two main segments: the long-chain high molecular weight diol, which is the soft phase, and the diisocyanate and chain-extending low molecular weight diol, which acts as the hard or rigid phase [173]. The mechanism of the shape memory transition involves the movement of the soft phase polymer chains. As the soft phase is melted, the hard, rigid phase is capable of springing back to its

original shape. Before melting, the crystalline form of the soft phase prevented this spring movement [174-175].

There are many different applications for shape memory polymers, as mentioned in Chapter I. There are also some applications which are not necessarily applicable for the traditional direct application of heat. These applications can include space technologies and especially medical devices. In space, the application of heat is not possible due to the presence of a vacuum. With respect to medical devices, the application of heat to the human body would often seem undesirable, unless it is very localized and low intensity. Regardless, an alternative form of triggering in which the body is not affected at all is desired.

This chapter investigates such an alternative form. Using gold nanorods, as detailed in Chapter III, a near-infrared laser will be utilized along with the nanorods' photothermal effect. The nanorods are incorporated into the polyurethane shape memory polymer and localized heat within the shape memory nanocomposite will be produced. This localized heat will then be used to trigger the shape memory effect. Thus, no heat would need to be applied to the body, as it would be produced indirectly from within the implanted medical device. The benefit of this technique is that near-infrared light, a range of wavelength that is invisible to the human body and passes through with no harm, is used [190].

This type of shape memory application has never before been examined, thus many of the steps have never been studied. First, the isolation and stability of the gold nanorods grown in Chapter III is examined. Due to the necessities of a non-aqueous solvent for polyurethane, the

nanorods have to be isolated and stabilized in a non-aqueous solution instead of the aqueous growth solution. Challenges include nanorod centrifugation without damage, removal of excess CTAB without agglomeration, and stabilization of the micelles. Next, the photothermal properties of the nanorods are explored in order to understand the possible control over heat production and eventual shape memory behavior. The shape memory polyurethanes are next examined, with respect to their thermal properties and shape memory behavior. Finally, the nanorods are incorporated into the polyurethane and the effects of the incorporation on the inherent properties, thermal, mechanical, shape memory, etc., of the polymer are examined. Following this, near-infrared light is utilized to determine the feasibility of triggering the shape memory effect with light and the many aspects of that triggering that can be manipulated in order to control the behavior of these novel nanocomposites.

MATERIALS AND METHODS

Isolation and Stability of Gold Nanorods

To isolate the nanorods from the growth solution, centrifugation occurred in a Beckman Coulter Microfuge 16. The typical time for centrifugation was 10 minutes and the typical speed was 14,462 xg. The centrifugation speed was varied, however, to test for minimum speed to isolate nanorods. These varied speeds were 0; 1,844; 4,722; 8,928; and 14,462 xg. In addition, the times were varied as well, with the times of 0, 8, 12, 16, and 20 minutes.

Typically, to remove excess CTAB from the system, washing cycles with water were utilized. The solution was centrifuged according to previous specifications and water was removed from the top of the vials. Normally, the amount was 1.8 mL of supernatant removed and the same

amount of water replaced. Tests were performed, however, of how much to remove and how many times to perform a washing cycle. Removal amounts ranged from 0.5 to 1.95 mL and the number of washing cycles varied from none to four. Regardless, supernatant was removed by careful pipette actions so as not to disturb the nanorods layered at the bottom of the vial.

To stabilize the nanorods as excess CTAB were being removed, polyacrylic acid (PAA), 35 wt.% solution in water and purchased from Sigma-Aldrich, was added by the same way that water was added in the washing steps. The PAA solution was created with 1 g of PAA in 1000 mL of DI water. Normally, 1.8 mL of the supernatant after centrifugation was discarded and 1.8 mL of the PAA solution was added. Tests were performed to determine how many washes were performed before and after the PAA step as well as how many PAA steps were included. There were as many as 3 washes before and as many as three washes afterward. There were also as many as three PAA steps.
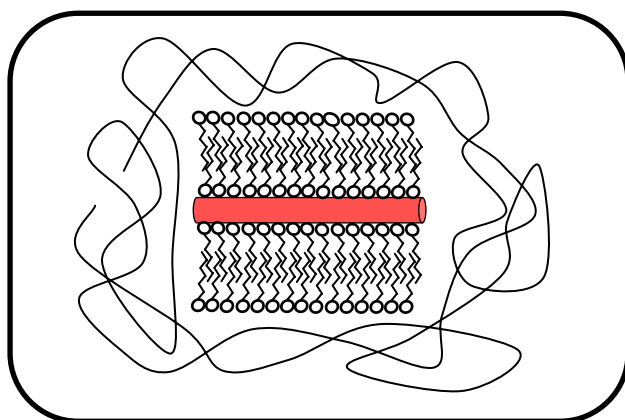
Figure IV-1. Representation of the stabilization of nanorods by PAA.

Incorporation into the Shape Memory Polyurethane

Nanorod incorporation into the shape memory polyurethane involved the use of centrifugation to stabilize the nanorods without excess CTAB and water. A separate method for isolating the rods was undertaken for when adding nanorods to the polyurethane. First, the solution of one growth solution was separated into five 2 mL centrifuge vials. The vials were centrifuged for 10 minutes at 14,462 xg and 1.8 mL of the supernatant was removed from each vial and discarded. 1.8 mL of DI water was replaced into each vial. Centrifugation took place again for the same time and at the same speed. Once again, 1.8 mL of the supernatant was removed and replaced by 1.8 mL of DI water. The centrifugation process was repeated one last time. The 0.2 mL of the bottom of the vial, including the nanorods, were then removed and recombined into a single container.
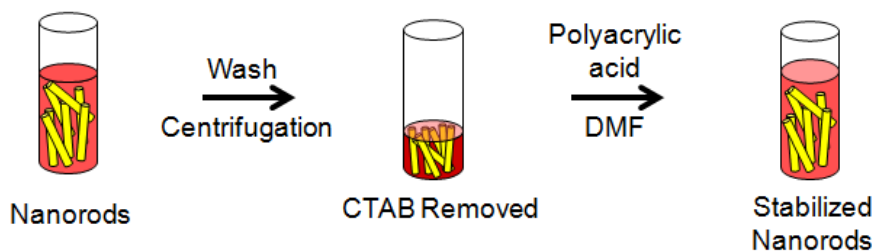
Figure IV-2. Nanorod Stabilization.

200 g of polyacrylic acid was added and mixed, followed by 15 mL of DMF. It was noticed that the solution warmed slightly after the addition of the DMF. Because the polyurethane will not accept water, the water was removed by evaporation. The bottom of the vial containing the solution was submerged into an oil bath until the level of the oil bath was above the level of the solution. The oil bath was then heated to 80°C for eight hours, after which the water

evaporated, leaving PAA-coated nanorods suspended in DMF. DMF was then added to obtain a 15 mL solution.

The final solution was added to 3.15 grams of the polyurethane pellets and then mixed in an agitation mixer. Finally, the mixture of polyurethane and gold nanorods was cast into the Teflon mold and the solvent allowed to evaporate in an 80°C oven.
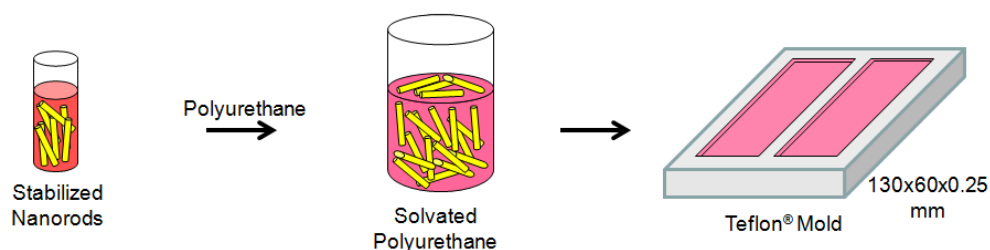
Figure IV-3. Addition of the nanorods to the polyurethane.

When the contents of more than one growth solution were to be added to a film, the process for preparing the nanorods was the same. The washing and stabilizing steps were performed for all solutions. The difference occurred when recombining the centrifuge vials. If more than one growth was being prepared, then all of the solutions were recombined together and PAA was added at 200 μL per growth solution (for example, 400 μL for two growth solutions). Then, 15 mL of DMF was added to finish the process. Following this, the procedure was, once again, the same in regards to addition to the polyurethane.

TECHNIQUES

UV-vis Spectrophotometry

Analysis under UV-vis was performed in the same manner as in Chapter III. The UV-vis was only used when examining the effectiveness of isolation and stabilization of the nanorods.

Differential Scanning Calorimetry

Thermal analysis was performed with a temperature-modulated differential scanning calorimeter (TA Instrument DSC Q2000). The modulated function of this DSC was utilized because of the presence of multiple melting and crystallization endotherms. Most procedures involved a multi-cycle program. The temperature was equilibrated at -80°C and then increased to 100°C at a rate of 10°C/min. A modulation of ±1.0°C every minute was used. The sample was then cooled back to -80°C at a rate of 10°C/min. This first cycle corresponded to the molecular rearrangement that is always present in the first heating of these types of polyurethanes. A second cycle was then utilized to collect the useable data. The sample was once again heated to 100°C at 10°C/min, followed by cooling to -80°C at 10°C/min. Finally, the sample was heated to 200°C at 10°C/min, followed by cooling back down to -80°C at 10°C/min. The second cycle captured data concerning the melting and crystallization of the soft segment of the polyurethane, while the third cycle captured the data corresponding to the melting and crystallization of the hard segment.

Tensile Analysis

Stress/Strain measurements was obtained using a Dynamic Mechanical Analyzer (DMA; TA Instruments DMA RSA III). The gauge length was 5 mm. Stress and strain values were found

at multiple temperatures. The film was elongated to a value of 300% strain at a rate of 0.06667 mm/sec. The slope of the initial part of the curve was considered the modulus.

Shape Memory Behavior

Thermal cyclic tests without the laser were performed on the Dynamic Mechanical Analyzer (DMA; TA Instruments DMA RSA III). These tests examined the shape memory behavior of the films using traditional direct heating. Strips of the shape memory polymer, pure and incorporated with nanorods, were placed inside the DMA, with a gauge length of 5 mm. The strips were then conditioned to the test temperature, normally 60°C, for two minutes. This temperature was above the melting temperature of the soft segment of the polyurethane. The film was then elongated to a value of 300% strain at a rate of 0.06667 mm/sec. The strips were then rapidly cooled to -25°C using the liquid nitrogen cooling function of the DMA and kept at this temperature for two minutes. This temperature was below the melting temperature of the soft segment. The sample was then unloaded at a speed of 0.06667 mm/sec, while still at -25°C. A wait time of ten minutes was observed, and then the cycle then began again, with temperature conditioning at 60°C for two minutes, followed by the same elongation, cooling, unloading procedures, and wait time. Depending on the test, as few as three, or as many as ten, of these cycles were utilized for one polyurethane strip. Figure IV-4 is a representation of the data gathered from this methodology.
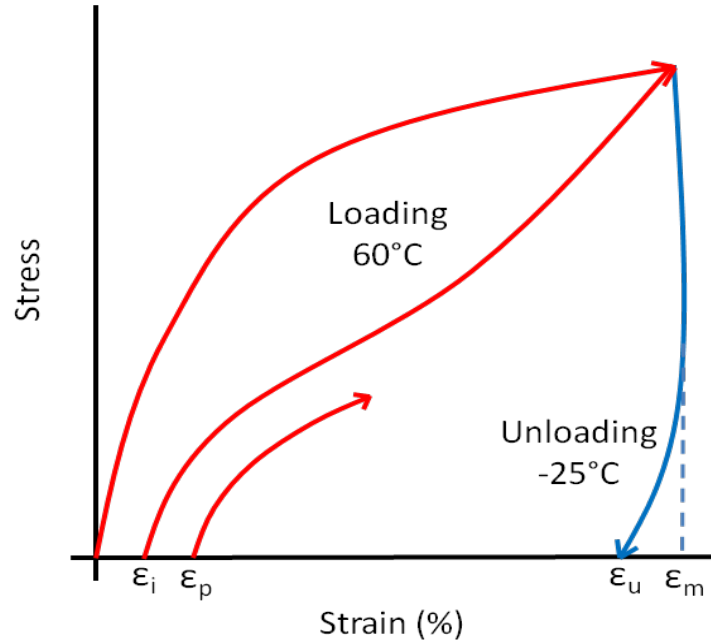
Figure IV-4. Representation of stress vs. strain graph for shape memory behavior.

Two valuable shape memory behavior parameters were gathered from these cycles. The first is called fixity, which is the ability of the polyurethane to keep its strain upon unloading. It is calculated according to Equation 4.

$$Fixity\ (\%) = \frac{\varepsilon_u}{\varepsilon_m}\ \text{x}\ 100 \tag{4}$$

The second parameter is called recovery, or the residual strain present in the polyurethane after the next heating cycle is applied. It is calculated according to Equation 5.

$$Recovery\ (\%) = \frac{\varepsilon_m - \varepsilon_p}{\varepsilon_m - \varepsilon_i}\ \text{x}\ 100 \tag{5}$$

where ε_m is the maximum strain in the cycle (300%), ε_u is the residual strain after unloading, ε_p is the residual strain after recovery, and ε_i is the residual strain after recovery of the previous cycle. The first cycle of Fig IV-4 is the characteristically different cycle of this type of polyurethane and is usually disregarded for data.

Shape Memory Behavior with the Laser

First, the shape memory effect test was preceded by a photothermal test involving nanorods still in the growth solution. This test would prove that heating is possible and the shape memory effect could be induced. The setup for this test included setting up a LD-WL206 infrared laser at 1.32 watts and a wavelength of 808nm, from Changchun New Industries Optoelectronics Tech Co Ltd. The laser was arranged to shine through a poly(methyl methacrylate) macrocuvette at a range of 3 mm. Heat produced as the laser interacts with the rod was measured by a thermocouple placed in the center of the macrocuvette. Temperature measurements were recorded every 30 seconds for 30 minutes.

Shape memory behavior initiated by the laser utilized a very similar procedure to when using direct heat. Once again, the thermal cyclic tests were performed on the Dynamic Mechanical Analyzer (DMA; TA Instruments DMA RSA III). Strips of the shape memory polymer, pure and incorporated with nanorods, were placed inside the DMA, with a gauge length of 5 mm. The strips were then conditioned to the test temperature, normally 60°C, for two minutes. The film was then elongated to a value of 300% strain at a rate of 0.06667 mm/min. The strips were then rapidly cooled to -25°C using the liquid nitrogen cooling function of the DMA and kept at this temperature for two minutes. This temperature is below the melting temperature of the soft segment. The sample was then unloaded at a speed of 0.06667 mm/min, while still at -25°C. A wait time of ten minutes was observed, and then the cycle then began again, with temperature conditioning at 60°C for two minutes, followed by the same elongation, cooling, and unloading procedures, and wait time. This type of cycle was normally performed three times, to get a baseline as to how the film responds to traditional heating. Following that, laser

cycles were analyzed, as many as eight or nine. To test with the laser, the only part of the procedure that changed was the heating and elongation part. When the heating cycle began from the previous cooling cycle, the furnace was opened and the LD-WL206 infrared laser at various power settings and distances, depending on the test, was shown onto the film. This initiated recovery. Following two minutes of the recovery, the strip was then elongated to 300% at 0.06667 mm/min with the laser still shining on the strip. As soon as a strain of 300% was reached, the furnace was closed again, and the traditional cooling cycle took over. Figure IV-5 is a representation of this methodology.

In panel D:

$$\text{Fixity (\%)} = \frac{\varepsilon_u}{\varepsilon_m} \times 100$$

$$\text{Recovery (\%)} = \frac{\varepsilon_m - \varepsilon_p}{\varepsilon_m - \varepsilon_i} \times 100$$

$$\varepsilon_m = 300\%$$
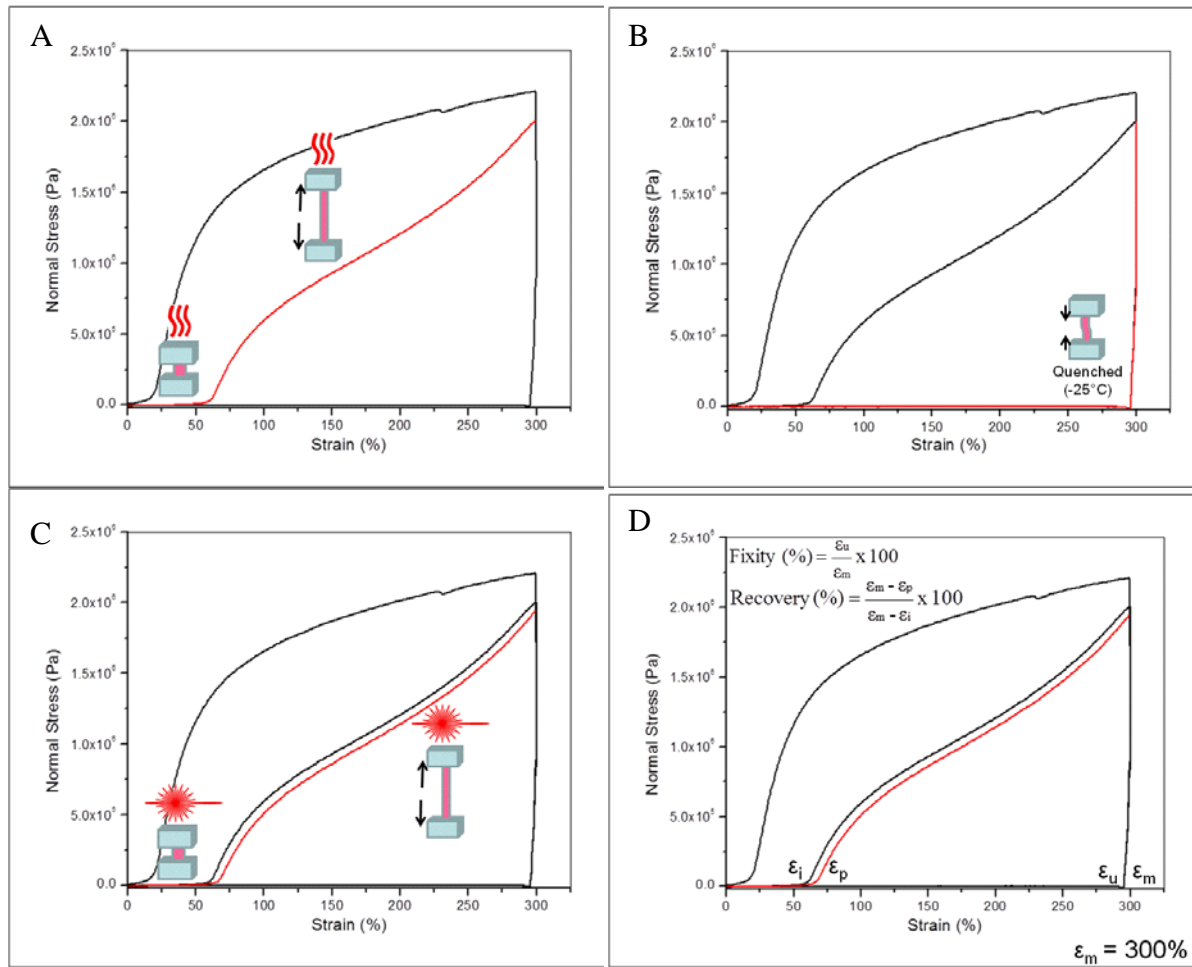
Figure IV-5. Representation of stress vs. strain graph for laser initiated shape memory behavior. A involves the use of direct heat from the furnace. C involves the use of the laser.

When calculating the fixity and recovery, the methodology was the same. The first cycle was disregarded, and fixity and recovery were calculated with ε_i from the previous curve. Alternatively, the recovery was also calculated based on the ε_i from the last oven curve. This was determined as relative recovery and allowed for a comparison of recoveries from direct heat and the laser.

RESULTS AND DISCUSSION

Isolation and Stability of Gold Nanorods

Due to the constraints of the type of shape memory polymer used for this research, certain reagents in use had to be removed before incorporation into the polymer. CTAB was used to stabilize the polymer during growth. After growth, however, there was an excess amount of CTAB in the system which needed to be removed. Once this occurred, however, there was not enough CTAB left in the system to maintain the micelles and stabilize the rods. To prevent this, another polymer was introduced to the system in solution form. The polymer chains coated the micelles, preventing instability from occurring when removing the rest of the CTAB.

Centrifugation

Centrifugation is a necessary step in separating the nanorods from the excess surfactant. To understand if the centrifugation was damaging the nanorods, a study was performed during which a nanorod solution was centrifuged and resuspended four times. During each resuspension, the nanorods were analyzed by UV-vis. Results indicate that neither wavelength nor absorption intensity changes, indicating that centrifugation does not damage the nanotubes.

112

Next, a study was undertaken to examine at what speeds and times were needed to centrifuge the nanotube solution in order to achieve maximum removal of the nanotubes from the supernatant. Figure IV-6 displays results for testing speed in xg, with a constant time of ten minutes. For this test, CTAB supernatant was removed after centrifugation and then replaced with fresh CTAB solution and the nanorods resuspended. The data at 0 xg is the baseline, or the nanorods not centrifuged at all. It can be seen that at lower speeds, there was not enough centrifugation to separate the nanorods from the supernatant and significant amounts of nanorods were lost in supernatant removal, as seen by the absorption intensity. At higher speeds, however, a vast majority of the nanorods were brought to the bottom of the vial during centrifugation. Wavelength value shows no distinct difference, meaning that rods were not damaged during centrifugation. If there was damage, then wavelength would decrease, due to decreasing aspect ratio. It can be determined that higher speeds are more desirable when separating the nanorods from the excess CTAB.
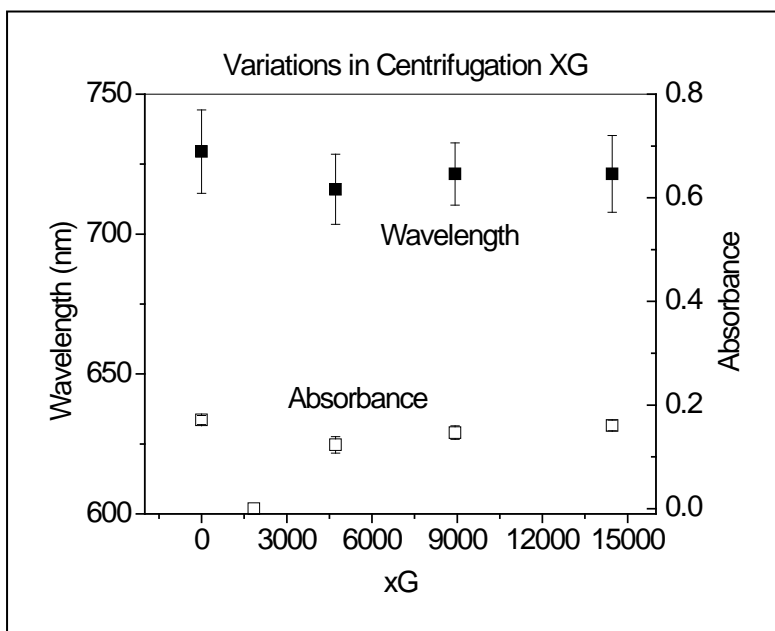
Figure IV-6. Variation in centrifugation speed. A speed of zero xg signifies no centrifugation and is the control of the test.

Figure IV-7 displays variation in time of centrifuge, at a constant speed of 14,462 xg. In this case, results show that there is no significant difference for different times of centrifugation, especially at high speeds. Once again, the data at 0 minutes indicates a control where the nanorod solution has not been centrifuged. This indicates that, while high speeds are necessary to separate the nanotubes, long times are not necessary and result in the same degree of separation as shorter times.
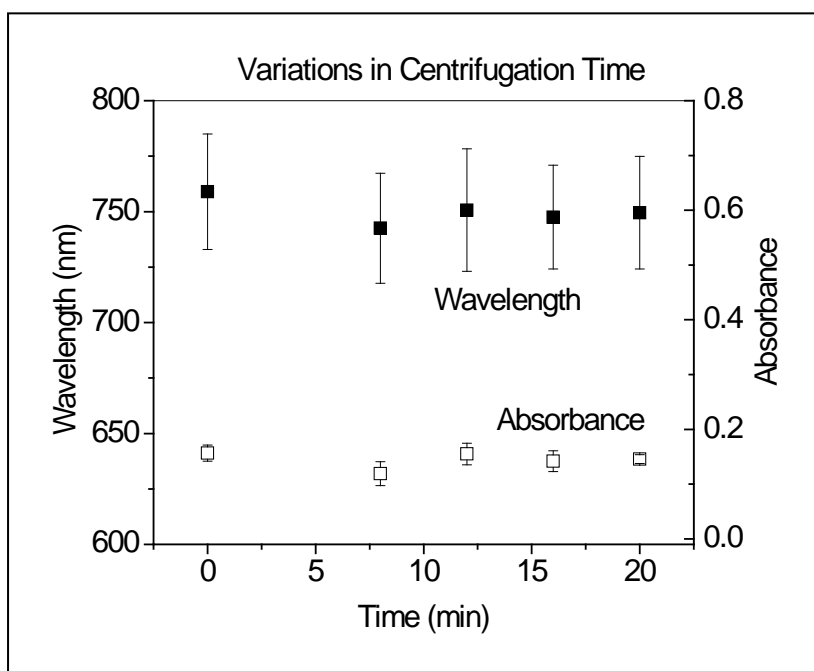
Figure IV-7. Variation in the centrifugation time. Time of zero minutes signifies no centrifugation and is the control of the test.

Elimination of Excess CTAB

The ideal process for removal of CTAB is through washing cycles. It is known, though, that at a critical point in washing, there remains not enough CTAB to stabilize the nanorods. To discover this point, washing cycles were performed in a series until nanorods could not be measured after each washing cycle and resuspension. 1.8 mL of supernatant were removed each time, with 1.8 mL of DI water added. Results are shown in Figure IV-8. Each successive

washing cycle brought a decrease in wavelength absorption value and absorption intensity. Logically, this makes sense. As CTAB is removed, nanorods are accidentally removed with it, even with careful centrifugation. In addition, with the removal of more and more CTAB, there is less to support the nanorods and less to keep the nanorods apart. Thus, nanorods begin to aggregate, effectively lowering the aspect ratio and lowering the absorption wavelength value. Eventually, the nanorods completely aggregated into a dark pellet that could not be resuspended. This is seen in literature as well. Becker et al. demonstrated the fact that after just two washes, nanorods agglomerated due to CTAB bilayer degradation [80]. While the study reported here demonstrates aggregation after three washes, Becker et al. utilized a less concentrated CTAB solution for growth, thus resulting in agglomeration after fewer centrifugation cycles.
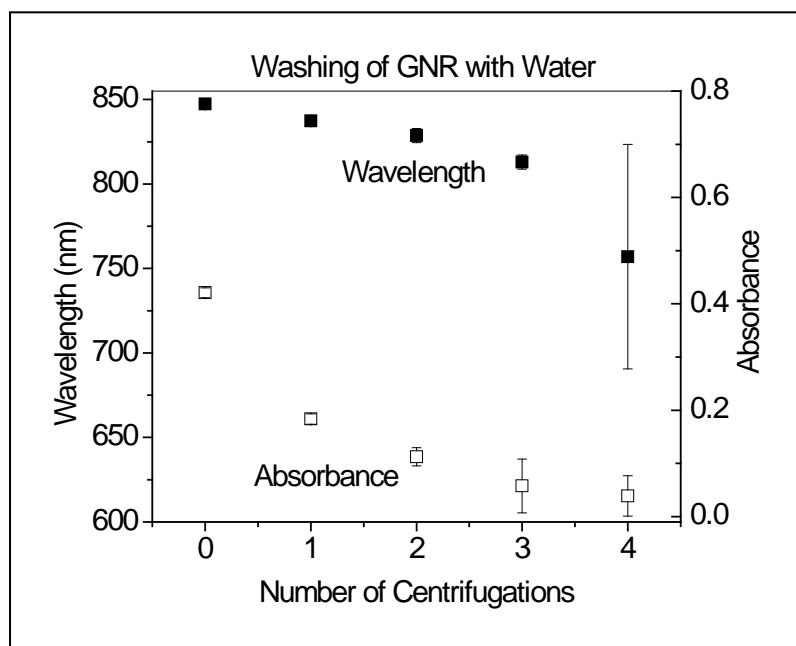
Figure IV-8. Number of washes performed on the nanorod solution. Zero centrifugations signify no centrifugation and is the control of the test.

Stabilization via Polymer Molecules

There are many factors to consider when coating the micelles with polyacrylic acid to stabilize them upon removal of excess CTAB. For one, how many washes with DI water need to be performed before PAA application? Should there be washes afterward?   How many applications of PAA to one solution of nanorods should there be?   All of these questions involve trying to stabilize the nanorods for inclusion into the shape memory polymer while also keeping the desired properties of the nanorods. Multiple studies have been performed. The first set of studies involved testing how many washes should be performed before adding PAA. Figure IV-9 details the results of each number of washes followed by the addition of PAA.
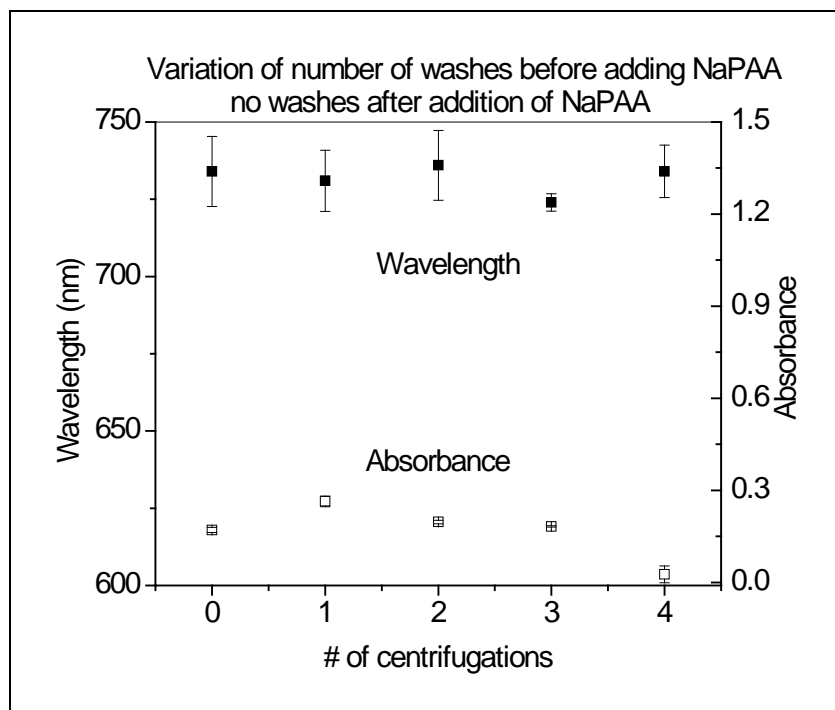
Figure IV-9. Number of washes before addition of PAA. Zero centrifugations signify no centrifugation and is the control of the test.

It can be seen that after the addition of PAA, there is a small rise in absorption intensity. This phenomenon is not yet understood, although has been seen before in the literature [191]. Regardless, wavelength fluctuates only slightly, while absorption intensity gradually decreases. This can mean that, once again, washes begin to destabilize the rods. No conclusion can be drawn from this study as to when PAA needs to be added to the system.

Another study investigated the variation of number of washes before and after addition of PAA. The total number of washes was kept the same throughout and there was only one addition of PAA. This means that the data series includes no centrifugations, addition of PAA followed by three washes, one wash followed by addition of PAA and two washes, two washes followed by addition of PAA and one wash, and three washes followed by addition of PAA. Results can be seen in Figure IV-10. Interestingly, addition of PAA, followed by three washes, results in complete agglomeration of the nanorods. It is not known if this was caused by early addition of PAA with no washes beforehand or if it was an effect of three washes afterward, although it took four washes in a row to effect full agglomeration in earlier tests. It is more likely that the early introduction of PAA results in a bubble effect, where large amounts of both nanorods and CTAB are stabilized together by the PAA, resulting in large agglomeration.
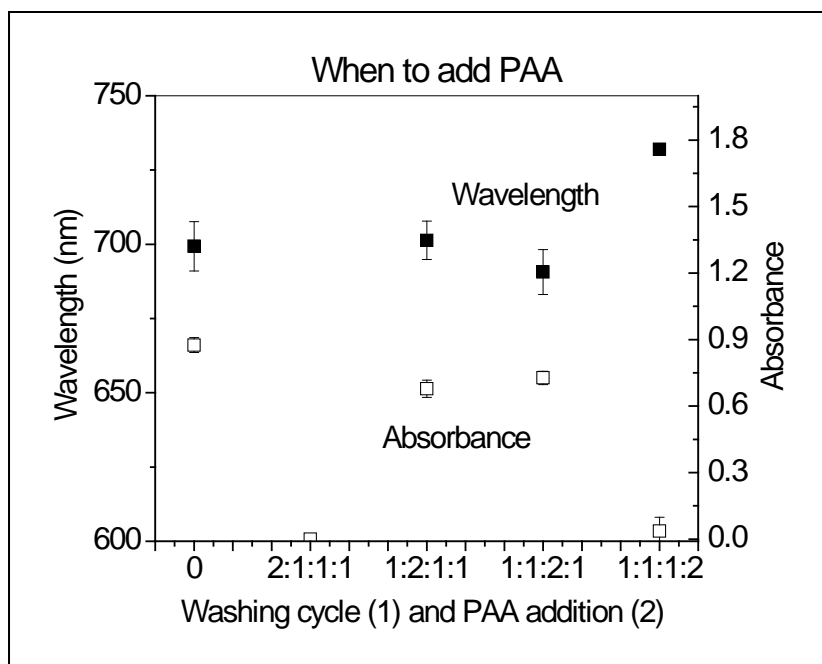
Figure IV-10. Longitudinal plasmon peak properties of washes before and after addition of PAA. Zero centrifugations signify no centrifugation and is the control of the test.

Additionally, three washes before addition of PAA also resulted in a large intensity drop, although the wavelength is still relatively high. Once again, the jump in the wavelength after PAA addition in relation to the control is still seen. Unusually, there are actually effects to the transverse plasmon peak in this experiment. Usually, this peak remains unchanged, especially in relation to the wavelength values. These effects can be seen in Figure IV-11.
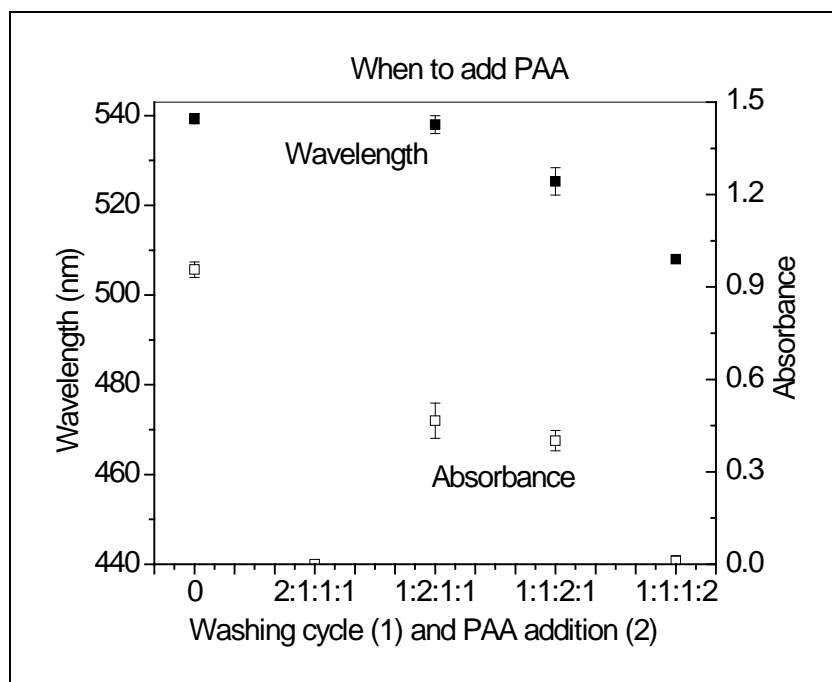
Figure IV-11. Transverse plasmon peak properties of washes before and after addition of PAA. Zero centrifugations signify no centrifugation and is the control of the test.

Absorbance intensity effects are the same, indicating the same conclusions. What is interesting, however, is that there is a red shift in the wavelength value with increasing number of washes before PAA addition and fewer washes afterward. Gole et al. supplies a possible explanation for this occurrence. While they did not test washing procedures, they discovered that thicker PAA shells resulted in larger peak wavelength values for the transverse plasmon peak [192]. This is due to the change in local refractive indices when moving from water to the PAA and the polymer absorption. Thus, in the constraints of this study, with more washes after the addition of the PAA, the layers stabilizing the nanorod are most likely thicker. This could result from larger amounts of CTAB removed with each washing process.

Photothermal Production of Heat

To ensure that the nanorods will produce heat by photothermal treatment inside the polyurethane, heat measurement of pure nanorods was initially studied. Nanorods were left in growth solution, after verifying that CTAB provided no additional heating effect. A laser of known wavelength was shone through a cuvette and temperature change was recorded by thermocouple. Heat production occurred very rapidly. To analyze the heat production, different formulations of nanorods were studied. Changes in reagent concentration served to create these different formulations, since it had already been established that varied reagent concentrations resulted in different and largely predictable nanorod changes. Figure IV-12 displays the results of heat produced from varied concentrations of silver nitrate.
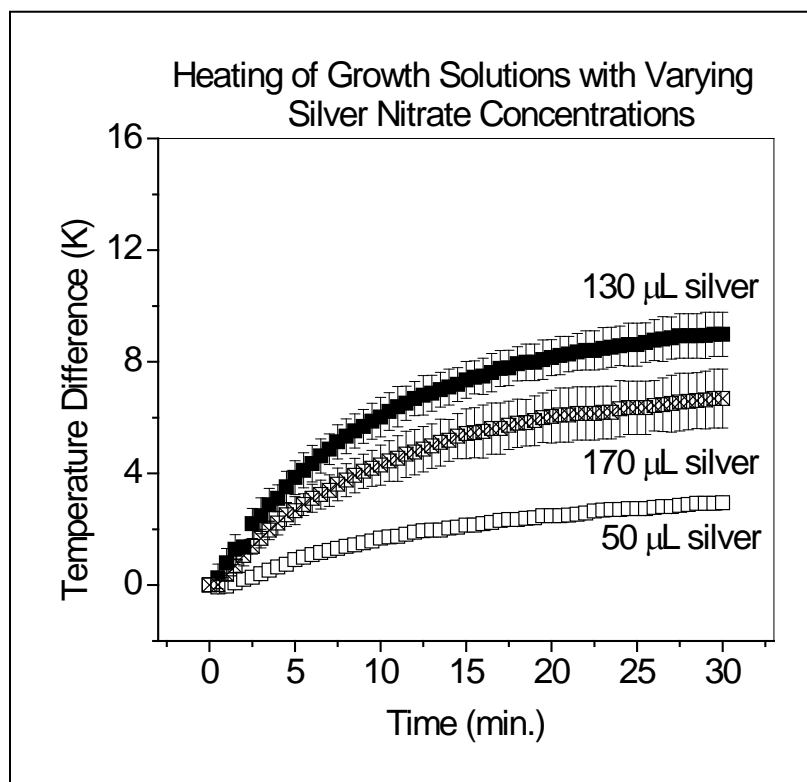
Figure IV-12. Temperature change as a result of photothermal heating of gold nanorods grown with different amounts of silver nitrate.

There are definite differences in heat production. Examining these results, it can be seen that the nanorods made with 130 μL of silver nitrate have the highest heating rate for the solution. This is due to the fact that the 130 μL variation has the highest absorption intensity at 808 nm, the wavelength of the laser, even though its peak wavelength is equidistant from 808 nm compared to the 170 μL variation. The absorbance value for the 130 μL variation is 0.103 and that for the 170 μL is 0.082. In addition, both are significantly higher in heat production than the 50 μL variation because its wavelength peak was much further away from 810 nm than either of the other two, and its absorbance at 808 nm is also much lower at 0.054.

Examining the plot in Figure IV-13, for heat production with relation to variation of seed amounts, similar results are documented.
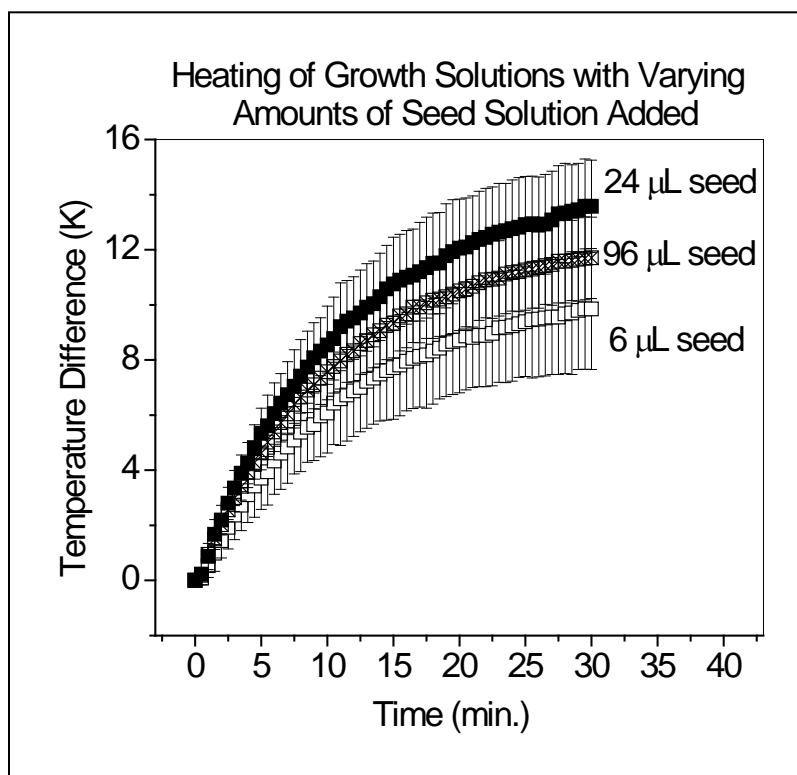
Figure IV-13. Temperature change as a result of photothermal heating of gold nanorods grown with different amounts of seed solution.

For the 6 μL variation, the absorbance at 808 nm is 0.253 and its peak wavelength is far from 808 nm. Similarly, the wavelength value for the 96 μL variation is closer to 810 nm than that of the 24 μL variation, but the absorption intensity of the 24 μL variation at 808 nm is once again higher, thus resulting in a higher heating effect due to an increased amount of nanorods (absorbance at 808 nm for the 96 μL variation is 0.341 and for the 24 μL variation is 0.353). Similar effects were described in studies performed by Wang et al., where the photothermal properties of multiple gold structures were compared [193]. When studying the gold nanorods, temperature differences in aqueous solutions were demonstrated to be up to 20°C, but with a higher concentration of gold and a higher-powered laser than with the current study. It was noted, however, that the gold structures that absorbed as close to the wavelength of the laser as possible, resulted in the highest heat production, giving support to the proposed explanation of temperature effects.

Shape Memory Polyurethanes

There are four commercial polyurethanes that were examined for the purpose of this research. Three were purchased from Irogran and include PS 455-203, A60E 4902, and A78E 4915 DP. The fourth was Pearlbond 508. For the purposes of this research, they have been renamed to SMPU 1, 2, 3, and 4, respectively. All four were tested for their thermal properties and their shape memory behavior for their viability.

Thermal Properties

The four polyurethanes in question were all examined in relation to their thermal properties, namely, their transition temperatures and enthalpies. These are the variables that make them viable as shape memory polyurethanes. The results are summarized in Table IV-1.

Table IV-1. Thermal Properties of Shape Memory Polyurethanes.

SMPU #	ΔH_{mSS} (J/g)	T_{mSS} (°C)	ΔH_{cSS} (J/g)	T_{cSS} (°C)	ΔH_{mHS} (J/g)	T_{mHS} (°C)	T_g (°C)
1	3.824	24.06	7.498	51.2	7.265	130.78	-44.64
2	0.9216	13.06	*	*	*	*	-49.16
3	*	*	*	*	4.585	134.4	-38.69
4	96.57	42.8	10.42	-6.71	*	*	*

ΔH is enthalpy, T_m is melting temperature, T_c is crystallization temperature, and T_g is the glass transition temperature. Subscripts "SS" and "HS" mean soft segment and hard segment, respectively. As can be seen, no soft segment melting temperature can be identified for SMPU 3, leaving this polyurethane as not viable for shape memory studies. In addition, the melting temperature for the soft segment of SMPU 4 is very high, with no visible hard segment melting temperature detected. This also leaves SMPU 4 unacceptable. Finally, SMPU 2 also has no detectable hard segment melting temperature. Its enthalpy of melting for the soft segment is also very low. With respect to thermal properties, SMPU 1 is much more acceptable. It has a reasonable soft segment melting temperature with high enough enthalpy to be a shape memory trigger.

Shape Memory Behavior

The four shape memory polymers were also tested for their shape memory behavior. Each polyurethane was solvent cast using DMF as the solvent to make a film. The standard DMA

test was utilized, but with a few differences. Instead of a heating temperature of 60°C, a 40°C heating temperature was used. Also, a -15°C quenching temperature was used instead of -25°C. The resulting shape memory data was gathered for each polyurethane and is displayed in Table IV-2.

Table IV-2. Shape Memory Behavior for polyurethanes.

SMPU #	Cycle #	Fixity (%)	Recovery (%)
1	1	99.65	*
	2	99.65	98.82
	3	99.65	98.33
	4	99.65	*
2	1	99.57	*
	2	99.57	98.29
	3	99.57	98.62
	4	99.57	*
3	1	99.45	*
	2	99.45	97.48
	3	99.45	97.71
	4	99.45	*

No data was collected for SMPU 4 due to the fact that the 40°C heating temperature was not high enough to reach the soft segment melting temperature. When tested in the DMA, the film slipped out of the jaws because there was not enough elasticity in the film. Of the three that showed shape memory behavior, however, the data was extremely similar. All three polyurethanes exhibited high and constant fixity values, meaning that when cooled, strain remained constant even when loading was released. In addition, all three exhibited high recovery rates related to the recovery of the previous recovery curve. SMPU 3 possessed slightly lower recovery values. Values are not shown for cycles 1 and 4 for each film because the first cycle has no previous cycle to compare to and the last cycle stopped at the cooling

phase, with no heating phase to calculate recovery. From both the thermal properties and shape memory behavior, SMPU 1 is chosen to continue the research. While there is no determinable difference in the shape memory behavior, the thermal properties of SMPU 1 are much more appropriate for this type of research.

Incorporation of Gold Nanorods

Gold nanorods were incorporated into the polyurethane films in six different concentrations. These concentrations stem from the amount of growth solutions that it takes to produce that exact number of gold nanorods. For example, one film was made with the nanorods grown with a quarter of a growth solution. This film is said to be a 0.25 film. Six films of varying concentrations were made: 0.25, 0.5, 1.5, 2, 3, and 5.

Films Created

Upon incorporation of the gold nanorods into the commercial polyurethane, a substantial color change was observed. Due to the fact that the DMF solution of nanorods has been observed to be a dull to vibrant red color, the films to which these solutions are added to take that hue as well. Of the six films of different concentrations made, all were observed to have the red coloration. What is interesting to note, however, is that as the concentration of nanorods in the films increase, the deeper and darker the red color becomes. While the film with 0.25 growth solutions appears almost colorless, with the only the slightest hint of red, the films made with 2, 3, and 5 growth solutions have a very dark coloration. This can be seen in Figure IV-14.
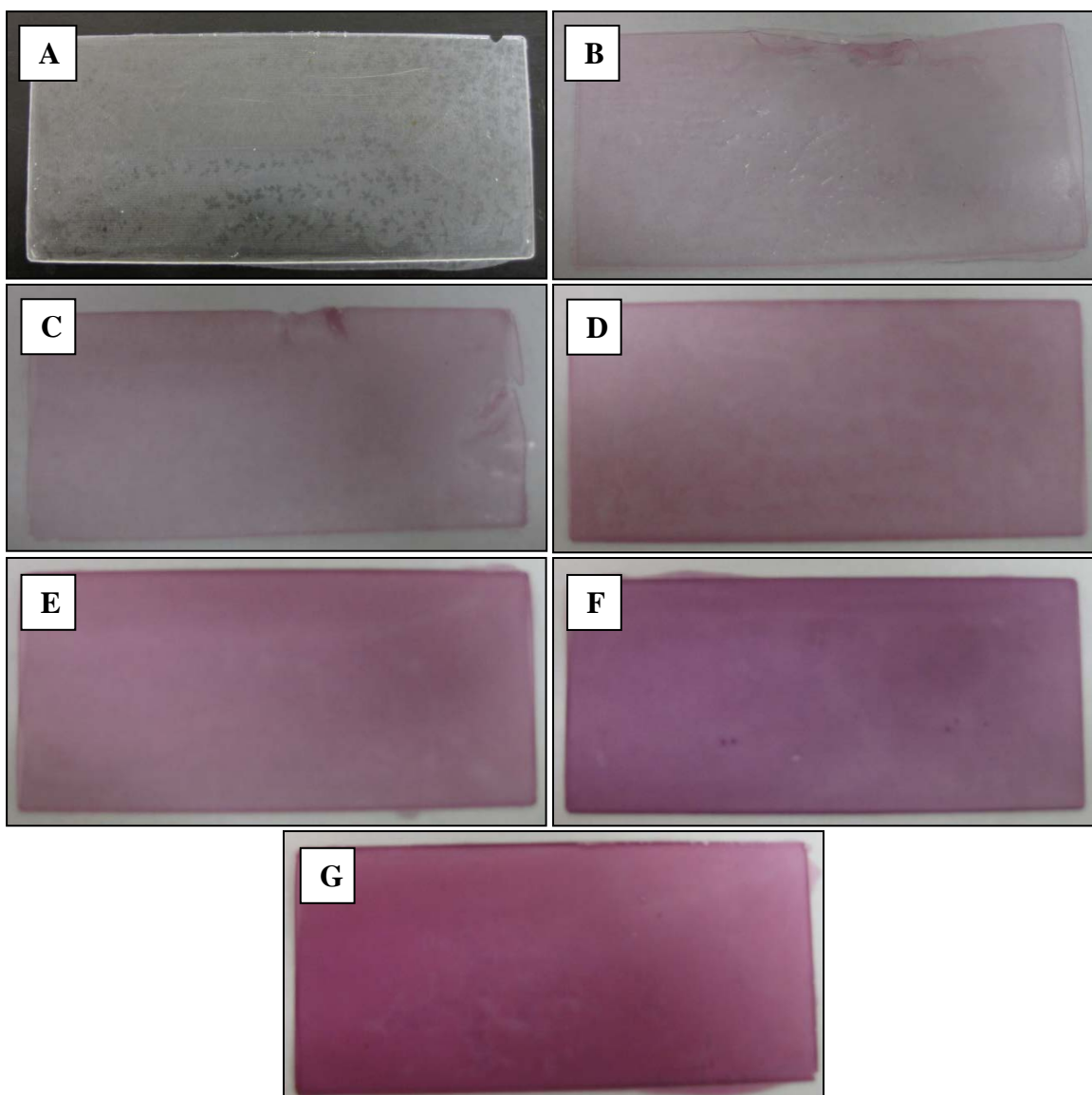
Figure IV-14. Polyurethane films incorporated with the nanorods from no growth solutions (A), 0.25 growth solutions (B), 0.5 growth solutions (C), 1.5 growth solutions (D), 2 growth solutions (E), 3 growth solutions (F), and 5 growth solutions (G)

In addition to the resultant color of the films, a difference in curing properties was noticed as well. The pure film and films with less than one growth solution in them cured very quickly, meaning that the DMF evaporated out during the solvent casting process at a quick rate. Indeed, the films were completely cured in less than twelve hours. The films with higher concentration, however, required a much longer time to cure. In fact, the film with five growth

solutions' worth of gold nanorods required as long as 48 hours for the DMF to completely evaporate. This observation could result, in part, due to the presence of a higher concentration of nanorods. With a higher concentration, there would be a more tortuous path for the escaping DMF to escape as it evaporates.

Thermal Properties

Thermal properties of the films were measured in order to determine if the incorporation of the gold nanorods affected the thermal properties inherent to the polyurethane. Normally, the incorporation of many nanoparticles can have a significant effect on these types of properties. The concentrations were so small, however, that there was not expected to be much difference between the films. All created films are compared to a film created of pure polyurethane. Table IV-3 displays the thermal properties measured by DSC.

Table IV-3. Thermal properties of gold nanocomposites.

Film (# of growth solutions in film)	T_g (°C)	T_{mSS} (°C)	ΔH_{mSS} (J/g)	T_{mHS} (°C)	ΔH_{mHS} (J/g)	T_c (°C)	ΔH_c (J/g)
0	-32.08	31.35	6.18	142.23	3.02	50.70	8.13
0.25	-35.51	30.60	5.35	142.87	3.27	50.79	7.27
0.5	-34.46	29.00	7.64	139.96	4.70	50.49	8.09
1.5	-36.80	30.82	7.36	141.77	3.43	49.89	7.31
2	-34.63	27.97	9.97	138.77	5.35	51.25	7.91
3	-37.32	29.64	9.67	140.06	4.14	50.14	9.11
5	-35.32	30.19	6.44	137.43	3.19	50.71	7.50

From the data in the table, it is necessary to review each set of data individually. The glass transition temperature is the lowest transition temperature measured for the films. Traditionally for polyurethanes, this temperature is a negative temperature. Indeed, the

temperature for the pure polyurethane film is about -32°C. If the glass transition temperatures for the other films are displayed graphically, as can be seen in Figure IV-15, there is no obvious trend in the temperatures.
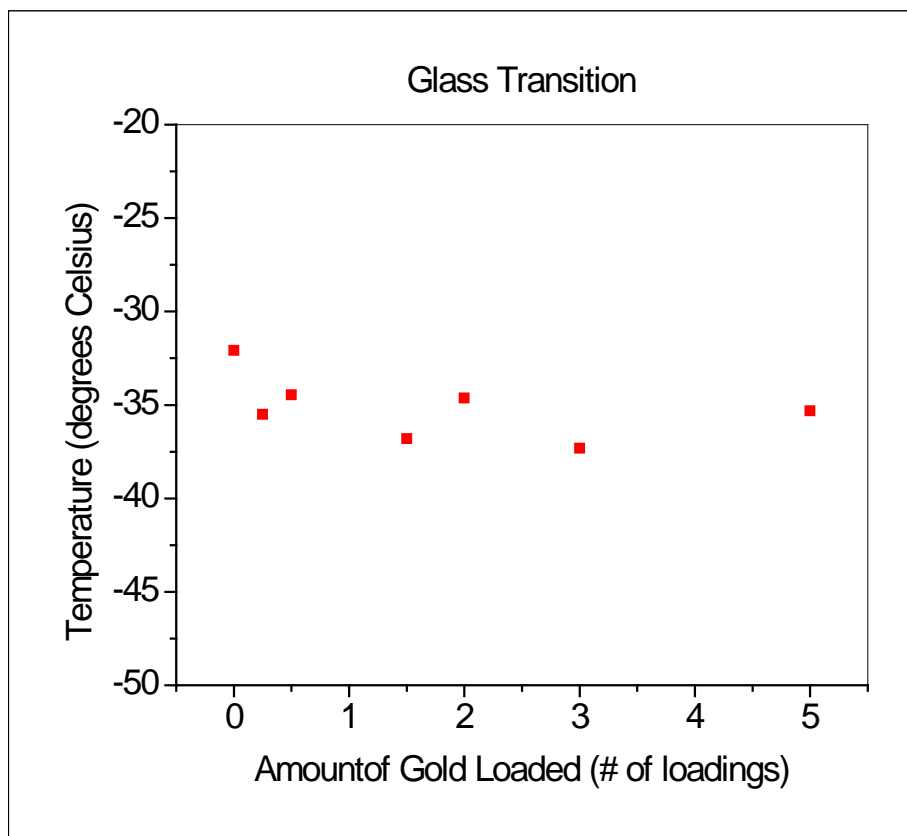
Figure IV-15. Glass transition temperatures of films with varying nanorod concentrations.

It can be inferred that there might be a slight drop in glass transition temperature when adding gold nanorods. This could be attributed to the conducting properties of the gold nanorods. The rods present may be able to more efficiently transfer heat, allowing for a lower transition temperature. Boucher et al. noticed a similar trend in decreasing glass transition temperature upon addition of gold nanorods [194]. They reasoned that the decrease in temperature could result from either conductive effects or from the hindrance of entanglement formation.

Furthermore, they wrote that this drop in glass transition temperature would become less noticeable with slower temperature ramps during measurement, leading the reader to believe that these effects could deal with temperature gradients within the sample.

Very similar results are seen with respect to crystallization properties. Included in Figure IV-16 are both the crystallization temperatures as well as the enthalpy of crystallization.
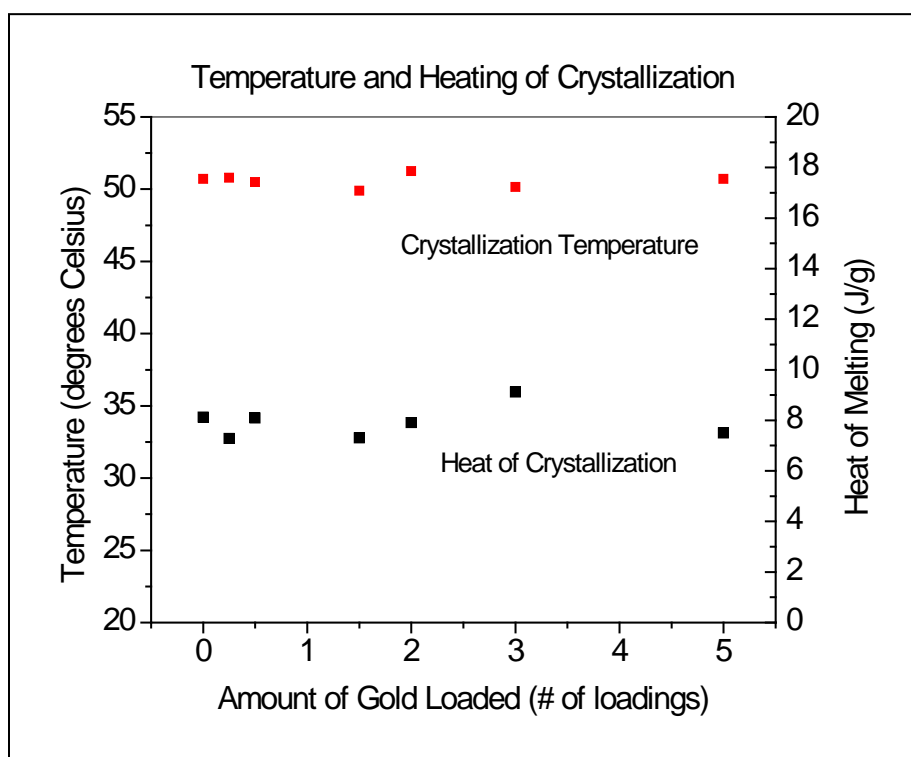
Figure IV-16. Crystallization temperatures and enthalpy of crystallization of films with varying nanorod concentrations.

While there is slight variation in the enthalpy of crystallization, there is no significant change to either parameter. This can mean that the introduction of the nanorods to the polyurethane has no effect on the formation of crystalline regions within the polymer. This is important, as

the crystalline regions and their transition to amorphous regions are the cause of shape memory behavior in this type of polyurethane.

The two final transitions, the soft and hard segment melting temperatures, are the most crucial transitions for the shape memory behavior. The soft segment transition is responsible for the actual triggering of movement as the crystalline regions melt, while the hard segment provides the rigidity needed for the elastic movement to return to the original shape after the soft segment has melted. Examining the effects on the soft segment melting characteristics in Figure IV-17, it can be seen that, while there is no effect on the actual temperature of the soft segment melting, there is a large amount of fluctuation within the enthalpy of melting.
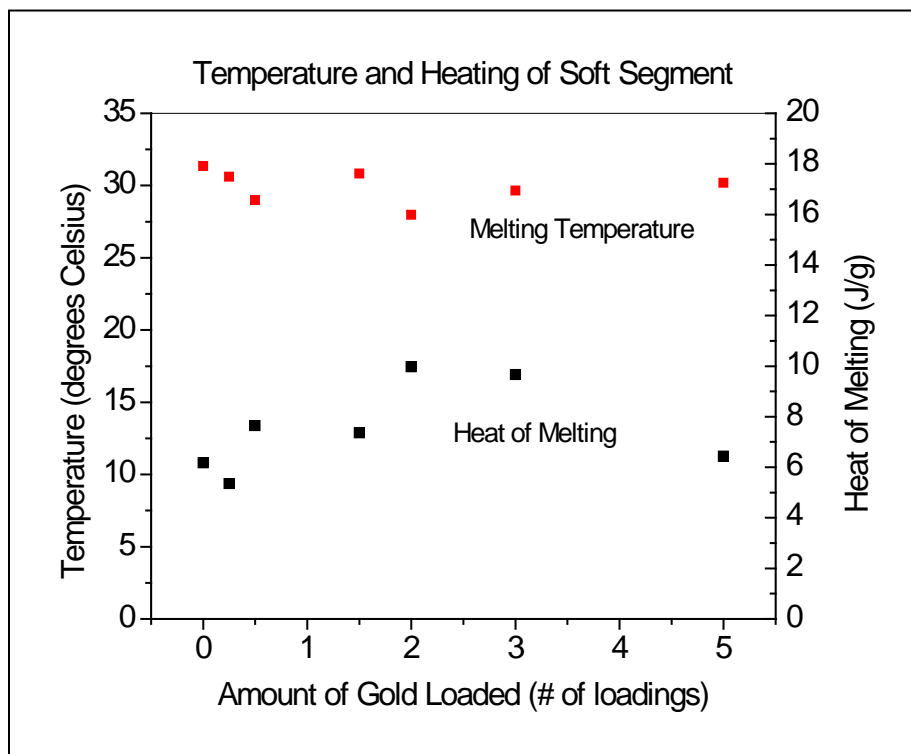
Figure IV-17. Melting temperatures and enthalpy of melting for the soft segment of films with varying nanorod concentrations.

It is interesting to note that it is possible for the nanorods to be associated more with one type of segment or the other, depending on the properties of the nanorods and their propensity to be attracted to either the soft or hard segments. If the nanorods were more closely associated with the soft segments, then the transition temperature would have more change as more nanorods were incorporated.

The same can be said to be true of the characteristics of hard segment melting, as seen in Figure IV-18.
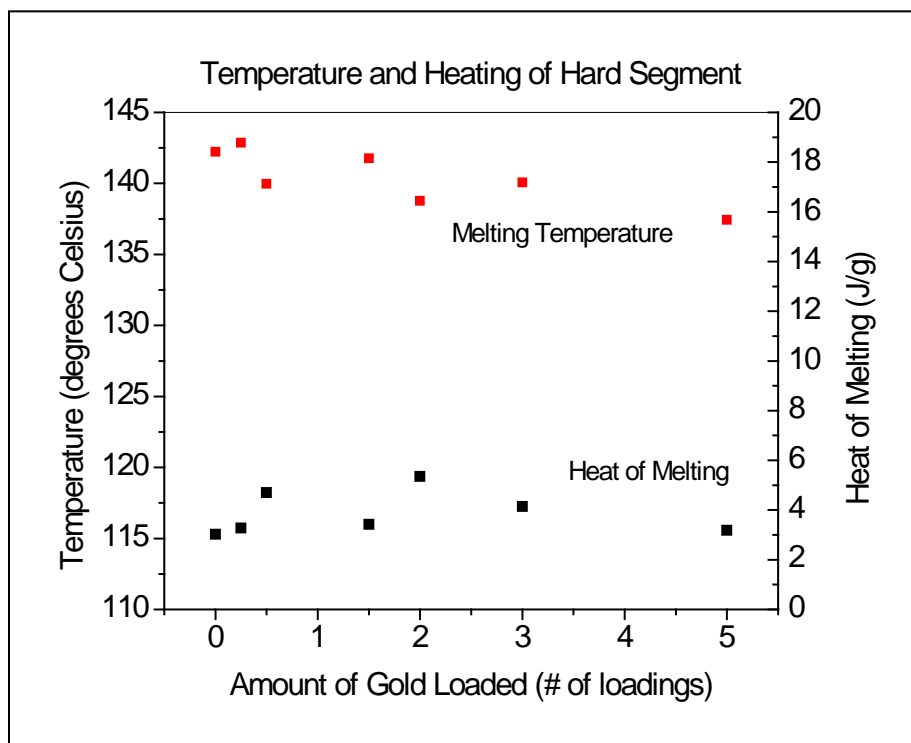
Figure IV-18. Melting temperatures and enthalpy of melting for the hard segment of films with varying nanorod concentrations.

There is not quite as much fluctuation. In these temperatures of the hard segment melting is where the nanorods begin to influence properties. As mentioned, the nanorods seem to be

more associated with the hard segments, due to the slight decreasing trend of the transition temperature. When compared together, as in Figure IV-19, it can be seen that there is a much larger trend of nanorod effects for the melting of the hard segment compared to the melting of the soft segment. While this would not have any effect on the shape memory behavior at lower temperatures, if the nanorods were incorporated more in the soft segment, then many effects on recovery would be seen. The reason for decreasing melting temperatures is due to the effect that the nanorods have on crystalline formation. Gunes et al. discussed this in regards to their polyurethane system incorporated with organoclays, carbon nanofibers, silicon carbide, and carbon black [195]. For all systems, the melting temperature of the soft segment decreased significantly upon nanoparticle incorporation.
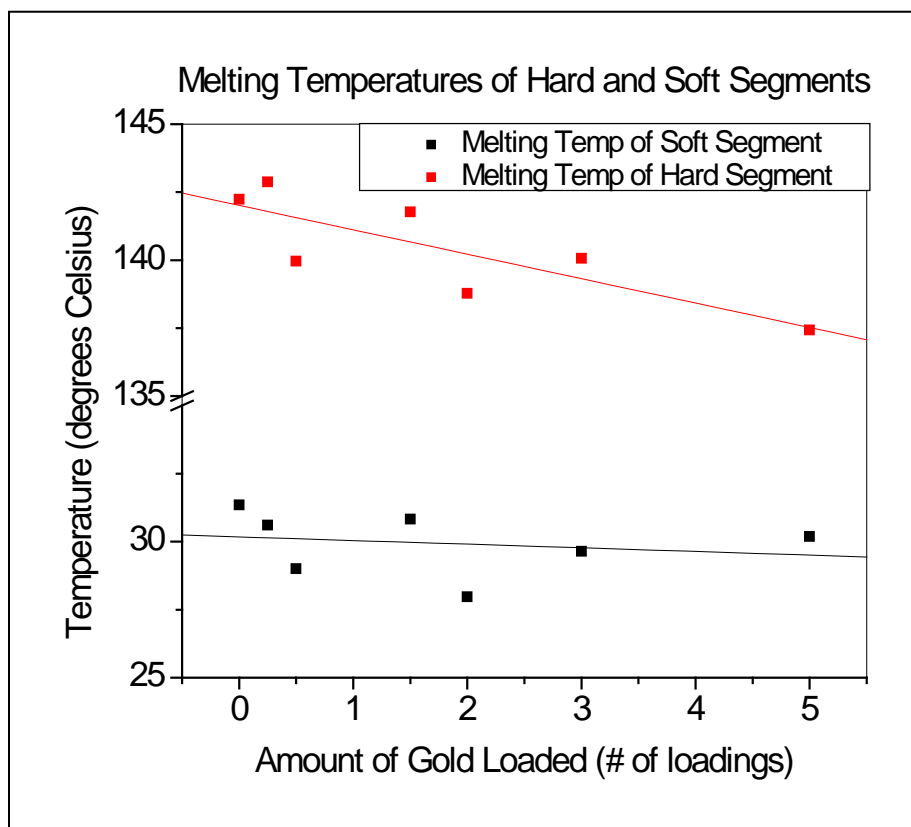
Figure IV-19. Melting temperatures of the soft and hard segments of films with varying nanorod concentrations.

Another thermal property to examine is the thermal degradation of the polyurethane. It is a concern that the application of the laser will not just cause the photothermal effect within the nanorods but will also cause a degradation of the polymer. To investigate this, the 5-growth film was subjected to the laser at the highest power and at a distance of 2 cm for 5 minutes and then for 30 minutes. Following this exposure, the DSC was used in order to determine if any of the thermal properties were affected by degradation of the polymer chains. Degradation should be most notable in the soft segments of the polymer, so the melting temperature of the soft segment would most likely show any effects. The thermal properties are shown in Table IV-4, compared to the properties of the film before irradiation.

Figure IV-4. Thermal properties of the 5-growth nanocomposite after 5 and 20 minutes of laser irradiation.

Time of Laser Irradiation (min.)	T_g (°C)	T_{mSS} (°C)	ΔH_{mSS} (J/g)	T_{mHS} (°C)	ΔH_{mHS} (J/g)	T_c (°C)	ΔH_c (J/g)
0	-40.95	30.22	6.62	134.58	6.57	50.45	5.74
5	-39.36	30.86	6.72	133.18	6.65	50.93	6.26
30	-41.09	29.38	7.70	134.84	5.77	50.85	5.03

There is clearly not much difference to the thermal properties due to sustained laser irradiation, especially to the melting temperature, which fluctuates by less than 1°C. In addition, with possible degradation, the enthalpy of the soft segment melting should decrease as the polymer chains break. However, the enthalpy of soft segment melting actually increases slightly once irradiated for 30 minutes, fully disproving the notion that laser irradiation damages the polyurethane itself. If damages were to occur, Rek et al. demonstrated that photocrosslinking is likely to occur with polyurethanes [196]. This would result in higher values of all thermal

properties, especially where the crosslinks occur. This only emphasizes the fact that no degradation occurs because of the UV irradiation.

Mechanical Properties

The mechanical properties are also an important inherent property of the polymer that can be affected by the inclusion of gold nanorods. In fact, enhancement of mechanical strength is one of the more popular applications of nanotechnology under research. To measure this, the initial modulus of the films at 60°C was examined. The films were placed in the DMA, heated to 60°C, and then stretched to 300% strain. This results in curves like that in Figure IV-20.
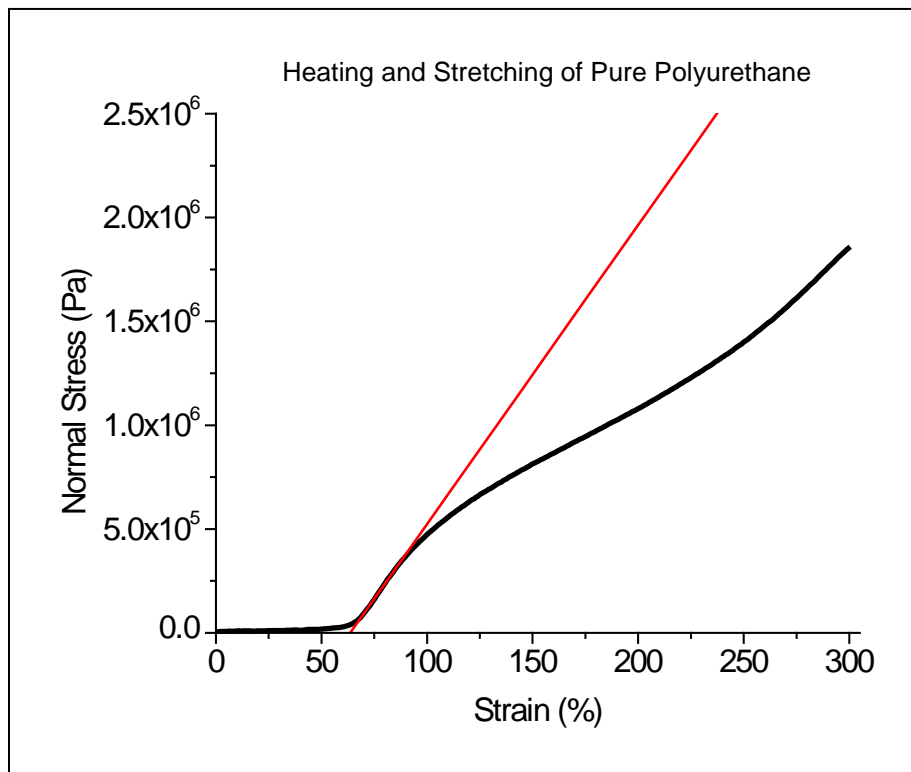
Figure IV-20. Curve to determine initial moduli of films.

The modulus was calculated by measuring the slope of the curve in the initial linear elastic region of the curves. The results are displayed in Figure IV-21.
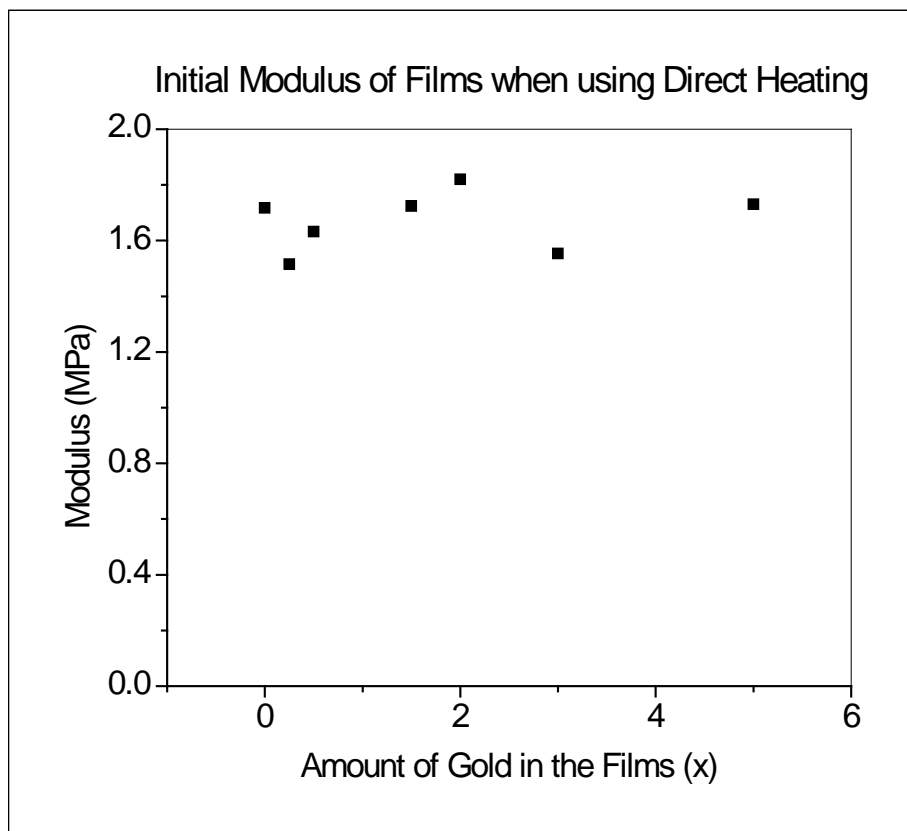
Figure IV-21. Initial modulus of nanocomposites when using direct heat.

While there is some slight fluctuation of the moduli between 1.5 and 1.9 MPa, there is no trend when increasing the amount of gold nanorods present in the film, meaning that the amount of nanorods present is small enough not to affect the inherent mechanical properties.

Shape Memory Behavior with Direct Heat

To understand the shape memory behavior of these nanocomposites when triggering the shape memory behavior with light, the effects on the traditional shape memory behavior using direct

heat need to be understood. With the incorporation of nanorods, the shape memory behavior

may change. The traditional application of heat to the shape memory polyurethane will cause

the soft segment to melt. With the incorporation of nanorods, the presence of nanoparticles

may hinder this transition, increasing the temperature needed to melt the soft segment.

Alternatively, the conductive properties of the nanorods may enhance the conduction of heat,

allowing for a lower melting temperature and providing for a faster shape memory transition.

In Figure IV-22, shape memory curves are shown for the pure polyurethane film, in which

direct heat from the DMA furnace is used as the shape memory triggering mechanism.
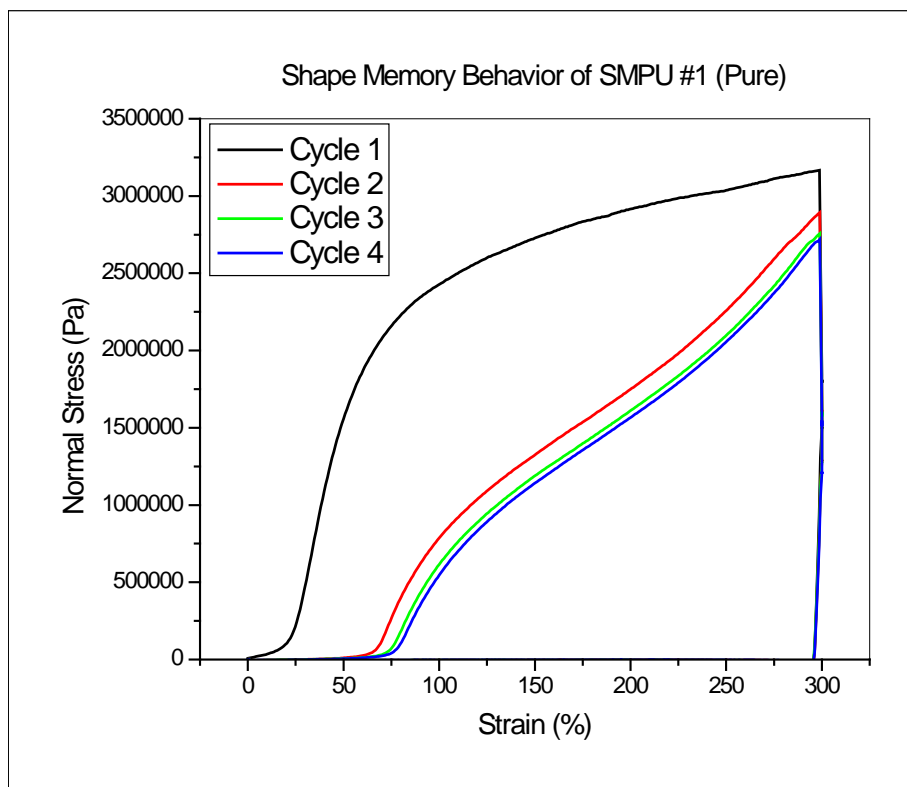
Figure IV-22. Shape memory behavior of pure polyurethane using direct heat.

As usual, the first cycle is completely different than the following cycles due to an annealing

process. This process occurs as the solvent cast film has significant molecular rearrangement

as the film is heated. Thus, the first cycle is usually disregarded and the following cycles are regarded as the valuable data. As can be seen in Figure IV-22, recovery for the second cycle begins around 70% strain. For the purposes of removing the faulty first cycle, this will be considered the starting point of the shape memory behavior analysis. The following cycles, while not recovering fully each time, remain very close in what percentage of the strain is recovered when heat is applied. Examining the fixity, values are very close to the 300% applied strain. This strain is held as the load is removed, with rapid cooling before loading is released. The small loss of strain when this load is removed is what is considered fixity. From Figure IV-22, the loss of strain is very low, with the final strain value still close to 300% once loading is completely removed. The analyzed recovery and fixity values are summarized in Table IV-5.

Table IV-5. Fixity and recovery values for a pure film and gold film (5 growths), using the heat from a furnace.

SMPU	Cycle #	Fixity (%)	Recovery (%)
Pure SMPU #1	Cycle 1	98.49	
	Cycle 2	98.02	
	Cycle 3	97.95	96.60
	Cycle 4	97.911	95.09
Gold Film w/ Furnace	Cycle 1	96.69	
	Cycle 2	94.39	
	Cycle 3	94.26	97.38
	Cycle 4	94.18	96.07

Also in Table IV-5 are recovery and fixity values for a gold film comprised of the gold from five growth solutions. Direct heat was also used for the shape memory triggering of this film.

137

Once again, the first cycle, and, subsequently, the recovery of the second cycle are omitted due to the first cycle rearrangements. It is interesting to note that the fixity values are lower for the film with gold nanorods. This is important to understand. What is likely happening is that the gold nanorods are slightly stiffening the film, allowing for slightly less strain to be retained when the load is removed. This is also seen in the work by Gunes et al [195]. As they added more of the nanoparticle fillers, the fixity values began to decrease dramatically due to stiffening of the films. Alternatively, the recovery is slightly more. This is most likely a result of the extra conduction of the nanorods. The nanorods more easily conduct the heat of the furnace, allowing for slightly more heating of the film, which results in a slightly higher recovery. The plot of this film with direct heat is shown in Figure IV-23.
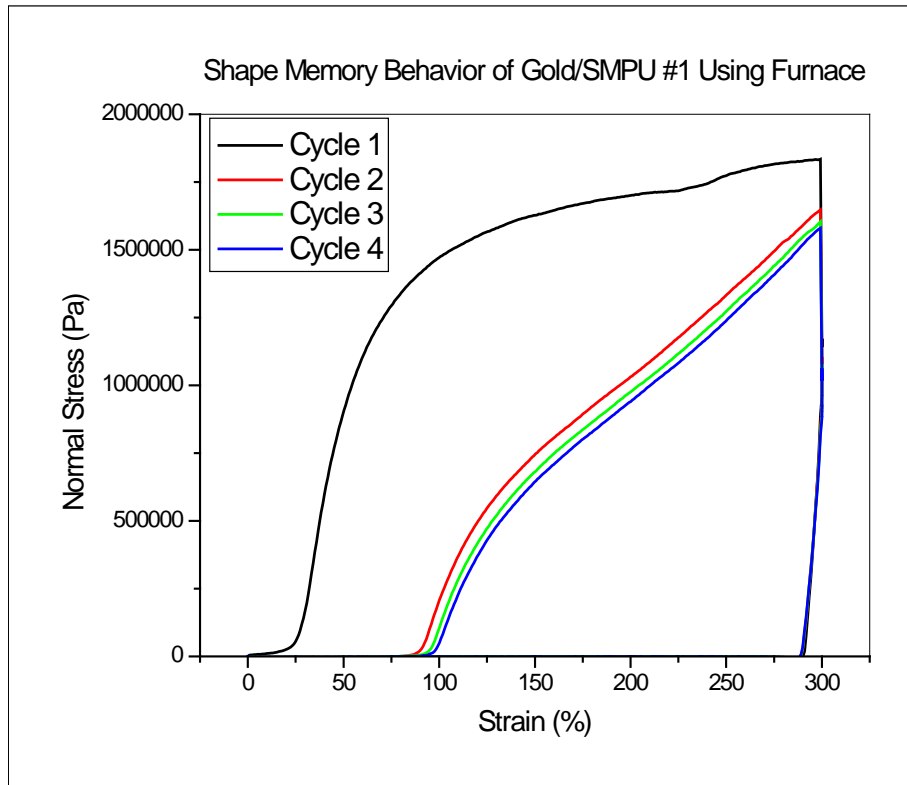
Figure IV-23. Shape memory behavior of a 5-growth film using direct heating.

When examining all of the films, the effects of nanorod incorporation on the fixity and recovery values remain very small. This can be beneficial if the desire is to provide a shape memory polymer with the exact same properties as those of pure polyurethane. The effects of nanorod incorporation on the fixities and recoveries of all film concentrations are displayed in Figures IV-24 and IV-25.
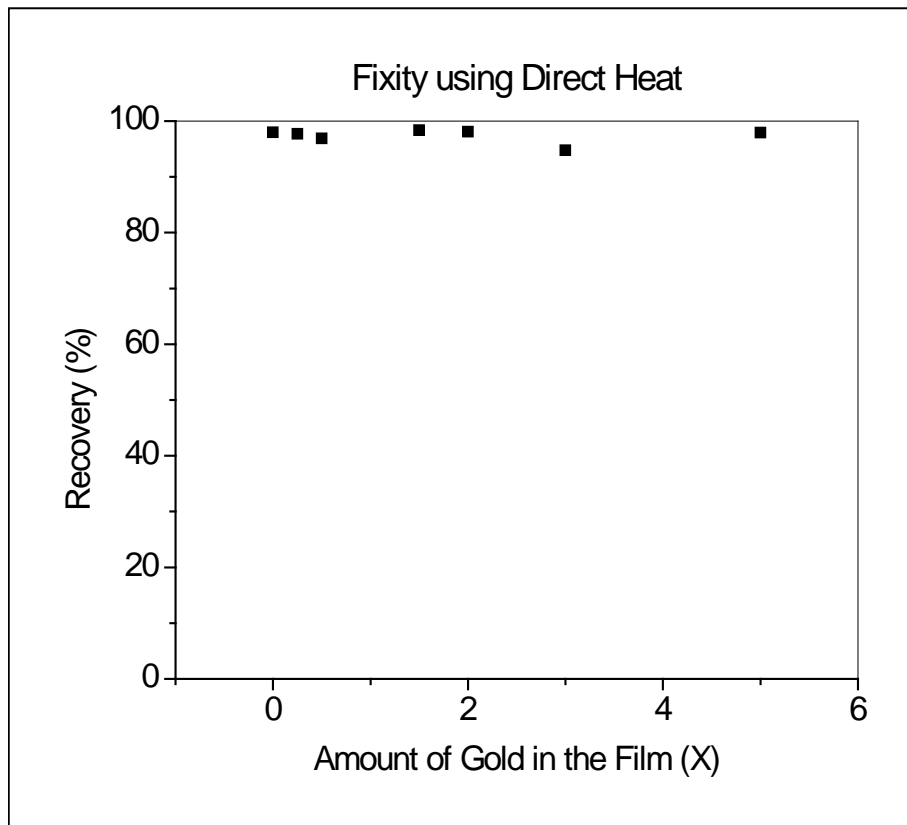
Figure IV-24. Fixities of films of varying gold composition using direct heat.
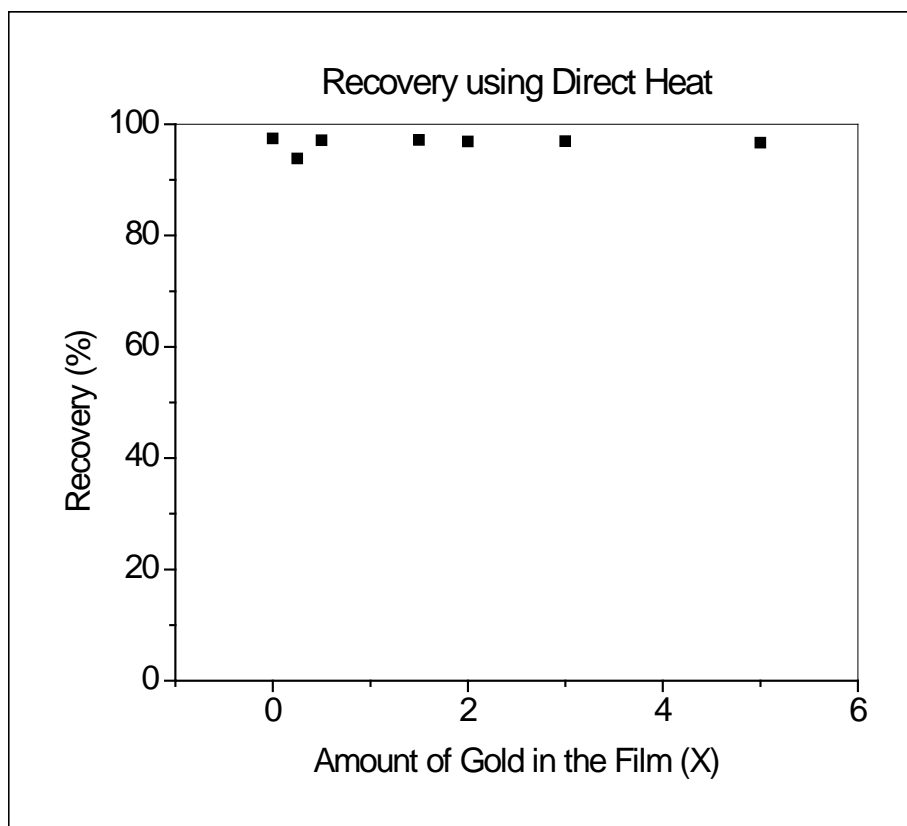
Figure IV-25. Recoveries of films of varying gold composition using direct heat.

As can be seen, there is very little effect, if any, on the inherent fixity and recovery when utilizing direct heat. The complete data for this information is displayed in Table IV-6.

Table IV-6. Fixity and recovery values for nanocomposites when using direct heat for the shape memory effect.

Film (# of growth solutions in the film)	Fixity (%)	Recovery (%)
0	97.97	97.45
0.25	97.68	93.82
0.5	96.91	97.12
1	98.34	97.18
2	98.09	96.91
3	94.76	96.96
5	97.90	96.67

Effect of Recovery Temperature

Recovery values are some of the most important shape memory behavior characteristics. To fully understand how the incorporation of gold nanorods has affected this behavior, the effect on the recovery values based on different temperatures was studied. This is important to understand because the presence of gold nanorods most likely affects the films' conduction properties and thus how the heat from the furnace affects recovery. In addition, when using the laser in a later section, understanding how different temperatures, as a result of different laser parameters, will affect the recovery of the nanocomposites is very important and crucial towards controlling the use of the nanocomposites and their final behavior. To thus understand how temperature affects recovery when just using direct heat from a furnace, a study was designed whereas four different temperatures were used during the recovery cycles during shape memory triggering: 40°C, 45°C, 50°C, and the normal 60°C. Recovery value results are shown in Table IV-7.

Table IV-7. Recovery values for a pure film and 5-growth film with various recovery temperatures (*all values are based off these recovery values as a relative full recovery).

Recovery Temperature (°C)	Recovery (%)	
	Pure Film	5-Growth Film
60	100*	100*
50	89.14	91.67
45	86.13	88.03
40	83.12	84.39

As can be seen, there is an obvious decrease in recovery values as the recovery temperature decreases. This results from the enhanced mobility of the soft segment as the temperature is higher. This behavior is evident for both films, although recovery values do seem to be slightly higher for the nanocomposite film than for the pure film. This could be a result of the

presence of the nanorods and their ability to slightly enhance heat conduction, thus resulting in slightly more recovery. The 100% values of the 60°C temperature need to be mentioned. The reason that these values are 100% is that the recovery values are all based off this recovery set, meaning that recovery is relative to this point. This just relates that recovery values are lower relative to the recovery at 60°C. Normally, recovery values are calculated based off the recovery values of the cycle immediately prior to it. In this case relative values are needed to understand just how the values change. Otherwise, values would be under 100% or over 100% depending on the order of testing the temperatures.

The full shape memory behavior curves are shown in Figures IV-26 and IV-27. The differences in recovery can be clearly seen when comparing at what point the heating curve begins to rise from the x-axis, heading towards 300% strain.

Figure IV-26. Shape memory behavior of the pure film with varying recovery temperatures.

142
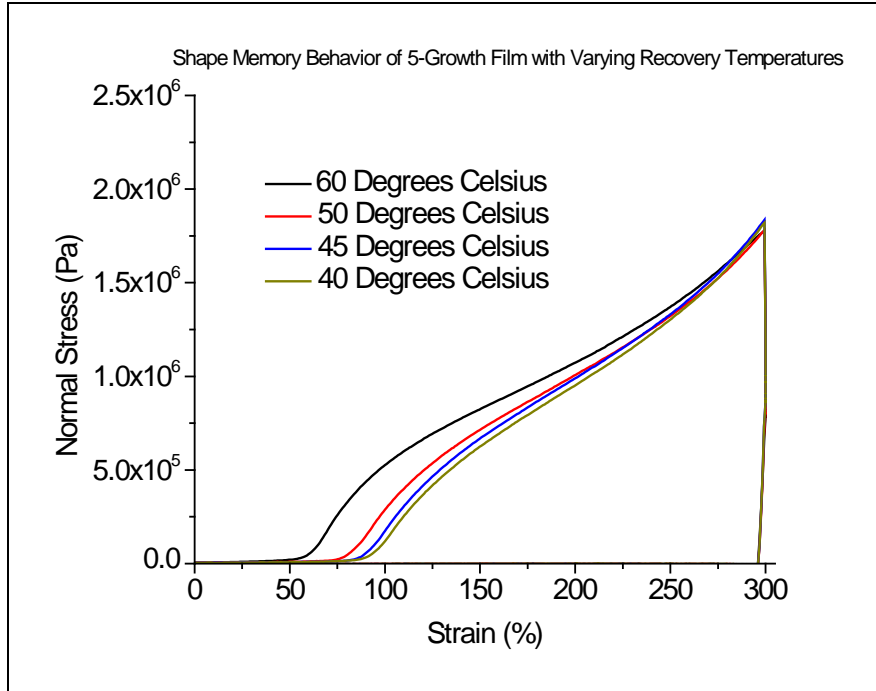
Figure IV-27. Shape memory behavior of the 5-growth film with varying recovery temperatures.

Effect of Quenching Temperature

The temperature at which the film is quenched after recovery has a major effect on the fixity of the film. Fixity is generally the ability of the film to hold at a given strain once the load is removed. As a rule, this quenching temperature must be below the melting temperature of the soft segment, since this temperature is the triggering temperature of the shape memory behavior. If the quenching temperature is not below this melting temperature then the soft segments will still flow and the strain will very quickly return to the original strain before loading. It is also possible that, even with the temperature below the melting temperature of the soft segment, quenching temperatures close enough to this melting temperature will still result in a lower fixity than desired. To determine the effect that different temperatures have on fixity, a study was performed that varies that temperature. The usual quenching temperature used is -25°C. For this study, quenching temperatures of -12°C, 0°C, and 12°C

143

were also examined. The resulting fixity values for a pure film and a 5-growth film are displayed in Table IV-8.

Table IV-8. Fixity values for a pure film and 5-growth film with various quenching temperatures (quenching time of 120 sec.).

Quenching Temperature (°C)	Fixity (%)	
	Pure Film	5-Growth Film
-25	87.49	96.47
-12	87.93	97.52
0	87.92	96.43
12	77.47	89.88

While the fixity values for pure polyurethane are usually much higher (this is not a result of change in quenching temperatures), there can still be seen a clear trend for both films. The fixity values remain high for -25°C, -12°C, and 0°C. When the quenching temperature reaches 12°C, however, the fixity values drop significantly. This can be explained by thermal properties of the films. While the thermal properties of the films detail that the melting temperature of the of the soft segments of the films are between 27°C and 32°C, the onsets of the melting temperature are, in fact, much lower. The onsets and offsets of this melting temperature for all films are displayed in Table IV-9.

Table IV-9. Onset and offset temperatures for the melting of the soft phase of the nanocomposite films.

Film (# of growth solutions in the film)	Onset of T_{mSS} (°C)	Offset of T_{mSS} (°C)
0	1.13	46.46
0.25	0.22	44.76
0.5	2.07	45.02
1.5	-0.31	45.55
2	-0.84	46.08
3	-1.94	44.08
5	5.90	47.48

From Table IV-9, it can be seen that for both the pure film and for the 5-growth film, the onset of melting for the soft phase begins above 0°C, but before 12°C. Thus, it is not surprising to see that fixity values begin to drop at 12°C. Melting of the soft segment has already begun and the ability to hold a strain will be diminished.

The actual shape memory behavior of the two films is displayed in Figures IV-28 and IV-29. The drop in fixity can be seen on the right portion of the return curve; the curve touches the x-axis further from 300% than is usual.
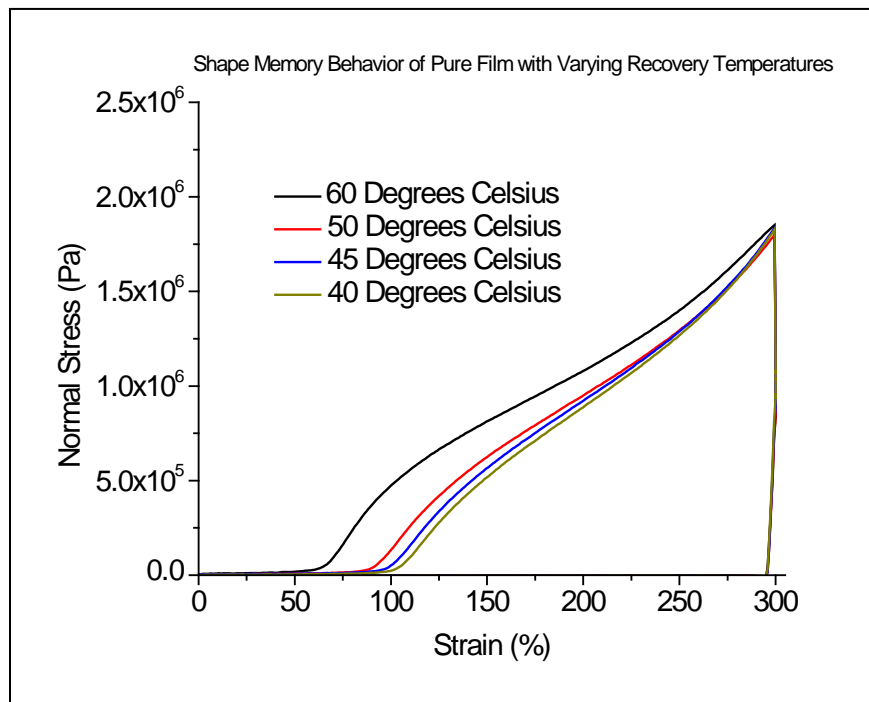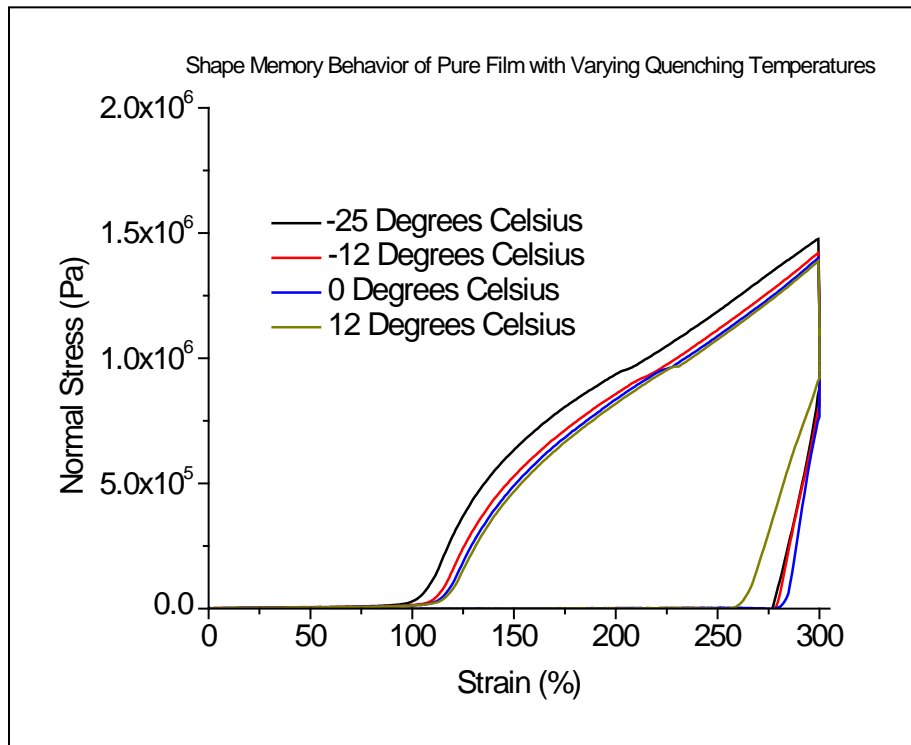

Figure IV-28. Shape memory behavior of the pure film with varying quenching temperatures.
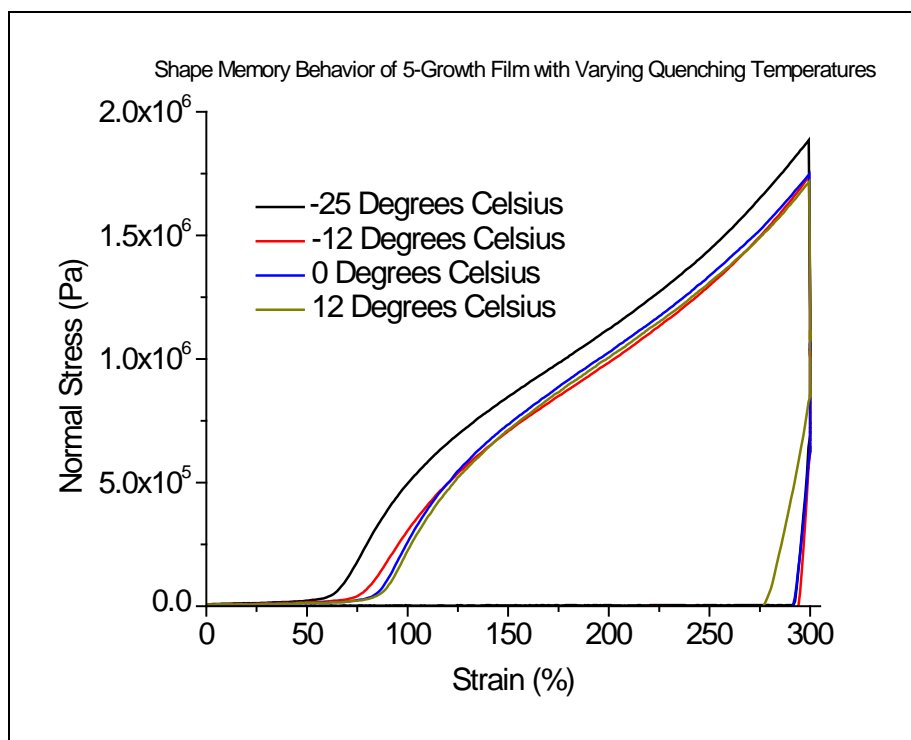
Figure IV-29. Shape memory behavior of the 5-growth film with varying quenching temperatures.

Effect of Quenching Time

Quenching time can also be an important factor in the values of fixity. While the films are thin, around 0.2 to 0.25 mm, cooling of the film is not instantaneous. In addition, the soft segment needs to fully recrystallize from the heating and loading section of the testing. If the soft segment has not fully recrystallized, then it will not support the temporary fixed condition and keep as much applied strain as possible when the load is released. Instead, the film will "give" a slight amount, resulting in a less desirable fixity value. This property of the soft segment was studied by varying the quenching time. The quenching temperature is held constant at -25°C, but the quenching times were varied between 30, 120, 300, and 600 seconds. This test was once again performed with both the pure film and the 5-growth film. Resultant fixity values are shown in Table IV-10.

Table IV-10. Fixity values for a pure film and 5-growth film with
various quenching times (quenching temperature of -25°C).

Quenching Time (sec.)	Fixity (%)	
	Pure Film	5-Growth Film
600	98.61	98.57
300	98.30	98.24
120	96.22	96.47
30	91.65	91.03

Results for both films are very similar. As can be seen, a trend is clearly present; as the quenching time decreases, the fixity values substantially decrease. While the values never leave the 90% range, an almost 10% reduction in fixity could be substantial in certain applications. It is apparent that, normally, at least 300 seconds should be devoted to quenching time in order to sustain a relatively stable fixity value between nanocomposite films. Any time amount smaller than that leads to substandard fixity values, unless the desired application calls for lower fixity values.

The actual shape memory behavior of the two films is displayed in Figures IV-30 and IV-31. There can be seen definite differences when the return of the cycles touches the x-axis at different values away from 300%.
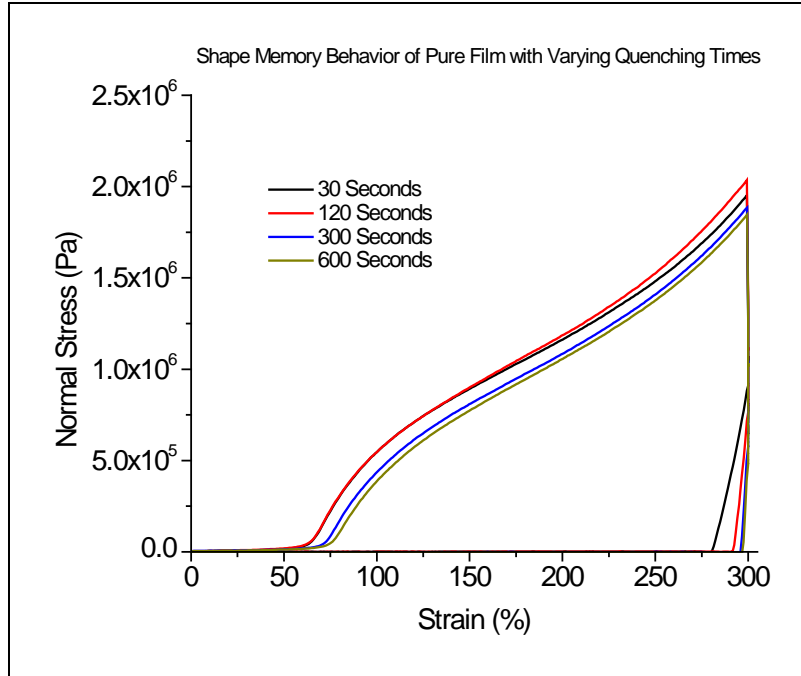
Figure IV-30. Shape memory behavior of the pure film with varying quenching times.
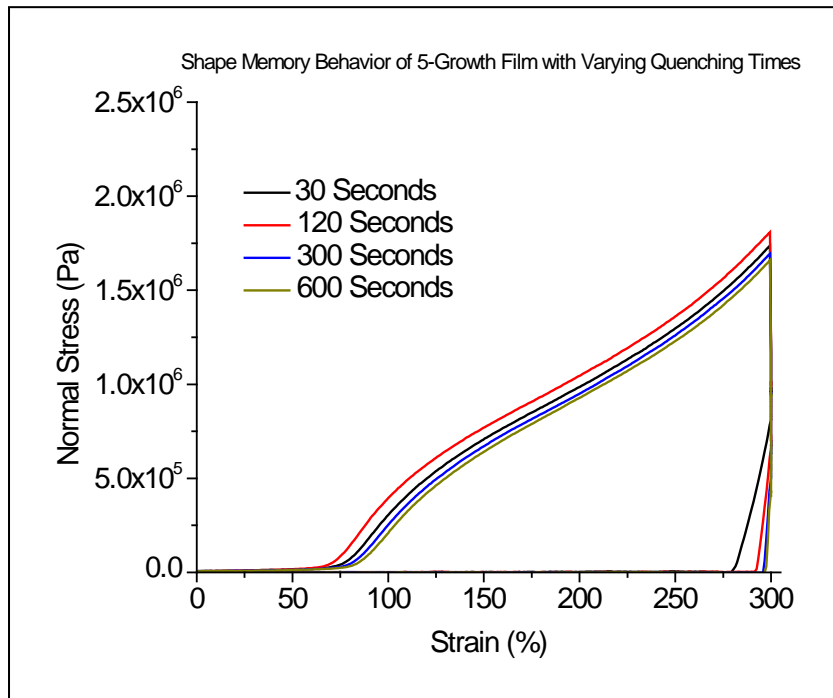
Figure IV-31. Shape memory behavior of the 5-growth film with varying quenching times.

Shape Memory Behavior with Laser Triggering

The main goal of this objective is to be able to trigger the shape memory effect of these nanocomposites with near-infrared light. Initial results were very promising. A film composed of nanorods from five growth solutions was used, under the pretense that the more gold present, then the higher the recovery would be. The resultant shape memory behavior was observed, shown in Figure IV-32.
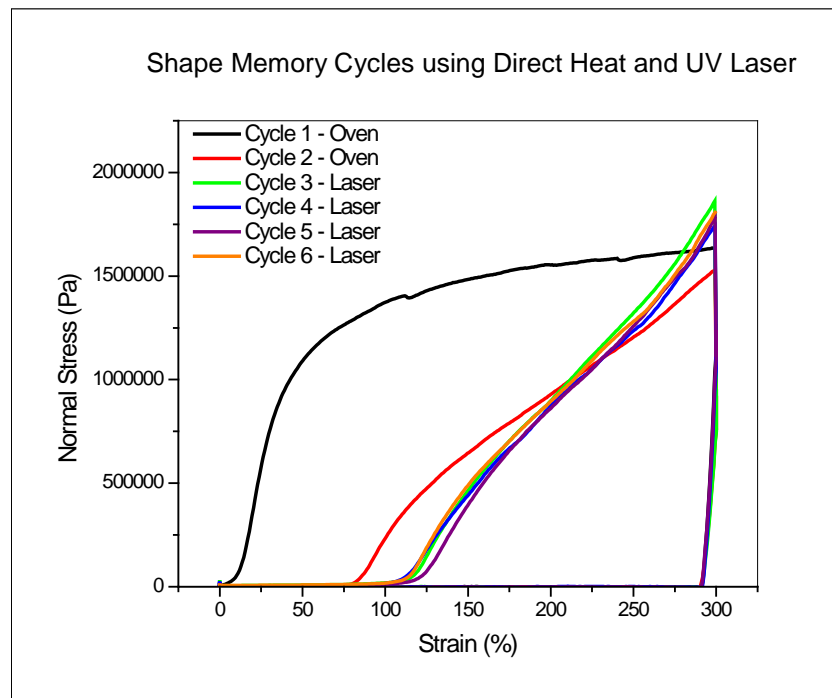
Figure IV-32. Shape memory cycles using direct heat (first two cycles) and a near-infrared laser (last four cycles).

From Figure IV-32, it can be seen that the shape memory behavior for the film is very similar to that of direct heat with a pure film. In fact, the curves for when using a laser are also very close to that when direct heat is used on the same film. Cycles 1 and 2 are when direct heat is used, whereas the next four cycles utilize the laser. Unfortunately, unlike when direct heat is used, there is strong overlap for the curves when a laser is used. This means that recovery

149

values will not decrease linearly cycle by cycle, as with direct heat. This decrease is natural, as fatigue slowly sets in on the film and less strain is able to be recovered. Most likely, this fatigue is still present when using the laser. However, as the procedure for using the laser is not quite perfected, and the ability to bathe the film in near-infrared light as you can bathe the film with heat is not possible. Thus, technique error is to blame for the overlapping of the curves. This could be due to slightly unequal distances of the laser from the films, small fluctuations with the power of the laser, or just user error at the time of recovery. Regardless, results still indicate that recovery of this film using the laser is, if not quite exactly, very close to the recovery when direct heating is used. Recovery and fixity values are reported in Table IV-11.

Table IV-11. Fixity and recovery values when using the laser for shape memory triggering (5-growth film; recovery values are based on the percentage of recovery when using direct heat instead of the laser).

SMPU	Cycle #	Fixity (%)	Recovery (%)
5-Growth Gold Film	Cycle 3	95.43	80.72
	Cycle 4	95.82	81.21
	Cycle 5	95.83	77.11
	Cycle 6	95.84	82.43

Cycle 1 and 2 have been left out of Table IV-11. All values of recovery are based on the recovery data for Cycle 2. This means that the cycles' recovery is a percentage on how direct heat is capable of triggering shape memory behavior. For example, in cycle 4, the laser is capable of stimulating about 81% of recovery versus a full recovery when using direct heat. As mentioned before, the recovery curves when using the laser are overlapping. This is shown in Figure IV-32 as well. The values for recovery increase, then decrease, followed by a final

150

increase. Results do indicate, however, that the laser, with these conditions and this film, triggers a shape memory behavior roughly 80% of that when using direct heat. The following sections will deal with improving these values and studying how different factors such as laser distance and power, as well as gold concentration, will affect the values.

Effect of Laser Distance

One of the main considerations when studying the laser-triggering of these films is the effects of various factors. One main factor is the distance of the laser from the film. When comparing how well a film can recover the applied strain when using the laser, the fixity and recovery are compared to when using direct heat. When changing the distance of the laser to the film however, different temperatures are produced. These temperatures are reported in Figure IV-33.
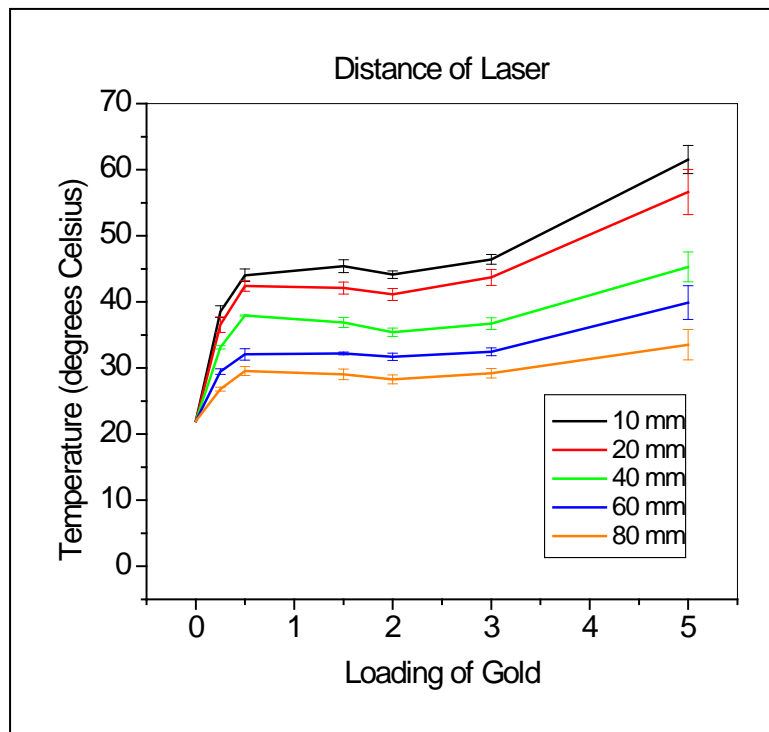
Figure IV-33. Temperatures produced at various laser distances for all gold films.

There can be seen a definite effect of laser distance. Logically, as the distance from the film increases, the resultant temperature due to the photothermal effect decreases. This occurs due to the spot size of the laser. The closer the laser is to the film, the smaller the spot size is and the more concentrated the energy is. The pure film, with no gold nanorods, stays at a constant room temperature of about 22°C, even when the laser is shined at all distances directly on the film. Alternatively, all other films result in higher temperatures than room temperature. There seems to be a plateau effect upon all of the films except for the highest concentration. Gradual increases in temperature are seen to begin with the film incorporated with the nanorods from 3 growth solutions. From this result, systems of experiments are designed in order to compare laser shape memory behavior more closely to that of direct heat triggering. For example, if the film is known to produce a temperature of 45°C with the laser shone at a 2 mm distance, then fixity and recovery values will be compared to those when a film is subjected to a temperature of 45°C utilizing the oven.

Effect of Nanorod Concentration and Laser Power

Ideally, as the nanorod concentration in a film increases, the amount of heat that the nanorods are capable of producing would increase as well. In addition, an increase in the power of the laser should result in the same increase in resultant temperature production. To study this, all films created were subjected to the laser at a set distance and their shape memory behavior was observed. Table IV-12 displays the resultant fixity and recovery values.

Table IV-12. Fixity and recovery values for nanocomposites with varying laser powers.

Film (# of growth solutions in film)	Fixity (%)				Recovery (%)			
Laser Power (W)	0.82	1.00	1.18	1.44	0.82	1.00	1.18	1.44
0.25	98.68	98.70	98.69	98.67	7.04	7.78	8.14	10.59
0.5	98.06	98.05	98.04	98.38	29.20	40.67	53.5	61.10
1.5	98.38	97.75	97.73	98.09	15.63	28.47	30.92	39.95
2	97.55	97.92	97.88	98.23	29.31	25.71	33.01	37.84
3	97.40	97.37	96.96	96.95	11.95	13.17	22.36	32.30
5	97.99	97.96	97.95	98.30	46.28	42.95	71.66	78.00

As can be seen, the fixity values remain virtually the same. The recovery values are vastly different, however. The data is displayed in Figure IV-34, with the amount of nanorods as the x-axis.
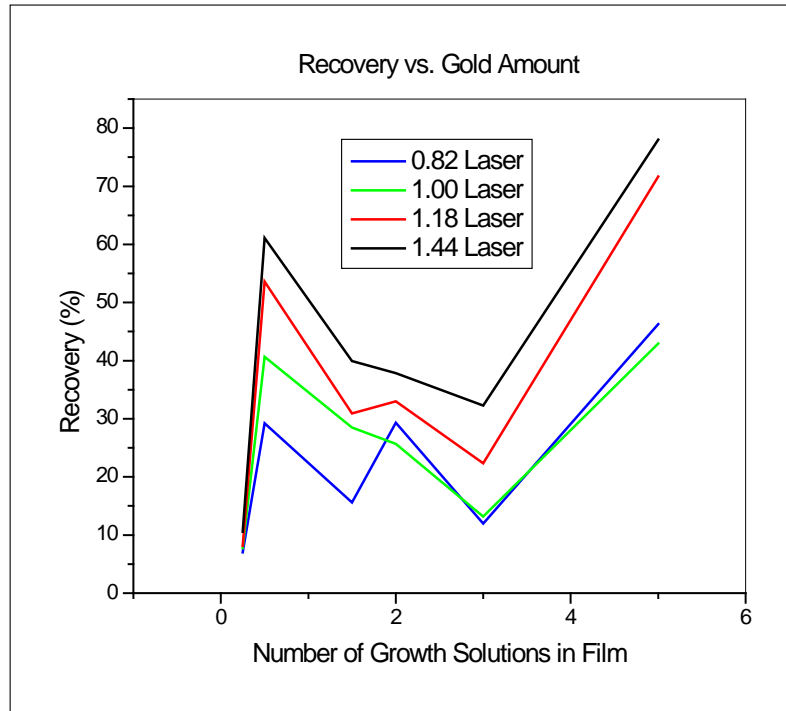
Figure IV-34. Recovery as a function of the amount of nanorods in the film, further categorized by the power of the laser.

As can be seen, recovery values fluctuate dramatically. The film containing five growths' worth of nanorods exhibits the highest recovery values. This is logical, as it should provide more heat than the other films upon application of the laser. In addition, the film containing 0.25 growths' worth of nanorods exhibits the smallest recovery amounts. This is logical as well. Hong et al. demonstrated that with higher nanorod concentrations, the temperature changes should increase [197], leading to higher recovery. The middle concentrations begin to fluctuate, however. This is troubling, as this leads to the rationale that either these films do not contain as many nanorods as they should, which is unlikely, or that there is some unknown factor inhibiting heat production. This factor could be poor dispersion of the nanorods, producing regions where there are no nanorods present and thus no heat production and uneven shape memory recovery. This factor could also be agglomeration of the nanorods, allowing localized heat in some areas and none in others. Agglomeration could even cause very little heat production at all, as the effective aspect ratio is altered. With this alteration, the agglomerated nanorods would no longer absorb at the correct wavelength of laser, resulting in no photothermal effect and no heat production for shape memory activation. Finally, the factor inhibiting recovery could be a change in shape memory behavior of the polyurethane itself. While it has been demonstrated that the inclusion of nanorods should not affect the thermal and physical properties, this could be an indication that there may be some effects after all.

The examination of the effects of laser power results in much clearer conclusions. The data is represented in Figure IV-35.
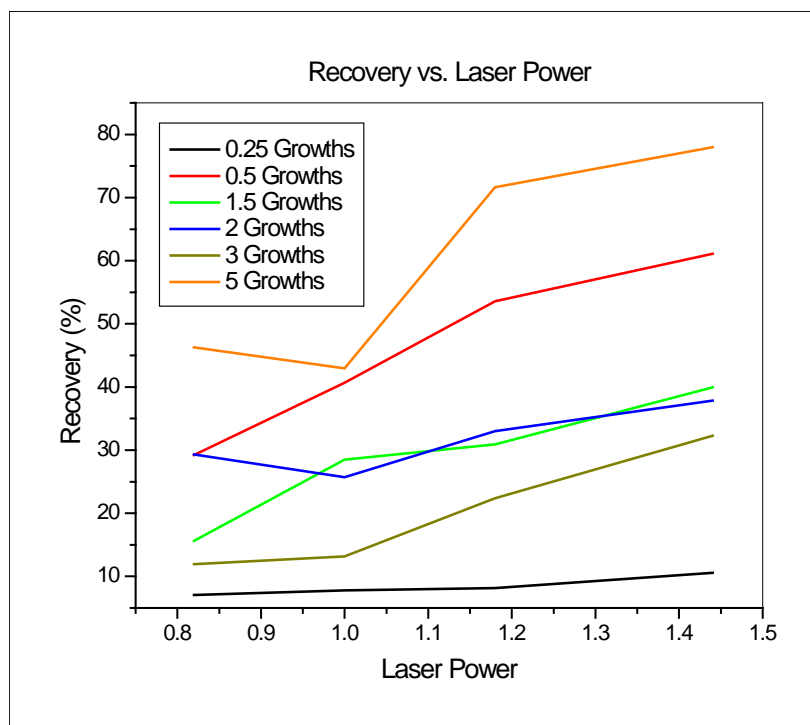
Figure IV-35. Recovery as a function of the power of the applied laser, further categorized by the amount of nanorods present in the film.

Results based on varying the laser power appear more consistent. It can clearly be seen that the general trend is for recovery to increase as laser power increases. This is only logical, as the more energy transferred to the nanorods at the same wavelength means that the energy has to be converted into more heat. This allows for the higher recovery values. There are a few slight fluctuations in the values when a higher laser power results in a lower recovery, but these very slight differences are most likely the cause of experimental error or the fluctuation of power within the laser itself. In general, it is shown that laser power can be a definite control over the recovery. While studies in literature have not focused on this aspect of photothermal heating of gold nanorods, a similar effect has been seen with tissue soldering. McNally et al. observed that as laser power increased, then the temperature production due to photothermal effects increases, due to increased energy absorption [198].

Design of Experiments (DOE)

As mentioned previously, recovery and fixity values have not fallen under predictive trends. For example, it would be logical to assume that as the concentration of nanorods increases, then if everything else is held constant, meaning the laser power, laser distance, etc., the temperature produced by the photothermal effect would increase as well. Following the results achieved in previous sections, whereas higher temperatures were demonstrated to result in higher recovery values, then increasing the nanorods concentration would logically increase the recovery values achieved, until a natural plateau of effects would probably be reached. While the highest concentration, 5 growths, did indeed result in the highest recovery values, and the smallest concentration, with 0.25 growths, resulted in the smallest recovery values, the concentrations in between resulted in a large fluctuation of values. As mentioned before, this could be a result of poor dispersion within the film or a large amount of agglomeration which the 5-growth film overcame with sheer number of nanorods. Due to the difficulty of accessing the concentration of nanorods within the film, a design of experiments was created in order to discover if the films are behaving according to their other properties, such as temperature production.

In a previous section, the temperature production of the films was displayed with regards to nanorods concentration and laser distance. The laser power was held constant at 1.44 W. The figure is reproduced here as Figure IV-36.
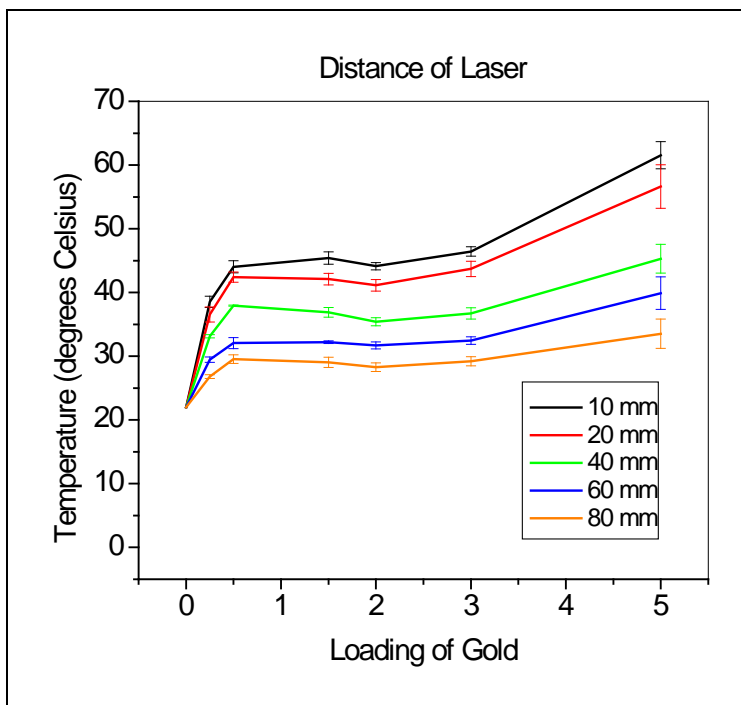
Figure IV-36. Temperatures produced at various laser distances for all gold films.

It can be seen that there is a plateau effect occurring for the films of concentrations 0.5, 1.5, 2, and 3. Thus, the first set of experiments was devised in order to determine if similar recovery values could be obtained if all recovery conditions were kept constant between the films. The top curve was chosen, so the laser is set at 10 mm away from the films during recovery. Thus, four shape memory behavior experiments were planned for this part of study. The second part of the study involved comparing different distances of the laser for the same film to study the differing recovery results. The 5-growth film was chosen since it has the greatest range of temperature production. Recovery when the laser is at 40, 20, and 10 mm will be compared to the film's recovery when it is subjected to direct heat at 45°C. This should result in increasing relative recovery as the distance of the laser grows smaller. Of course, at a distance of 40 mm, according to Figure IV-36, the temperature production should be 45°C, thus resulting in a relative recovery of 100%. This would mean that closer differences would also result in

157

relative recoveries of 100%, since temperature production should be higher. That is what this experiment determines, however. It determines if temperature production with a laser according to a thermometer is the same as direct heat application. Finally, a third part of the study involved experiments to determine if the same relative recoveries could be achieved with the same film, but with different distances. For example, the 5-growth film produces a temperature of 45°C at a laser distance of 40 mm, a temperature of 55°C at a laser distance of 20 mm, and a temperature of 60°C at a laser distance of 10 mm. Thus, for those three situations, if compared to the recoveries by direct heat at temperatures of 45°C, 55°C, and 60°C, respectively, then all three should result in relative recoveries of 100%. Thus, the third part of the study used those exact conditions in order to try to achieve all 100% relative recoveries. A summary of the sections of the study are presented in Table IV-13.

Table IV-13. Summary of Design of Experiments.

Experimental Section	Film (# of growths solutions in the film)	Laser Distance (mm)	Predicted Temperature (°C)	Direct Heat Comparison Temperature (°C)
1	0.5	10	45	45
	1.5	10	45	45
	2	10	45	45
	3	10	45	45
2	5	10	60	45
	5	20	55	45
	5	40	45	45
3	5	10	60	60
	5	20	55	55
	5	40	45	45

The first part of the study was to determine if using the four films from the plateau area of the temperature figure would result in the same recovery values when compared to direct heat recovery at 45°C. The results are shown in Table IV-14. Note that the first recovery column is the traditionally-calculated recovery based on the previous cycle. The second recovery column

is the relative recovery based off of the direct heat recovery. Also note that the cycle numbers start at 3, due to the fact that the first cycle is disregarded like usual and the second cycle is the direct heat cycle, of which the data is not displayed, but is used for calculation of the relative recovery.

Table IV-14. Results of section one of the DOE study.

Loading	Laser Distance (mm)	Comparison Temperature (°C)	Max Temperature Predicted (°C)	Cycle #	Fixity (%)	Recovery (%)	Relative Recovery (%)
0.5	10	45	45	3	98.35	80.93	80.93
				4	97.58	105.44	85.28
				5	97.72	96.13	81.98
				6	98.02	104.01	85.33
				7	97.79	95.69	81.62
1.5	10	45	45	3	97.83	74.76	74.76
				4	97.63	94.33	70.61
				5	96.96	108.24	76.31
				6	97.19	103.56	79.03
				7	97.24	102.47	80.97
2	10	45	45	3	98.16	61.70	61.70
				4	96.45	111.06	68.36
				5	96.80	99.40	67.95
				6	96.80	105.32	71.57
				7	96.96	98.88	70.77
3	10	45	45	3	98.28	84.74	84.74
				4	98.01	99.99	84.74
				5	97.99	97.81	82.88
				6	97.97	95.53	79.17
				7	97.85	105.64	83.63

Examining the data, once again, there are inconsistencies. The 0.5-growth film exhibits a very high relative recovery, around 80% - 85%. All other films exhibit relative recovery lower than that, with the 3-growth film the closest with recovery around 79% - 84%. It is obvious that these films are not exhibiting the desired properties of increasing concentration resulting in

increased recovery. Thus, regardless of the fact that all four of these films are predicted to produce a temperature of about 45°C within the film at the stated conditions, none of the four exhibit similar recovery when compared to the recovery achieved with direct heating at 45°C. Otherwise, all four films would have relative recovery of around 100%. In addition, they are different from one another, contrary to what testing the temperature output states. The actual shape memory curves for these four tests are shown in Figure IV-37. It can be seen that the distances from the furnace cycle are completely different from one another and are not even close to 100%.
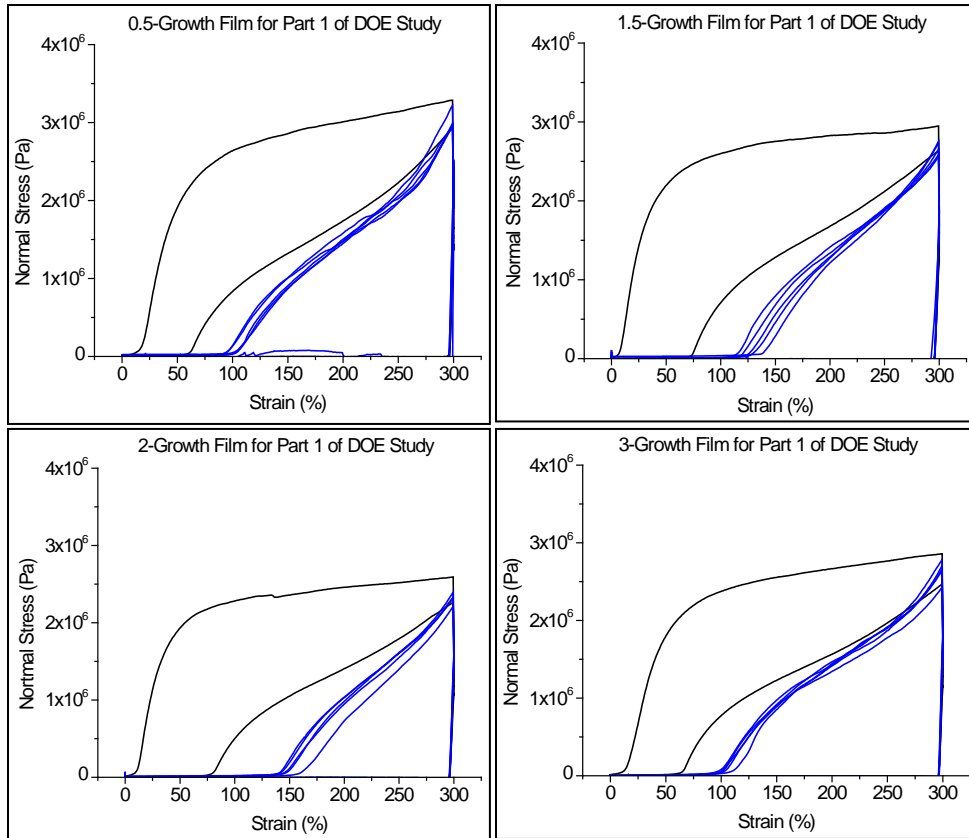
Figure IV-37. Shape memory behavior for the films in part 1 of the DOE study.

The second part of the study involved comparing the same film, but at different laser distances. These distances included 10 mm, 20 mm, and 40 mm. In addition, all three were compared to

the recovery obtained with direct heat triggering at 45°C. It is predicted that as the distance grows, then the relative recovery based on comparison to the same direct heating temperature should decrease. It is important to note, however, that according to the temperature production experiment, at a distance of 40 mm, the 5-growth film should produce a temperature of 45°C. Thus, all three should technically have a full relative recovery. From the last section, however, it is unlikely. Regardless, this section of the study was created in order to determine if temperature production with a laser according to a thermometer is the same as direct heat application. Recovery results, similar in structure to the last section's results, are displayed in Table IV-15.

Table IV-15. Results of section two of the DOE study.

Loading	Laser Distance (mm)	Comparison Temperature (°C)	Max Temperature Predicted (°C)	Cycle #	Fixity (%)	Recovery (%)	Relative Recovery (%)
5	10	45	60	3	98.23	97.70	97.70
				4	98.18	96.86	94.63
				5	98.12	103.64	98.07
				6	98.20	98.83	96.92
				7	97.81	97.64	94.62
5	20	45	55	3	97.80	82.84	82.84
				4	97.37	102.41	84.83
				5	96.93	102.33	86.74
				6	97.45	98.18	85.21
				7	97.84	101.42	86.48
5	40	45	45	3	98.24	52.08	52.08
				4	96.71	105.95	55.19
				5	96.85	123.33	68.06
				6	97.44	90.83	61.82
				7	97.17	99.36	61.43

Results are more promising for this section. Relative recovery is actually very close to 100% for the film at a laser distance of 10 mm. Further examination, however, reveals that the film

with a laser distance of 40 mm should have 100% percent relative recovery, but only has around 60% relative recovery. In addition, the laser at 20 m only produces a relative recovery of about 85%. While the trend of increasing laser distance results in decreasing relative recovery, as predicted, all relative recovery values should technically be 100%, even with the laser at 40 mm. The 10 mm film is expected to produce a temperature of 60°C and the 20 mm film is expected to produce a temperature of 55°C, and in comparison to 45°C direct heat; in all actually, however, the produced temperature inside the films are much less. Shape memory behavior is displayed in Figure IV-38. The general trend of decreasing recovery can be seen when examining that the distance between the furnace curve and the others increases.
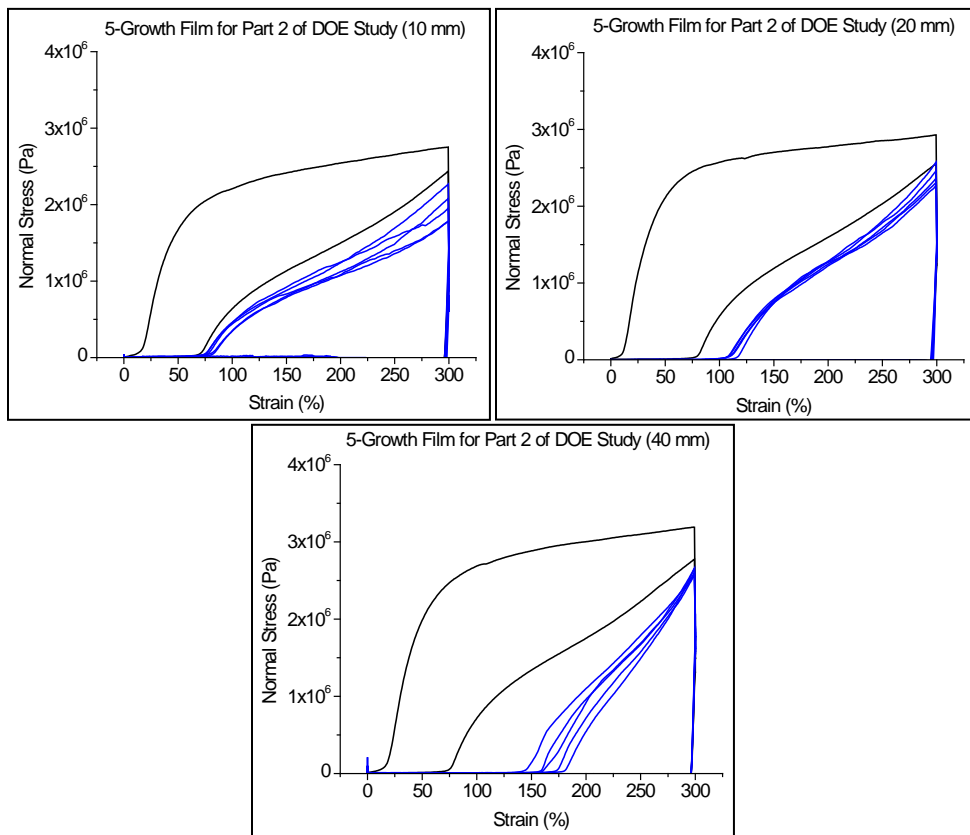
Figure IV-38. Shape memory behavior for the films in part 2 of the DOE study.

The final section of the DOE study involved the effort to achieve 100% relative recovery for the same film, but different distances. It is basically is an experiment to test for control over shape memory behavior. The 5-growth film has been shown, in the temperature production study, to exhibit a temperature of 45°C at a laser distance of 40 mm, a temperature of 55°C at a laser distance of 20 mm, and a temperature of 60°C at a laser distance of 10 mm. If those three situations were used and compared to the recovery at direct heat temperatures of 45°C, 55°C, and 60°C, respectively, then all three should result in relative recoveries of 100%. The recovery results are detailed in Table IV-16.

Table IV-16. Results of section three of the DOE study.

Loading	Laser Distance (mm)	Comparison Temperature (°C)	Max Temperature Predicted (°C)	Cycle #	Fixity (%)	Recovery (%)	Relative Recovery (%)
5	10	60	60	3	97.24	90.35	90.35
				4	97.37	98.78	89.29
				5	98.11	102.05	91.19
				6	97.79	99.20	90.43
				7	97.34	101.63	91.87
5	20	55	55	3	97.95	70.77	70.77
				4	97.63	102.04	72.32
				5	97.19	98.49	71.12
				6	97.63	95.39	67.95
				7	97.03	104.31	70.76
5	40	45	45	3	98.24	52.08	52.08
				4	96.71	105.95	55.19
				5	96.85	123.33	68.06
				6	97.44	90.83	61.82
				7	97.17	99.36	61.43

Once again, when using the laser on the 5-growth film at a distance of 1 mm results indicate a relatively high recovery. As well, however, full recovery is not seen for all three situations,

when all should read 100% relative recovery. The shape memory behavior curves are displayed in Figure IV-39.
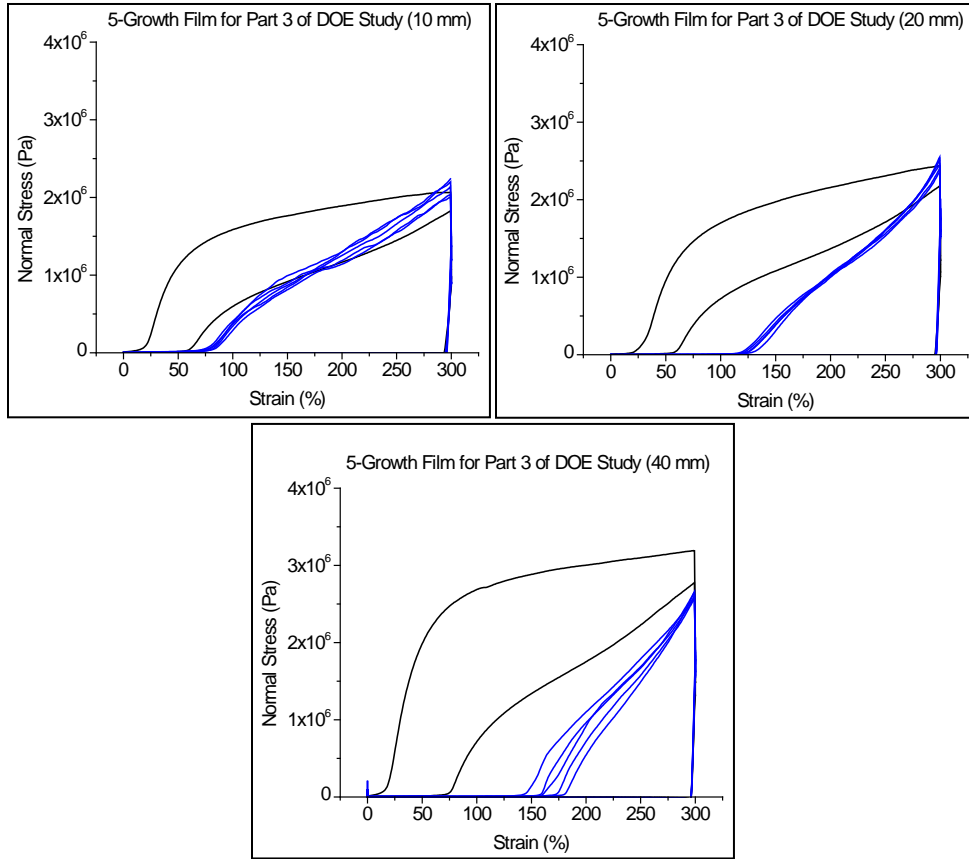
Figure IV-39. Shape memory behavior for the films in part 3 of the DOE study.

From all three sections of the DOE study, it can be stated that the predicted temperatures from the temperature productions experiments are not the same temperatures reached when utilizing the laser for shape memory behavior. This could be due to the fact that when taking the temperature of the films, that temperature was only a surface temperature, while the temperature inside the relatively thin film is lower. It could also be that, while the nanorods may amplify, by conduction, the heat of direct heat to help with shape memory effects, the conduction of heat due to the photothermal effects may be lower. Finally, it is also a

possibility that the production of heat is only localized around the gold nanorods and dispersal of the nanorods may be poor. For the temperature experiment, the nanorods could be more concentrated on the surface of the film, producing a higher temperature at the surface.

In an attempt to reconcile the data, a further experiment was performed where the moduli of the films at different temperatures were determined using the direct heat of the oven. Those moduli could then be compared to the moduli of the films during laser triggering. With higher temperatures of the films, the modulus should be lower. Thus, by comparing the modulus of the film at a known temperature with the modulus of the film during light triggering, then a general temperature of that film could be estimated. For example, the modulus of the 3-growth film during the initial stage of elongation was 1.88 MPa. Once the modulus at different temperatures is tested under direct heat, a curve could be created in which the 1.88 MPa could be inserted and solved for the estimated temperature of the film. This calculation is a possible reason as to why the films are not performing as well with the light as with direct heat. The temperature for the films may be lower than anticipated. For this experiment, only the two larger concentrations have been tested, 3 and 5 growths. Testing the moduli at four different temperatures, 60°C, 50°C, 40°C, and 30°C, the resulting moduli for the 3-growth film are displayed in Table IV-17.

Figure IV-17. Moduli for the 3-growth film at varying temperatures.

Temperature (°C)	Modulus (MPa)
60	1.797
50	1.878
40	1.945
30	2.0079

Once graphed, the resulting plot is displayed in Figure IV-40, with the modulus on the x-axis and the temperature on the y-axis. A linear fit line is already applied.
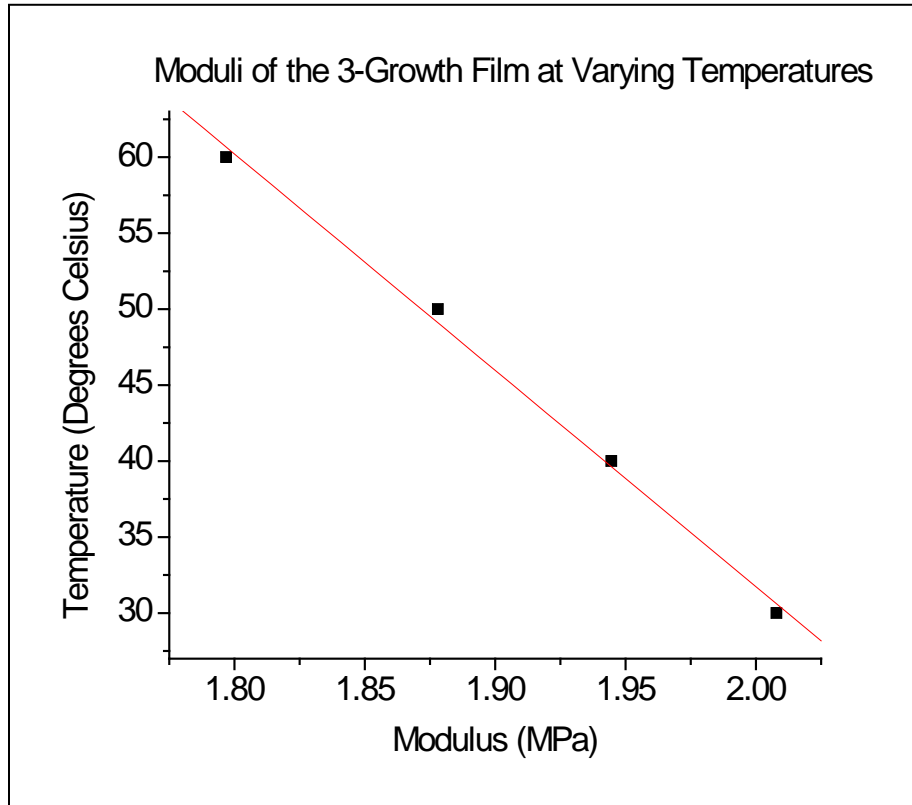
Figure IV-40. Moduli of the 3-growth film at varying temperatures with a linear fit.

The equation of the fit line is y = -142.388*x + 316.512. Analyzing the modulus of the 3-growth film from the first part of the DOE study, it was discovered that the modulus was 1.8819 MPa. When inserting this into the equation, it was found that the calculable temperature would be 48.55°C. This is actually close to what was predicted at the beginning of the DOE study, which was 45°C. It is, thus, still puzzling as to why recovery values were so low.

The other film analyzed was the 5-growth film. Moduli values calculated for it at various

temperatures are shown in Table IV-18.

Figure IV-18. Moduli for the 5-growth film at
varying temperatures.

Temperature (°C)	Modulus (MPa)
60	1.7028
50	1.8169
40	1.8672
30	1.9694

The graphical version of this data is shown in Figure IV-41.
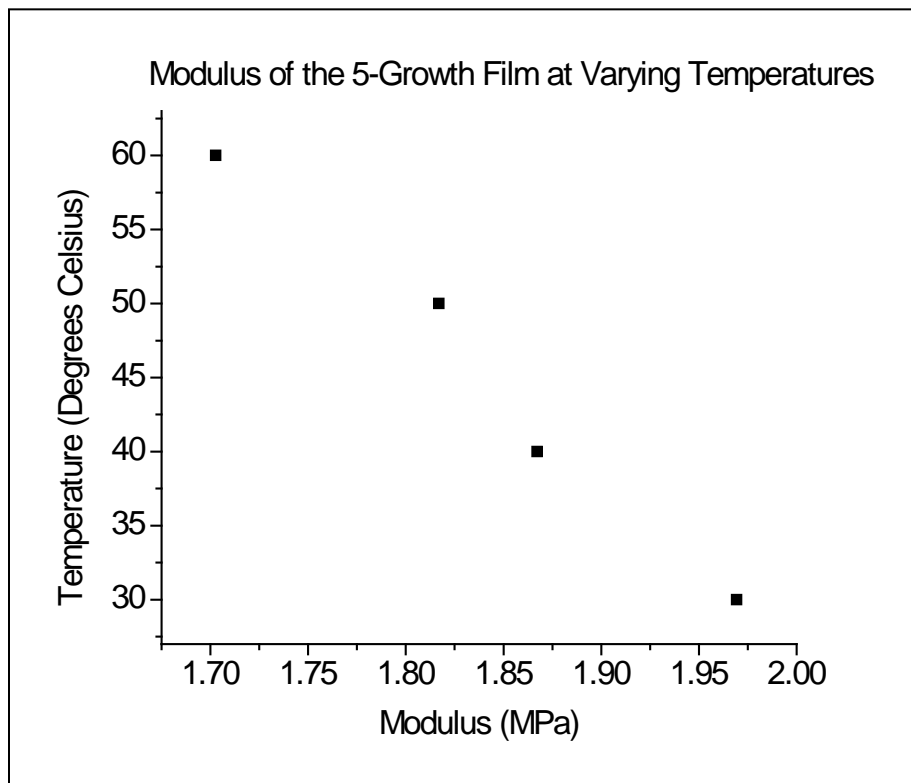
Figure IV-41. Moduli of the 5-growth film at varying temperatures.

Results here are not quite as linear. Reviewing the thermal properties of the films, however, at

a temperature of 30.19°C, the melting temperature of the soft segment is reached. In fact, the

onset of melting has been reached even sooner. Thus, as the film cools past 30°C, then the film becomes stiffer more rapidly, most likely following a different linear function. Unfortunately, no more data points exist, so an attempt at a linear fit is not attempted. In general, however, it is still believed that poor dispersion has played a role in the lower actual temperatures than desired and, thus, the lower recovery values than desired.

Shape Memory Recovery Using the Laser

Shape memory recovery of the nanocomposite films occurs very quickly. For the purposes of this chapter, time lapses of a video are shown in Figures IV-42 and IV-43, of a pure film and a 5-growth film. Both films were pre-stretched in hot water to 300% extension for 30 seconds. Both then have the laser shone on them, but only the nanocomposite film exhibits shape memory recovery.
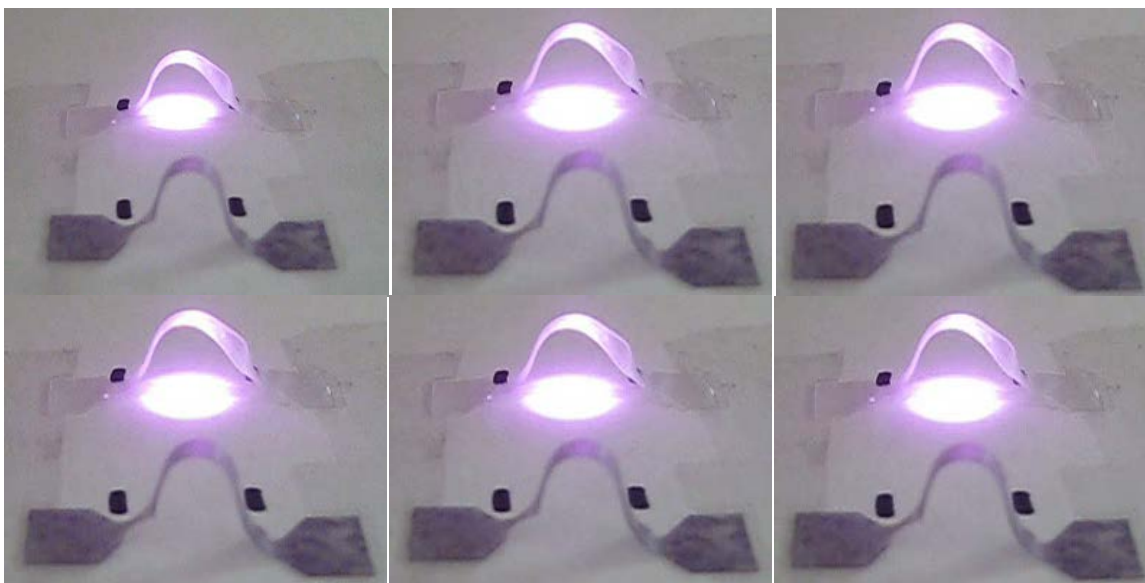
Figure IV-42. 808 nm laser shone on pure polyurethane film, with no shape memory recovery (starting with 0 seconds, each time lapse is 3 seconds apart).
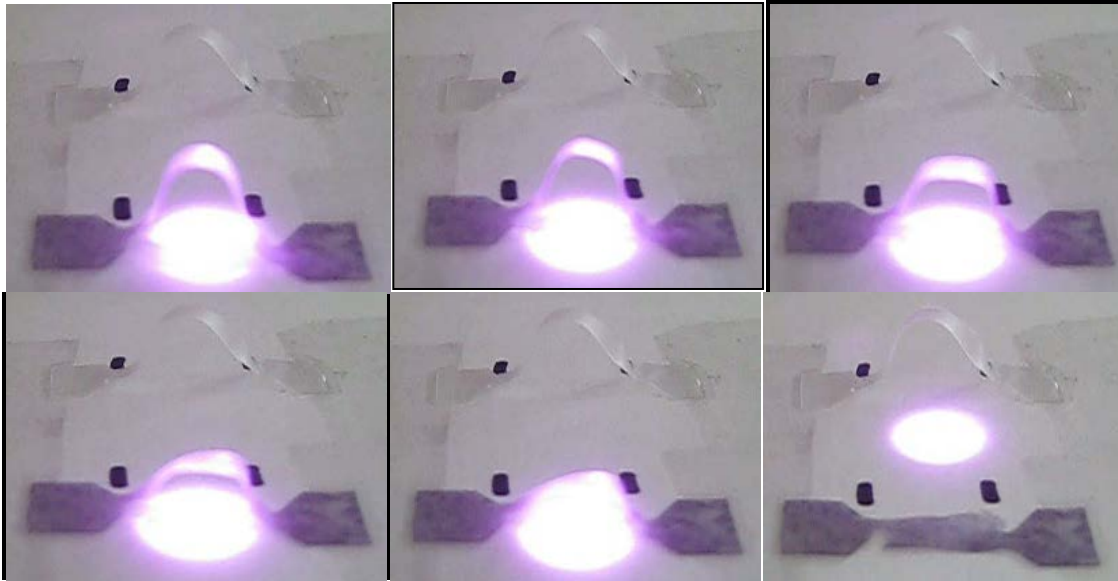
Figure IV-43. 808 nm laser shone on 5-growth nanocomposite film, with resultant shape memory recovery (starting with 0 seconds, each time lapse is 3 seconds apart).

CONCLUSIONS

Shape memory polymers can be found in many commercial applications today. These applications can range from mattresses and pillows to clothing and aerospace industries. There are some applications, however, that need special types of shape memory polymers. Chapter IV investigated one such polymer, focusing on light-induced remote-triggered shape memory polyurethane. Instead of utilizing direct heat as the method for shape memory transition triggering, near–infrared light was shown to be a viable alternative. To do this, gold nanorods were incorporated into the polymer, with the nanorods' photothermal effect the key property.

This is a novel approach to light-induced shape memory effects. While they do exist in certain forms, mainly with the presence of photo-crosslinking, this method of using light for shape memory triggering is a novel approach. Thus, many of the steps for research are new and had to be approached with no previous knowledge.

First, the challenge of isolating and stabilizing the nanorods in a non-aqueous solution was addressed, with a result that the growth can be centrifuged only three times without full agglomeration of the nanorods. In addition, only a limited amount of excess CTAB can be removed before agglomeration once again occurs. To solve this, a polyacrylic acid solution was found to be capable of surrounding the micelles and inhibiting agglomeration.

Shape memory polyurethanes were next studied, with the result that only one of four possible commercial polyurethanes was suitable according to both thermal and shape memory properties. Gold nanorods were successfully incorporated into the polyurethane and the effects on thermal and mechanical properties were observed. These studies resulted in the conclusion that such small amounts of gold nanorods had virtually no effect on the inherent properties of the polyurethane. Following this conclusion, studies were then performed on the shape memory behavior of the new nanocomposites, but still utilizing direct heat as the triggering method. Results indicated that the fixity and recovery values, even for the highest concentration of gold nanorods, were still virtually the same, meaning that even the inherent shape memory characteristics were not affected. Furthermore, this line of study was continued to see whether or not different recovery temperatures, quenching temperatures, or quenching times would affect the nanocomposites any differently than pure polyurethane. While there were distinct changes in recovery and fixity values because of these manipulations, these changes were accurately predicted and were almost identical when comparing the pure polyurethane and 5-growth film.

Finally, a study could be attempted on using the near-infrared laser to try and trigger the shape memory effect. First, a proof-of-concept test was undertaken, with the result that significant recovery was observed when using the laser. This proved irreversibly that this novel concept of using gold nanorods to remotely trigger a shape memory effect with light is successful. Following the proof of concept, multiple experiments were designed in order to understand the behavior with the laser. The first study provided a correlation between laser distance, nanorod concentration, and temperature produced by the film. It was found that a plateau of temperatures exist for the middle ranges of nanorod concentration. In addition, while it was confirmed that with higher laser powers, higher recovery values are produced, it was also observed that the predicted trend of increasing nanorod concentration leading to increased recovery values could not be verified. There were multiple contradictions, most notably with the 1.5, 2, and 3-growth films.

To solve these contradictions, a design of experiment study was conducted, in which the previously mentioned temperature production results were utilized in order to try and predict resulting recovery values. Predictable trends were seen, especially when examining laser distances and decreasing recovery trends with increasing laser distances. In contrast, however, results still reported that recovery values were lower than expected. This trend seemed only to increase the further the laser was taken from the film, as the recovery values strayed further and further away from the predicted values. It was concluded that this is most likely a result of nanorod inhibition, either through agglomeration or poor dispersion.

A final experiment produced visual time lapses of the shape memory behavior of the nanocomposites, proving that this light-triggered shape memory behavior is only possible when the nanorods are incorporated into the polyurethane and that the resulting shape memory recovery is very fast.

CHAPTER V

CONCLUSIONS

This work details the study of two distinct nanomaterials for unique uses in possible medical applications and devices. The first nanomaterial is the naturally-occurring clay nanotube, halloysite. Its rolled and hollow nature is ideal for the loading and subsequent release of compounds. Thus, its controlled release capabilities were examined. The second nanomaterial is gold nanorods. Their photothermal effect is a property unique to certain metallic nanomaterials, and one that has potential in the shape memory polymer field. Thus, incorporation into a shape memory polyurethane was investigated in order to investigate the possibility of triggering shape memory effects with a near-IR light source.

During initial studies on drug-loading methods of halloysite, it was discovered that the second method, utilizing a 1:1 drug solution to halloysite ratio, resulted in typical controlled release and a calculable loaded amount. Furthermore, this second method resulted in smaller initial bursts, but virtually the same release profile after initial burst. This led to the conclusion that further loading of the drug would likely result in only an increase in the burst, not a difference in release profile. It was further discovered that this burst effect could be eliminated by careful washing methods and that, with careful application, these methods would not hinder or degrade the controlled release performance of the halloysite. These factors have previously never been examined in the literature.

173

A dye study resulted in the conclusion that loaded compound properties affect release in multiple ways. First, solubility plays an important role. Higher solubility of the loaded compound in the release medium resulted in a quicker release. In addition, more negatively charged compounds demonstrated quicker release, due to the repelling action from the "like" charged halloysite. Finally, it was observed that the larger-sized compounds might release more slowly due to their hindrance from escaping the lumen of the nanotubes, but charge effects are more dominant.

Polymeric matrix studies demonstrated that with the incorporation of the drug-loaded halloysite into the polymer, poly(methyl methacrylate), true controlled release was achieved. Release was demonstrated over multiple days, with a potential release of much longer. In addition, the burst effect was virtually eliminated.

Studies were performed regarding the roles of reagent amounts on nanorod growth. Within seed preparation, chloroauric acid, the gold ion source, was shown to be crucial to the size of the seeds. Increased amounts of chloroauric acid resulted in larger seeds. This results in shorter-aspect-ratio nanorods due to larger diameter of starting seed templates. Increased temperature of seed growth was then shown to result in smaller aspect-ratio nanorods.

Within the nanorod growth solution, the added amounts of seed solution, chloroauric acid, ascorbic acid, the ratio between the two previous, and silver nitrate were examined. It was found that a larger amount of seeds present will result in smaller aspect-ratio nanorods. This is a result of the availability of the gold ions. As more seeds are present, there are fewer gold

ions available for growth at each seed. Chloroauric acid and ascorbic acid have also been demonstrated to be very interrelated. Too many gold ions or too little ascorbic acid have been shown to result in no nanorod growth. In addition, the ratio between the two has been demonstrated to be very important. As the ratio was increased, an increase in wavelength and decrease in intensity was observed. Finally, in regards to the role of silver nitrate, two wavelength peaks were characterized with a result that many impacting factors created a complicated response curve.

Following growth off nanorods, the incorporation of the gold nanorods into a shape memory polyurethane was examined. During stabilization studies, it was found that the nanorods could only be centrifuged and washed a limited number of times before agglomeration. To solve this, a polyacrylic acid solution was demonstrated to be able to surround the micelles, inhibit agglomeration, and allow resuspension in a DMF solution.

It was the concluded, after a study on the thermal and mechanical properties of the resultant nanocomposites, that such small amounts of nanorods had virtually no effect on the polyurethane's inherent properties, such as thermal transitions and mechanical strength. Results of shape memory examinations using direct heat indicated that the fixity and recovery values were still virtually the same, meaning that the inherent shape memory characteristics of the polyurethane were also not affected. Furthermore, it was found that recovery temperatures, quenching temperatures, and quenching times do affect the shape memory behavior of both pure polyurethane and nanocomposites, but in exactly the same way. This is very important, as many applications might desire the usual properties of the polyurethane, but with the added

benefit of photothermal triggering. It was demonstrated that recovery temperature and recovery percentage are directly related, meaning that as recovery temperature increases, higher recovery values result. This can be attributed to increased soft segment mobility at higher temperatures. With respect to quenching temperature, it was discovered that the temperatures do not have an effect on fixity until the temperature reaches the onset temperature of soft segment melting. At this point, the soft segment has not fully recrystallized and full fixity cannot be reached. Finally, it was discovered that there is also a direct correlation between quenching times and fixity values. Higher fixity values resulted from longer quenching time, with a plateau of fixity values expected to be reached upon longer quenching times.

Initial results for light-activated shape memory effects were very positive, with significant recovery observed. Upon investigation of the characteristics, it was concluded that there is a direct correlation between laser power and shape memory recovery, due to enhanced heat production when the laser is placed closer to the film. Furthermore, no connection could be made when examining recovery values and gold nanorod concentration.

Shape memory behavior was further studied with respect to correlation between nanorod concentration, laser distance, and predicted heat production. Results led to the conclusion that, while laser distance effect was verified, there was still no direct proof between nanorod concentration and recovery. In addition, however, it was discovered that that the further the laser was taken from the film, the less accurate the recovery values came when compared to the

predicted values. It was concluded that poor nanorod dispersion was most likely the cause, aggregation causing only localized heat production.

Regardless, shape memory behavior triggered by the photothermal effect of gold nanorods and the application of a near-IR laser was demonstrated. This topic has never been examined and could prove to be invaluable to situations where known triggering methods are not as applicable.

The future direction of the halloysite research could include such studies as environmental effects on release as well as the initial creation of a controlled release structure. Environmental effects are expected to play a very important role in the release of loaded compounds, not only from pure halloysite, but also from the halloysite/polymer nanocomposites. Depending on the pH, temperature, or salinity of the release environment, factors such as solubility of the drug and degradation or diffusion of the polymer matrix could be extremely affected. In addition, as the properties of the loaded compound were demonstrated to have effects on controlled release profiles, the effects of the environment on those properties deserve to be investigated as well. It is already known that temperature has a negative effect on tetracycline. It can be assumed that increased temperature would thus have a negative effect on release. In addition, it would be very interesting to examine the possible creation of drug-releasing structures composed of a polymer matrix and halloysite nanotubes. Structures such as scaffolds have been demonstrated to be a viable cell growth device. The incorporation of loaded halloysite into an electrospun scaffold would be particularly interesting to explore.

Future directions of the gold/polyurethane nanocomposites are even more exciting. While future studies on dispersion quality of the gold nanorods inside the polyurethane are a requirement, the medical industry alone could provide a multitude of uses for this type of nanocomposite. Future directions of study, however, could include such facets as preferential locations of nanorods within the polyurethane. For instance, if the nanorods could be located preferentially to the soft segment domains of the polyurethane, then perhaps fewer nanorods would be required in order to achieve the same type of shape memory results. A lower laser power could possibly be used. The energy requirements could become less. Furthermore, this could result in an increase in shape memory response, whether a faster response or an enhancement in repeatable cycles. A different type of location study would be interesting as well, in which nanorods of different aspect ratio could be located within different sections of a designed polyurethane structure. Due to the differing absorption characteristics of a change in aspect ratio, as shown in the current research, this could lead to different sections of the device responding to different wavelengths of light. This could be very attractive for applications that require a complicated movement or unfolding mechanism, even in controlled release studies where a multi-stage release is desirable.

REFERENCES

1.   Franklin, M.R., *Drug Absorption, Action, and Disposition*, in *Remington: the science and practice of pharmacy*, D.B. Troy, Editor. 1995, Lippincott Williams & Wilkins: Baltimore. p. 1142-1170.

2.   Venkatraman, S., N. Davar, A. Chester and L. Kleiner, *An Overview of Controlled Release Systems*, in *Handbook of Pharmaceutical Controlled Release Technology*, D.L. Wise, Editor. 2000, Marcel Dekker, Inc.: New York. p. 431-463.

3.   Comer, R.J., *Substance-Related Disorders*, in *Abnormal Psychology*. 2004, Worth Publishers: New York. p. 359-398.

4.   Edlin, G. and E. Golanty, *Health and Wellness*. 2010, Sudbury: Jones and Bartlett Publishers, LLC.

5.   Berner, B. and S. Dinh, *Fundamental Concepts in Controlled Release*, in *Treatise on Controlled Drug Delivery*, A. Kydonieus, Editor. 1992, Marcel Dekker, Inc.: New York. p. 1-35.

6.   Gupta, P.K. and J.R. Robinson, *Oral Controlled-Release Delivery*, in *Treatise on Controlled Drug Delivery*, A. Kydonieus, Editor. 1992, Marcel Dekker, Inc.: New York. p. 255-313.

7.   Nilsson, T., *An Introduction to Neurophysiology*, in *International Encyclopedia of Ergonomics and Human Factors*, W. Karwowski, Editor. 2006, CRC Press: Boca Raton. p. 412-424.

8.   Ward, C.J., M. DeWitt and E.W. Davis, *Halloysite Nanoclay for Controlled Release Applications*, in *Nanomaterials for Biomedicine*. 2012, American Chemical Society. p. 209-238.

9.   Kydonieus, A.F., *Fundamental Concepts of Controlled Release*, in *Controlled Release Technologies: Methods, Theory, and Applications*, A.F. Kydonieus, Editor. 1980, CRC Press: Boca Raton. p. 1-19.

10.   Martini, L.G. and P.J. Crowley, *Controlling Drug Release in Oral Product Development Programs: An Industrial Perspecitve*, in *Controlled Release in Oral Drug Delivery*, C.G. Wilson and P.J. Crowley, Editors. 2011, Springer Science + Business Media, LLC: New York. p. 49-70.

11. Ballard, B.E., *An Overview of Prolonged Action Drug Dosage Forms*, in *Sustained Controlled Release Drug Delivery*, J.R. Robinson, Editor. 1978, Marcel Dekker, Inc.: New York. p. 1-69.

12. Lee, P.I. and W.R. Good, *Overview of Controlled-Release Drug Delivery*, in *ACS Symposium Series*. 1987, American Chemical Society: Washington, D.C. p. 1-13.

13. Cramer, J.A., A. Roy, A. Burrell, C.J. Fairchild, M.J. Fuldeore, D.A. Ollendorf and P.K. Wong, *Medication Compliance and Persistance: Terminology and Definitions.* Value in Health, 2008. **2**(1): p. 44-47.

14. Li, V.H.K., V.H.L. Lee and J.R. Robinson, *Influence of Drug Properties and Routes of Drug Administration on the Design of Sustained and Controlled Release Systems*, in *Controlled Drug Delivery*, J.R. Robinson and V.H.L. Lee, Editors. 1987, Marcel Dekker, Inc.: New York. p. 3-94.

15. Bruck, S.D., *Pharmacological Basis of Controlled Drug Delivery*, in *Controlled Drug Delivery*, S.D. Bruck, Editor. 1983, CRC Press, Inc.: Boca Raton. p. 1-13.

16. Dash, A. and G. Cudworth Ii, *Therapeutic applications of implantable drug delivery systems.* Journal of Pharmacological and Toxicological Methods, 1998. **40**(1): p. 1-12.

17. Theeuwes, F. and S.I. Yum, *Principles of the Design and Operation of Generic Osmotic Pumps for the Delivery of Semisolid or Liquid Drug Formulations.* Annals of Biomedical Engineering, 1976. **4**(4): p. 343-353.

18. Uhrich, K.E., S.M. Cannizzaro, R.S. Langer and K.M. Shakesheff, *Polymeric Systems for Controlled Drug Release.* Chemical Reviews, 1999. **99**(11): p. 3181-3198.

19. Betancourt, T., A. Doiron, K.A. Homan and L. Brannon-Peppas, *Controlled Release and Nanotechnology*, in *Nanotechnology in Drug Delivery*, M.M.d. Villers, P. Aramwit, and G.S. Kwon, Editors. 2009, American Association of Pharmaceutical Scientists: New York. p. 283-312.

20. Galeska, I., T.-K. Kim, S.D. Patil, U. Bhardwaj, D. Chatttopadhyay, F. Papadimitrakopoulos and D.J. Burgess, *Controlled Release of Dexamethasone from PLGA Microspheres Embedded Within Polyacid-COntining PVA Hydrogels.* The AAPS Journal, 2005. **7**(1): p. 231-240.

21. Daniels, A.U., K.P. Andriano, W.P. Smutz, M.K. Chang and J. Heller, *Evaluation of absorbable poly(ortho esters) for use in surgical implants.* Journal of Applied Biomaterials & Biomechanics, 1994. **5**(1): p. 51-64.

22. Davis, S.S., P.B. Daly, J.W. Kennerley, M. Frier, J.G. Hardy and C.G. Wilson, *Design and evaluation of sustained release formulations for oral and buccal administration.* Advanced Pharmacotherapy I, 1982. **17**.

23. Schmuhl, N., E. Davis and H.M. Cheung, *Morphology of Thermally Polymerized Microporous Polymer Materials Prepared from Methyl Methacrylate and 2-Hydroxyethyl Methacrylate Microemulsions.* Langmuir, 1998. **14**(4): p. 757-761.

24. Boder, N., *Novel approaches to the design of safer drugs: soft drugs and site-specific chemical delivery systems.* Advances in Drug Research, 1984. **13**: p. 255.

25. Bundgaard, H., *Drug Targeting: Prodrugs*, in *Topics in Pharmaceutical Sciences 1983*, D.D. Breimer and P. Speiser, Editors. 1983, Elsevier Science Publishers. p. 329-343.

26. Burger, J.J., E. Tomlinson, E.M. Mulder and J.G. McVie, *Albumin microspheres for intraarterial tumor targeting. I. Pharmaceutical aspects.* International Journal of Pharmaceutics, 1985. **23**: p. 333.

27. Odland, G.F., *Structure of the Skin*, in *Biochemistry and Physiology of the Skin*, L.A. Goldsmith, Editor. 1983, Oxford University Press: New York. p. 3-63.

28. Nachum, Z., A. Shupak and C.R. Gordon, *Transdermal Scopolamine fr Prevention of Motion Sickness: Clinical Pharmacokinetics and Therapeutic Applications.* Clinical Pharmacokinetics, 2006. **45**(6): p. 543-566.

29. Reichek, N., C. Priest, D. Zimrin, T. Chandler and M.S.J. Sutton, *Antianginal effects of nitroglycerin patches.* The American Journal of Cardiology, 1984. **54**(1): p. 1-7.

30. Fiore, M.C., S.S. Smith, D.E. Jorenby and T.B. Baker, *The Effectiveness of the Nicotine Patch for Smoking Cessation.* The Journal of the American Medical Association, 1994. **271**(24): p. 1940-1947.

31. Trueblood, J.H., R.M. Rossomondo, W.H. Carlton and L.A. Wilson, *Corneal contact times of ophthalmic vehicles. Evaluation by microscintigraphy.* Archives of Ophthalmology, 1974. **91**: p. 313.

32. Gürsel, İ., F. Korkusuz, F. Türesin, N. Gürdal Alaeddinoğlu and V. Hasırcı, *In vivo application of biodegradable controlled antibiotic release systems for the treatment of implant-related osteomyelitis.* Biomaterials, 2000. **22**(1): p. 73-80.

33. Whang, K., T.K. Goldstick and K.E. Healy, *A biodegradable polymer scaffold for delivery of osteotropic factors.* Biomaterials, 2000. **21**(24): p. 2545-2551.

34. Wischke, C. and S.P. Schwendeman, *Degradable Polymeric Carriers for Parenteral Controlled Drug Delivery*, in *Fundamentals and Applications of Controlled Release Drug Delivery*, J. Siepmann, R.A. Siegel, and M.J. Rathbone, Editors. 2012, Springer Science and Business Media, LLC: New York.

35. Pitt, C.G., *The controlled parenteral delivery of polypeptides and proteins.* International Journal of Pharmaceutics, 1990. **59**(3): p. 173-196.

36.   Andrews, D.A., A. Ben-Jebria and R. Langer, *Recent advances in puomonary drug delivery using large, porous inhaled particles.* Hournal of Applied Physiology, 1998. **85**(2): p. 379-385.

37.   Karmouty-Quintana, H., F. Tamimi, T.K. McGovern, L.M. Grover, J.G. Martin and J.E. Barralet, *Sustained steroid release in pulmonary inflammation model.* Biomaterials, 2010. **31**(23): p. 6050-6059.

38.   Abramson, D.I., *Blood Vessels and Lymphatics*. 1962, New York: Academic Press.

39.   Tieppo, A., C.J. White, A.C. Paine, M.L. Voyles, M.K. McBride and M.E. Byrne, *Sustained in vivo release from imprinted therapeutic contact lenses.* Journal of Controlled Release, (0).

40.   Rabbe, O.G., H.C. Yeh, G.J. Newton, R.F. Phalen and D.J. Velasquez, *Inhaled Particles IV, Part I*. 1977, Edinburgh: British Occupational Hygiene Society.

41.   Jain, K.K., *Drug Delivery Systems - An Overview*, in *Drug Delivery Systems*, K.K. Jain, Editor. 2008, Humana Press: Totowa. p. 1-50.

42.   Fulekar, M.H., *Nanotechnology: Importance and Applications*. 2010, New Delhi: I.K. International Publishing House Pvt. Ltd.

43.   Sahoo, S.K. and V. Labhasetwar, *Nanotech approaches to drug delivery and imaging.* Drug Discovery Today, 2003. **8**(24): p. 1112-1120.

44.   Thassu, D., Y. Pathak and M. Deleers, *Nanoparticulate Drug-Delivery Systems: An Overview*, in *Nanoparticle Drug Delivery Systems*, D. Thassu, Y. Pathak, and M. Deleers, Editors. 2007, Informa Healthcare USA, Inc.: New York. p. 1-32.

45.   Storm, G. and D.J.A. Crommelin, *Liposomes: quo vadis?* Pharmaceutical Science & Technology Today, 1998. **1**(1): p. 19-31.

46.   Babul, N., A.C. Darke, J.A. Anslow and T.N. Krishnamurthy, *Pharmacokinetics of two novel rectal controlled-release morphine formulations.* Journal of Pain and Symptom Management, 1992. **7**(7): p. 400-405.

47.   Dufreshne, M.H., D.L. Garrec, V. Sant, J.C. Leroux and M. Ranger, *Preparation and characterization of water-soluble pH-sensitive nanocarriers for drug delivery.* International Journal of Pharmaceutics, 2004. **277**(1-2): p. 81-90.

48.   Donald A, T., *Birth of a new macromolecular architecture: dendrimers as quantized building blocks for nanoscale synthetic polymer chemistry.* Progress in Polymer Science, 2005. **30**(3–4): p. 294-324.

49.   Tripathi, P.K., A.J. Khopade, S. Nagaich, S. Shrivastava, S. Jain and N.K. Jain, *Dendrimer grafts for delivery of 5-fluorouracil.* Pharmazie, 2002. **57**(4): p. 261264.

50. Uddin, F., *Clays, Nanoclays, and Montmorillonite Minerals.* Metall. Mater. Trans. A, 2008. **39A**(12): p. 2804-2814.

51. Patel, H.A., R.S. Somani, H.C. Bajaj and R.V. Jasra, *Nanoclays for polymer nanocomposites, paints, inks, greases and cosmetics formulations, drug delivery vehicle and waste water treatment.* Bull. Mater. Sci., 2006. **29**(2): p. 133-145.

52. Patil, N.V., *Nanoclays make polymers stronger.* Adv. Mater. Processes, 2005. **163**(12): p. 39-40.

53. Franchini, E., J. Galy and J.-F. Gérard, *Sepiolite-based epoxy nanocomposites: Relation between processing, rheology, and morphology.* Journal of Colloid and Interface Science, 2009. **329**(1): p. 38-47.

54. Xu, B., Q. Zheng, Y. Song and Y. Shangguan, *Calculating barrier properties of polymer/clay nanocomposites: Effects of clay layers.* Polymer, 2006. **47**(8): p. 2904-2910.

55. Maiti, M., S. Mitra and A.K. Bhowmick, *Effect of nanoclays on high and low temperature degradation of fluoroelastomers.* Polymer Degradation and Stability, 2008. **93**(1): p. 188-200.

56. Das, G. and N. Karak, *Vegetable oil-based flame retardant epoxy/clay nanocomposites.* Polymer Degradation and Stability, 2009. **94**(11): p. 1948-1954.

57. El-Sherif, H. and M. El-Masry, *Superabsorbent nanocomposite hydrogels based on intercalation of chitosan into activated bentonite.* Polymer Bulletin, 2010.

58. Joshi, G.V., B.D. Kevadiya, H.A. Patel, H.C. Bajaj and R.V. Jasra, *Montmorillonite as a drug delivery system: Intercalation and in vitro release of timolol maleate.* International Journal of Pharmaceutics, 2009. **374**(1–2): p. 53-57.

59. Du, M., B. Guo and D. Jia, *Newly emerging applications of halloysite nanotubes: a review.* Polym. Int., 2010. **59**(5): p. 574-582.

60. Hedicke-Hoechstoetter, K., G.T. Lim and V. Altstaedt, *Novel polyamide nanocomposites based on silicate nanotubes of the mineral halloysite.* Compos. Sci. Technol., 2009. **69**(3-4): p. 330-334.

61. Li, C., J. Liu, X. Qu and Z. Yang, *A general synthesis approach toward halloysite-based composite nanotube.* J. Appl. Polym. Sci., 2009. **112**(5): p. 2647-2655.

62. Lvov, Y.M. and R.R. Price, *Halloysite nanotubules, a novel substrate for the controlled delivery of bioactive molecules.* Bio-Inorg. Hybrid Nanomater., 2008: p. 419-484.

63. Lvov, Y.M., D.G. Shchukin, H. Mohwald and R.R. Price, *Halloysite Clay Nanotubes for Controlled Release of Protective Agents.* ACS Nano, 2008. **2**(5): p. 814-820.

64.   Shchukin, D., S.V. Lamaka, K.A. Yasakua, M.L. Zheludkevich, M.G.S. Ferreira and H. Moehwald, *Active Anticorrosion Coatings with Halloysite Nanocontainers.* Journal of Physical Chemistry C, 2008. **112**(4): p. 958-964.

65.   Zhou, Y., *Nanotubes: a new carrier for drug delivery systems.* Open Nanosci. J., 2008. **2**: p. 1-5.

66.   Abdullayev, E., R. Price, D. Scchukin and Y. Lvov, *Halloysite Tubes as Nanocontainers for Anticorrosion Coating with Benzotriazole.* Applied Materials and Interfaces, 2009. **1**(7): p. 1437-1443.

67.   Shchukin, D. and H. Mohwald, *Surface-Engineered Nanocontainers for the Entrapment of Corrosion Inhibitors.* Advanced Functional Materials, 2007. **17**: p. 1451-1458.

68.   Shchukin, D., M. Zheludkevich, K. Yasakau, S. Lamaka, M.G. Ferreira and H.H. Mohwald, *Nanocontainers for Self-Healing Corrosion Protection.* Advanced Materials, 2006. **18**: p. 1672-1678.

69.   R. Price, B.P.G., Y. Lvov, R., *In-vitro release characteristics of tetracycline HCl, khellin and nicotinamide adenine dineculeotide from halloysite; a cylindrical mineral.* Journal of Microencapsulation, 2001. **18**(6): p. 713-722.

70.   Veerabadran, N.G., D. Mongayt, V. Torchilin, R.R. Price and Y.M. Lvov, *Organized Shells on Clay Nanotubes for Controlled Release of Macromolecules.* Macromolecular Rapid Communications, 2009. **30**(2): p. 99-103.

71.   Kelly, H.M., P.B. Deasy, E. Ziaka and N. Claffey, *Formulation and preliminary in vivo dog studies of a novel drug delivery system for the treatment of periodontitis.* International Journal of Pharmaceutics, 2004. **274**: p. 167-183.

72.   Levis, S.R. and P.B. Deasy, *Use of coated microtubular halloysite for the sustained release of diltiazem hydrochloride and propranolol hydrochloride.* International Journal of Pharmaceutics, 2003. **253**: p. 145-157.

73.   Guimaraes, L., A.N. Enyashin, J. Frenzel, T. Heine, H.A. Duarte and G. Seifert, *Imogolite Nanotubes: Stability, Electronic, and Mechanical Properties.* ACS Nano, 2007. **1**(4): p. 362-368.

74.   Ward, C.J., S. Song and E.W. Davis, *Controlled Release of Tetracycline-HCl from Halloysite-Polymer Composite Films.* Journal of Nanoscience and Nanotechnology, 2010. **10**(10): p. 6641-6649.

75.   Murphy, C.J., T.K. Sau, A.M. Gole, C.J. Orendorff, J. Gao, L. Gou, S.E. Hunyadi and T. Li, *Anisotropic metal nanoparticles: synthesis, assembly, and optical applications.* J. Phys. Chem. B, 2005. **109**(29): p. 13857-13870.

76.   Pérez-Juste, J., I. Pastoriza-Santos, L.M. Liz-Marzán and P. Mulvaney, *Gold nanorods: Synthesis, characterization and applications.* Coordination Chemistry Reviews, 2005. **249**(17–18): p. 1870-1901.

77.   Huang, X., S. Neretina and M.A. El-Sayed, *Gold Nanorods: From Synthesis and Properties to Biological and Biomedical Applications.* Adv. Mater. (Weinheim, Ger.), 2009. **21**(48): p. 4880-4910.

78.   Sharma, V., K. Park and M. Srinivasarao, *Colloidal dispersion of gold nanorods: Historical background, optical properties, seed-mediated synthesis, shape separation and self-assembly.* Materials Science and Engineering: R: Reports, 2009. **65**(1–3): p. 1-38.

79.   Alekseeva, A.V., V.A. Bogatyrev, B.N. Khlebtsov, A.G. Mel'nikov, L.A. Dykman and N.G. Khlebtsov, *Gold nanorods: Synthesis and optical properties.* Colloid J., 2006. **68**(6): p. 661-678.

80.   Becker, R., B. Liedberg and P.-O. Käll, *CTAB promoted synthesis of Au nanorods – Temperature effects and stability considerations.* Journal of Colloid and Interface Science, 2010. **343**(1): p. 25-30.

81.   García, M.A., V. Bouzas and N. Carmona, *Influence of stirring in the synthesis of gold nanorods.* Materials Chemistry and Physics, 2011. **127**(3): p. 446-450.

82.   Long, N.N., L.V. Vu, C.D. Kiem, S.C. Doanh, C.T. Nguyet, P.T. Hang, N.D. Thien and L.M. Quynh, *Synthesis and optical properties of colloidal gold nanoparticles.* J. Phys.: Conf. Ser., 2009. **187**: p. No pp. given.

83.   Murphy, C.J., L.B. Thompson, D.J. Chernak, J.A. Yang, S.T. Sivapalan, S.P. Boulos, J. Huang, A.M. Alkilany and P.N. Sisco, *Gold nanorod crystal growth: From seed-mediated synthesis to nanoscale sculpting.* Current Opinion in Colloid & Interface Science, 2011. **16**(2): p. 128-134.

84.   Orendorff, C.J. and C.J. Murphy, *Quantitation of Metal Content in the Silver-Assisted Growth of Gold Nanorods.* The Journal of Physical Chemistry B, 2006. **110**(9): p. 3990-3994.

85.   Park, W.M., Y.S. Huh and W.H. Hong, *Aspect-ratio-controlled synthesis of high-aspect-ratio gold nanorods in high-yield.* Current Applied Physics, 2009. **9**(2, Supplement): p. e140-e143.

86.   Nikoobakht, B. and M.A. El-Sayed, *Preparation and growth mechanism of gold nanorods (NRs) using seed-mediated growth method.* Chem. Mater., 2003. **15**(10): p. 1957-1962.

87.   Toderas, F., M. Iosin and S. Astilean, *Luminescence properties of gold nanorods.* Nuclear Instruments and Methods in Physics Research Section B: Beam Interactions with Materials and Atoms, 2009. **267**(2): p. 400-402.

88.   Huang, X., P.K. Jain, I.H. El-Sayed and M.A. El-Sayed, *Plasmonic photothermal therapy (PPTT) using gold nanoparticles.* Lasers Med Sci, 2008. **23**: p. 217-228.

89.   Jain, P.K., X. Huang, I.H. El-Sayed and M.A. El-Sayed, *Noble Metals on the Nanoscale: Optical and Photothermal Properties and Some Applications in Imaging, Sensing, Biology, and Medicine.* Accounts of Chemical Research, 2008. **41**(12): p. 1578-1586.

90.   Zharov, V.P., K.E. Mercer, E.N. Galitovskaya and M.S. Smeltzer, *Photothermal Nanotherapeutics and Nanodiagnostics for Selective Killing of Bacteria Targeted with Gold Nanoparticles.* Biophysical Journal, 2006. **90**(2): p. 619-627.

91.   Pissuwan, D., S. Valenzuela, M. Killingsworth, X. Xu and M. Cortie, *Targeted destruction of murine macrophage cells with bioconjugated gold nanorods.* Journal of Nanoparticle Research, 2007. **9**(6): p. 1109-1124.

92.   Alkilany, A.M., L.B. Thompson, S.P. Boulos, P.N. Sisco and C.J. Murphy, *Gold nanorods: Their potential for photothermal therapeutics and drug delivery, tempered by the complexity of their biological interactions.* Advanced Drug Delivery Reviews, 2012. **64**(2): p. 190-199.

93.   Hormozi-Nezhad, M.R., M. Jalali-Heravi, H. Robatjazi and H. Ebrahimi-Najafabadi, *Controlling aspect ratio of colloidal silver nanorods using response surface methodology.* Colloids and Surfaces A: Physicochemical and Engineering Aspects, 2012. **393**(0): p. 46-52.

94.   Foss, C.A., G.L. Hornyak, J.A. Stockert and C.R. Martin, *Optical properties of composite membranes containing arrays of nanoscopic gold cylinders.* The Journal of Physical Chemistry, 1992. **96**(19): p. 7497-7499.

95.   Martin, C., F. Gimenez, K.N. Bangchang, J. Karbwang, R. Farinotti and I.W. Wainer, *Whole blood concentrations of mefloquine enantiomers in healthy Thai volunteers.* European Journal of Clinical Pharmacology, 1994. **47**(1): p. 85-87.

96.   Martin, C.R., *Membrane-Based Synthesis of Nanomaterials.* Chemistry of Materials, 1996. **8**(8): p. 1739-1746.

97.   Foss, C.A., G.L. Hornyak, J.A. Stockert and C.R. Martin, *Template-Synthesized Nanoscopic Gold Particles: Optical Spectra and the Effects of Particle Size and Shape.* The Journal of Physical Chemistry, 1994. **98**(11): p. 2963-2971.

98.   Cepak, V.M. and C.R. Martin, *Preparation and Stability of Template-Synthesized Metal Nanorod Sols in Organic Solvents.* The Journal of Physical Chemistry B, 1998. **102**(49): p. 9985-9990.

99.   van der Zande, B.M.I., M.R. Böhmer, L.G.J. Fokkink and C. Schönenberger, *Aqueous Gold Sols of Rod-Shaped Particles.* The Journal of Physical Chemistry B, 1997. **101**(6): p. 852-854.

100. C. Hulteen, J. and C.R. Martin, *A general template-based method for the preparation of nanomaterials.* Journal of Materials Chemistry, 1997. **7**(7): p. 1075-1087.

101. Jirage, K.B., J.C. Hulteen and C.R. Martin, *Nanotubule-Based Molecular-Filtration Membranes.* Science, 1997. **278**(5338): p. 655-658.

102. van der Zande, B.M.I., M.R. Böhmer, L.G.J. Fokkink and C. Schönenberger, *Colloidal Dispersions of Gold Rods: Synthesis and Optical Properties.* Langmuir, 1999. **16**(2): p. 451-458.

103. Ling, T.P., K.A. Razak and A.A. Aziz, *Properties of gold nanoparticles synthesized in aqueous solution.* AIP Conf. Proc., 2012. **1455**: p. 219-224.

104. Chang, S.-S., C.-W. Shih, C.-D. Chen, W.-C. Lai and C.R.C. Wang, *The Shape Transition of Gold Nanorods.* Langmuir, 1998. **15**(3): p. 701-709.

105. Yu, S.-S. Chang, C.-L. Lee and C.R.C. Wang, *Gold Nanorods: Electrochemical Synthesis and Optical Properties.* The Journal of Physical Chemistry B, 1997. **101**(34): p. 6661-6664.

106. Törnblom, M. and U. Henriksson, *Effect of Solubilization of Aliphatic Hydrocarbons on Size and Shape of Rodlike C16TABr Micelles Studied by 2H NMR Relaxation.* The Journal of Physical Chemistry B, 1997. **101**(31): p. 6028-6035.

107. Kang, S.K., Y. Kim, M.S. Hahn, I. Choi, J. Lee and J. Yi, *Aspect ratio control of Au nanorods via temperature and hydroxylamine concentration of reaction medium.* Current Applied Physics, 2006. **6**(0): p. e114-e120.

108. Kooij, E.S., W. Ahmed, C. Hellenthal, H.J.W. Zandvliet and B. Poelsema, *From nanorods to nanostars: Tuning the optical properties of gold nanoparticles.* Colloids and Surfaces A: Physicochemical and Engineering Aspects, 2012(0).

109. Huang, X., I.H. El-Sayed, W. Qian and M.A. El-Sayed, *Cancer Cell Imaging and Photothermal Therapy in the Near-Infrared Region by Using Gold Nanorods.* Journal of the American Chemical Society, 2006. **128**(6): p. 2115-2120.

110. Huang, X. and M.A. El-Sayed, *Gold nanoparticles: Optical properties and implementations in cancer diagnosis and photothermal therapy.* Journal of Advanced Research, 2010. **1**(1): p. 13-28.

111. Cao, J., E.K. Galbraith, T. Sun and K.T.V. Grattan, *Effective surface modification of gold nanorods for localized surface plasmon resonance-based biosensors.* Sensors and Actuators B: Chemical, 2012. **169**(0): p. 360-367.

112. Li, J.L., D. Day and M. Gu, *Ultra-Low Energy Threshold for Cancer Photothermal Therapy Using Transferrin-Conjugated Gold Nanorods.* Advanced Materials, 2008. **20**(20): p. 3866-3871.

113. Gormley, A.J., K. Greish, A. Ray, R. Robinson, J.A. Gustafson and H. Ghandehari, *Gold nanorod mediated plasmonic photothermal therapy: A tool to enhance macromolecular delivery.* International Journal of Pharmaceutics, 2011. **415**(1–2): p. 315-318.

114. C.S, R., J. Kumar, R. V, V. M and A. Abraham, *Laser immunotherapy with gold nanorods causes selective killing of tumour cells.* Pharmacological Research, 2012. **65**(2): p. 261-269.

115. Jain, P.K., K.S. Lee, I.H. El-Sayed and M.A. El-Sayed, *Calculated Absorption and Scattering Properties of Gold Nanoparticles of Different Size, Shape, and Composition: Applications in Biological Imaging and Biomedicine.* The Journal of Physical Chemistry B, 2006. **110**(14): p. 7238-7248.

116. Pissuwan, D., T. Niidome and M.B. Cortie, *The forthcoming applications of gold nanoparticles in drug and gene delivery systems.* Journal of Controlled Release, 2011. **149**(1): p. 65-71.

117. Yamashita, S., Y. Niidome, Y. Katayama and T. Niidome, *Photochemical Reaction of Poly(ethylene glycol) on Gold Nanorods Induced by Near Infrared Pulsed-laser Irradiation.* Chemistry Letters, 2009. **38**(3): p. 226-227.

118. Shiotani, A., T. Mori, T. Niidome, Y. Niidome and Y. Katayama, *Stable Incorporation of Gold Nanorods into N-Isopropylacrylamide Hydrogels and Their Rapid Shrinkage Induced by Near-Infrared Laser Irradiation.* Langmuir, 2007. **23**(7): p. 4012-4018.

119. Kawano, T., Y. Niidome, T. Mori, Y. Katayama and T. Niidome, *PNIPAM Gel-Coated Gold Nanorods for Targeted Delivery Responding to a Near-Infrared Laser.* Bioconjugate Chemistry, 2009. **20**(2): p. 209-212.

120. Brown, K.R., L.A. Lyon, A.P. Fox, B.D. Reiss and M.J. Natan, *Hydroxylamine Seeding of Colloidal Au Nanoparticles. 3. Controlled Formation of Conductive Au Films.* Chemistry of Materials, 1999. **12**(2): p. 314-323.

121. Brown, K.R. and M.J. Natan, *Hydroxylamine Seeding of Colloidal Au Nanoparticles in Solution and on Surfaces.* Langmuir, 1998. **14**(4): p. 726-728.

122. Brown, K.R., D.G. Walter and M.J. Natan, *Hydroxylamine Seeding of Colloidal Au Nanoparticle Solutions. 2. Improved Control of Particle Size and Shape.* Chemistry of Materials, 1999. **12**(2): p. 306-313.

123. Jana, N.R., L. Gearheart and C.J. Murphy, *Evidence for Seed-Mediated Nucleation in the Chemical Reduction of Gold Salts to Gold Nanoparticles.* Chemistry of Materials, 2001. **13**(7): p. 2313-2322.

124. Cheng, J., L. Ge, B. Xiong and Y. He, *Investigation of pH Effect on Gold Nanorod Synthesis.* Journal of the Chinese Chemical Society, 2011. **58**(6): p. 822-827.

125. Johnson, C.J., E. Dujardin, S.A. Davis, C.J. Murphy and S. Mann, *Growth and form of gold nanorods prepared by seed-mediated, surfactant-directed synthesis.* J. Mater. Chem., 2002. **12**: p. 1765-1770.

126. Gou, L. and C.J. Murphy, *Fine-tuning the shape of gold nanorods.* Chem. Mater., 2005. **17**: p. 3668-3672.

127. Jana, N.R., L. Gearheart and C.J. Murphy, *Wet Chemical Synthesis of High Aspect Ratio Cylindrical Gold Nanorods.* The Journal of Physical Chemistry B, 2001. **105**(19): p. 4065-4067.

128. Busbee, B.D., S.O. Obare and C.J. Murphy, *An Improved Synthesis of High-Aspect-Ratio Gold Nanorods.* Advanced Materials, 2003. **15**(5): p. 414-416.

129. Kang, S.K., I. Choi, J. Lee, Y. Kim and J. Yi, *Investigation on shape variation of Au nanocrystals.* Current Applied Physics, 2008. **8**(6): p. 810-813.

130. Si, S., C. Leduc, M.-H. Delville and B. Lounis, *Short gold nanorod growth revisited: the critical role of the bromide counterion.* Chemphyschem, 2012. **13**(1): p. 193-202.

131. Sau, T.K. and C.J. Murphy, *Seeded High Yield Synthesis of Short Au Nanorods in Aqueous Solution.* Langmuir, 2004. **20**(15): p. 6414-6420.

132. Seo, S., X. Wang and D. Murray, *Direct monitoring of gold nanorod growth.* Ionics, 2009. **15**(1): p. 67-71.

133. Pérez-Juste, J., M.A. Correa-Duarte and L.M. Liz-Marzán, *Silica gels with tailored, gold nanorod-driven optical functionalities.* Applied Surface Science, 2004. **226**(1–3): p. 137-143.

134. Li, Q., T. Bürgi and H. Chen, *Preparation of gold nanorods of high quality and high aspect ratio.* Journal of Wuhan University of Technology-Mater. Sci. Ed., 2010. **25**(1): p. 104-107.

135. Jiang, X.C. and M.P. Pileni, *Gold nanorods: Influence of various parameters as seeds, solvent, surfactant on shape control.* Colloids and Surfaces A: Physicochemical and Engineering Aspects, 2007. **295**(1–3): p. 228-232.

136. Park, H.J., C.S. Ah, W.-J. Kim, I.S. Choi, K.-P. Lee and W.S. Yun, *Temperature-induced control of aspect ratio of gold nanorods.* J. Vac. Sci. Technol., A, 2006. **24**(4): p. 1323-1326.

137. Zou, R., Q. Zhang, Q. Zhao, F. Peng, H. Wang, H. Yu and J. Yang, *Thermal stability of gold nanorods in an aqueous solution.* Colloids and Surfaces A: Physicochemical and Engineering Aspects, 2010. **372**(1–3): p. 177-181.

138. Nikoobakht, B. and M.A. El-Sayed, *Evidence for Bilayer Assembly of Cationic Surfactants on the Surface of Gold Nanorods.* Langmuir, 2001. **17**(20): p. 6368-6374.

139.   Murphy, C.J. and N.R. Jana, *Controlling the Aspect Ratio of Inorganic Nanorods and Nanowires.* Advanced Materials, 2002. **14**(1): p. 80-82.

140.   Gao, J., C.M. Bender and C.J. Murphy, *Dependence of the Gold Nanorod Aspect Ratio on the Nature of the Directing Surfactant in Aqueous Solution.* Langmuir, 2003. **19**(21): p. 9065-9070.

141.   Nikoobakht, B., Z.L. Wang and M.A. El-Sayed, *Self-Assembly of Gold Nanorods.* The Journal of Physical Chemistry B, 2000. **104**(36): p. 8635-8640.

142.   Hu, J., Y. Zhu, H. Huang and J. Lu, *Recent advances in shape–memory polymers: Structure, mechanism, functionality, modeling and applications.* Progress in Polymer Science, 2012.

143.   Liu, C., H. Qin and P.T. Mather, *Review of progress in shape-memory polymers.* Journal of Materials Chemistry, 2007. **17**(16): p. 1543-1558.

144.   Rousseau, I.A., *Challenges of shape memory polymers: A review of the progress toward overcoming SMP's limitations.* Polymer Engineering & Science, 2008. **48**(11): p. 2075-2089.

145.   Cao, F. and S.C. Jana, *Nanoclay-tethered shape memory polyurethane nanocomposites.* Polymer, 2007. **48**(13): p. 3790-3800.

146.   Buckley, C.P., C. Prisacariu and A. Caraculacu, *Novel triol-crosslinked polyurethanes and their thermorheological characterization as shape-memory materials.* Polymer, 2007. **48**(5): p. 1388-1396.

147.   Gall, K., P. Kreiner, D. Turner and M. Hulse, *Shape-memory polymers for microelectromechanical systems.* Microelectromechanical Systems, Journal of, 2004. **13**(3): p. 472-483.

148.   Liu, Y., K. Gall, M.L. Dunn, A.R. Greenberg and J. Diani, *Thermomechanics of shape memory polymers: Uniaxial experiments and constitutive modeling.* International Journal of Plasticity, 2006. **22**(2): p. 279-313.

149.   Ota, S., *Current status of irradiated heat-shrinkable tubing in Japan.* Radiation Physics and Chemistry (1977), 1981. **18**(1–2): p. 81-87.

150.   Liu, C., S.B. Chun, P.T. Mather, L. Zheng, E.H. Haley and E.B. Coughlin, *Chemically Cross-Linked Polycyclooctene: Synthesis, Characterization, and Shape Memory Behavior.* Macromolecules, 2002. **35**(27): p. 9868-9874.

151.   Sakurai, K., H. Tanaka, N. Ogawa and T. Takahashi, *Shape-memorizable styrene-butadiene block copolymer. I. Thermal and mechanical behaviors and structural change with deformation.* Journal of Macromolecular Science, Part B, 1997. **36**(6): p. 703-716.

152. Kagami, Y., J.P. Gong and Y. Osada, *Shape memory behaviors of crosslinked copolymers containing stearyl acrylate.* Macromolecular Rapid Communications, 1996. **17**(8): p. 539-543.

153. Koerner, H., G. Price, N.A. Pearce, M. Alexander and R.A. Vaia, *Remotely actuated polymer nanocomposites[mdash]stress-recovery of carbon-nanotube-filled thermoplastic elastomers.* Nat Mater, 2004. **3**(2): p. 115-120.

154. Ahir, S.V. and E.M. Terentjev, *Photomechanical actuation in polymer-nanotube composites.* Nat Mater, 2005. **4**(6): p. 491-495.

155. Vaia, R., *Nanocomposites: Remote-controlled actuators.* Nat Mater, 2005. **4**(6): p. 429-430.

156. Wei, Z.G., R. Sandstroröm and S. Miyazaki, *Shape-memory materials and hybrid composites for smart systems: Part I Shape-memory materials.* Journal of Materials Science, 1998. **33**(15): p. 3743-3762.

157. Winzek, B., S. Schmitz, H. Rumpf, T. Sterzl, R. Hassdorf, S. Thienhaus, J. Feydt, M. Moske and E. Quandt, *Recent developments in shape memory thin film technology.* Materials Science and Engineering: A, 2004. **378**(1–2): p. 40-46.

158. Razzaq, M.Y. and L. Frormann, *Thermomechanical studies of aluminum nitride filled shape memory polymer composites.* Polymer Composites, 2007. **28**(3): p. 287-293.

159. Lendlein, A. and R. Langer, *Biodegradable, Elastic Shape-Memory Polymers for Potential Biomedical Applications.* Science, 2002. **296**(5573): p. 1673-1676.

160. Maitland, D.J., M.F. Metzger, D. Schumann, A. Lee and T.S. Wilson, *Photothermal properties of shape memory polymer micro-actuators for treating stroke.* Lasers in Surgery and Medicine, 2002. **30**(1): p. 1-11.

161. Schmidt, A.M., *Electromagnetic Activation of Shape Memory Polymer Networks Containing Magnetic Nanoparticles.* Macromolecular Rapid Communications, 2006. **27**(14): p. 1168-1172.

162. Gall, K., C.M. Yakacki, Y. Liu, R. Shandas, N. Willett and K.S. Anseth, *Thermomechanics of the shape memory effect in polymers for biomedical applications.* Journal of Biomedical Materials Research Part A, 2005. **73A**(3): p. 339-348.

163. Wache, H.M., D.J. Tartakowska, A. Hentrich and M.H. Wagner, *Development of a polymer stent with shape memory effect as a drug delivery system.* Journal of Materials Science: Materials in Medicine, 2003. **14**(2): p. 109-112.

164. Ratna, D. and J. Karger-Kocsis, *Recent advances in shape memory polymers and composites: a review.* Journal of Materials Science, 2008. **43**(1): p. 254-269.

165.   Kim, B.K., S.Y. Lee and M. Xu, *Polyurethanes having shape memory effects.* Polymer, 1996. **37**(26): p. 5781-5793.

166.   Li, F., J. Hou, W. Zhu, X. Zhang, M. Xu, X. Luo, D. Ma and B.K. Kim, *Crystallinity and morphology of segmented polyurethanes with different soft-segment length.* J. Appl. Polym. Sci., 1996. **62**(4): p. 631-638.

167.   Jeong, H.M., J.B. Lee, S.Y. Lee and B.K. Kim, *Shape memory polyurethane containing mesogenic moiety.* Journal of Materials Science, 2000. **35**(2): p. 279-283.

168.   Ni, X. and X. Sun, *Block copolymer of trans-polyisoprene and urethane segment: Shape memory effects.* J. Appl. Polym. Sci., 2006. **100**(2): p. 879-885.

169.   Cho, J.W., Y.C. Jung, Y.-C. Chung and B.C. Chun, *Improved mechanical properties of shape-memory polyurethane block copolymers through the control of the soft-segment arrangement.* J. Appl. Polym. Sci., 2004. **93**(5): p. 2410-2415.

170.   Pérez-Foullerat, D., S. Hild, A. Mücke and B. Rieger, *Synthesis and Properties of Poly(ketone-co-alcohol) Materials: Shape Memory Thermoplastic Elastomers by Control of the Glass Transition Process.* Macromolecular Chemistry and Physics, 2004. **205**(3): p. 374-382.

171.   Charlesby, A., *Atomic Radiation and Polymers* International Series of Monographs on Radiation Effects in Materials. 1960: Pergamon Press.

172.   Zhu, G., S. Xu, J. Wang and L. Zhang, *Shape memory behaviour of radiation-crosslinked PCL/PMVS blends.* Radiation Physics and Chemistry, 2006. **75**(3): p. 443-448.

173.   Maiti, P., G. Radhakrishnan, P. Aruna and G. Ghosh, *Novel Polyurethane Gels: The Effect of Structure on Gelation.* Macromolecular Symposia, 2006. **241**(1): p. 51-59.

174.   Hu, J.L., F.L. Ji and Y.W. Wong, *Dependency of the shape memory properties of a polyurethane upon thermomechanical cyclic conditions.* Polym. Int., 2005. **54**(3): p. 600-605.

175.   Auad, M.L., M.A. Mosiewicki, T. Richardson, M.I. Aranguren and N.E. Marcovich, *Nanocomposites made from cellulose nanocrystals and tailored segmented polyurethanes.* J. Appl. Polym. Sci., 2010. **115**(2): p. 1215-1225.

176.   Biercuk, M.J., M.C. Llaguno, M. Radosavljevic, J.K. Hyun, A.T. Johnson and J.E. Fischer, *Carbon nanotube composites for thermal management.* Applied Physics Letters, 2002. **80**(15): p. 2767-2769.

177.   Li, F., L. Qi, J. Yang, M. Xu, X. Luo and D. Ma, *Polyurethane/conducting carbon black composites: Structure, electric conductivity, strain recovery behavior, and their relationships.* J. Appl. Polym. Sci., 2000. **75**(1): p. 68-77.

178. Mohr, R., K. Kratz, T. Weigel, M. Lucka-Gabor, M. Moneke and A. Lendlein. *Initiation of shape-memory effect by inductive heating of magnetic nanoparticles in thermoplastic polymers* in *Proceedings of the National Academy of Sciences of the United States*. 2006.

179. Yang, B., W.M. Huang, C. Li, C.M. Lee and L. Li, *On the effects of moisture in a polyurethane shape memory polymer.* Smart Materials and Structures, 2004. **13**(1): p. 191.

180. Huang, W.M., B. Yang, L. An, C. Li and Y.S. Chan, *Water-driven programmable polyurethane shape memory polymer: Demonstration and mechanism.* Applied Physics Letters, 2005. **86**(11): p. 114105-3.

181. Chae Jung, Y., H. Hwa So and J. Whan Cho, *Water-Responsive Shape Memory Polyurethane Block Copolymer Modified with Polyhedral Oligomeric Silsesquioxane.* Journal of Macromolecular Science, Part B, 2006. **45**(4): p. 453-461.

182. Lendlein, A., H. Jiang, O. Junger and R. Langer, *Light-induced shape-memory polymers.* Nature, 2005. **434**(7035): p. 879-882.

183. Behl, M. and A. Lendlein, *Shape-memory polymers.* Materials Today, 2007. **10**(4): p. 20-28.

184. Chun, B.C., T.K. Cho and Y.-C. Chung, *Blocking of soft segments with different chain lengths and its impact on the shape memory property of polyurethane copolymer.* J. Appl. Polym. Sci., 2007. **103**(3): p. 1435-1441.

185. Li, F., X. Zhang, J. Hou, M. Xu, X. Luo, D. Ma and B.K. Kim, *Studies on thermally stimulated shape memory effect of segmented polyurethanes.* J. Appl. Polym. Sci., 1997. **64**(8): p. 1511-1516.

186. Tobushi, H., R. Matsui, S. Hayashi and D. Shimada, *The influence of shape-holding conditions on shape recovery of polyurethane-shape memory polymer foams.* Smart Materials and Structures, 2004. **13**(4): p. 881.

187. Gan, Q., D. Dai, Y. Yuan, J. Qian, S. Sha, J. Shi and C. Liu, *Effect of size on the cellular endocytosis and controlled release of mesoporous silica nanoparticles for intracellular delivery.* Biomed. Microdevices, 2012. **14**(Copyright (C) 2013 American Chemical Society (ACS). All Rights Reserved.): p. 259-270.

188. Loftin, K.A., C.D. Adams, M.T. Meyer and R. Surampalli, *Effects of ionic strength, temperature, and pH on degradation of selected antibiotics.* J. Environ. Qual., 2008. **37**(Copyright (C) 2013 American Chemical Society (ACS). All Rights Reserved.): p. 378-386.

189. Wei, W., E. Abdullayev, A. Goeders, A. Hollister, Y. Lvov and D. Mills, *Clay nanotube/poly(methyl methacrylate) bone cement composite with sustained antibiotic*

release. PMSE Prepr., 2011(Copyright (C) 2013 American Chemical Society (ACS). All Rights Reserved.): p. No pp. given.

190. Tanaka, E., S. Ohnishi, R.G. Laurence, H.S. Choi, V. Humblet and J.V. Frangioni, *Real-Time Intraoperative Ureteral Guidance Using Invisible Near-Infrared Fluorescence.* The Journal of Urology, 2007. **178**(5): p. 2197-2202.

191. Wang, J., B. Dong, B. Chen, Z. Jiang and H. Song, *Selective photothermal therapy for breast cancer with targeting peptide modified gold nanorods.* Dalton Trans., 2012. **41**(Copyright (C) 2013 American Chemical Society (ACS). All Rights Reserved.): p. 11134-11144.

192. Gole, A. and C.J. Murphy, *Polyelectrolyte-Coated Gold Nanorods: Synthesis, Characterization and Immobilization.* Chemistry of Materials, 2005. **17**(6): p. 1325-1330.

193. Wang, Y., K.C.L. Black, H. Luehmann, W. Li, Y. Zhang, X. Cai, D. Wan, S.-Y. Liu, M. Li, P. Kim, Z.-Y. Li, L.V. Wang, Y. Liu, and Y. Xia, *Comparison Study of Gold Nanohexapods, Nanorods, and Nanocages for Photothermal Cancer Treatment.* ACS Nano, 2013. **7**(3): p. 2068-2077.

194. Boucher, V.M., D. Cangialosi, A. Alegria, J. Colmenero, I. Pastoriza-Santos and L.M. Liz-Marzan, *Physical aging of polystyrene/gold nanocomposites and its relation to the calorimetric Tg depression.* Soft Matter, 2011. **7**(7): p. 3607-3620.

195. Gunes, I.S., F. Cao and S.C. Jana, *Evaluation of nanoparticulate fillers for development of shape memory polyurethane nanocomposites.* Polymer, 2008. **49**(9): p. 2223-2234.

196. Rek, V., M. Bravar, T. Jocic and E. Govorcin, *A contribution to the UV degradation of polyurethanes.* Angew. Makromol. Chem., 1988. **158-159**(Copyright (C) 2013 American Chemical Society (ACS). All Rights Reserved.): p. 247-63.

197. Hong, Y., E. Lee, J. Choi, S.J. Oh, S. Haam, Y.-M. Huh, D.S. Yoon, J.-S. Suh and J. Yang, *Gold Nanorod-Mediated Photothermal Modulation for Localized Ablation of Cancer Cells.* Journal of Nanomaterials, 2012.

198. Karen, M.M., S.S. Brian, J.W. Ashley, M.D. Judith and R.O. Earl, *Photothermal effects of laser tissue soldering.* Physics in Medicine and Biology, 1999. **44**(4): p. 983.